Winter 1-31-2022

Selective GSK3β inhibition mediates an Nrf2-independent anti-inflammatory microglial response

Mohamed H. Yousef
The American University in Cairo AUC, mhyosef@aucegypt.edu

Selective inhibition of GSK3β mediates an Nrf2-independent anti-inflammatory microglial response

A thesis submitted to the Biotechnology Graduate Program in partial fulfillment of the requirements for the degree of Master of Science

By:

Mohamed Hesham Hassanien Mahmoud Yousef

Under the supervision of:

Dr. Anwar Abdelnaser (Advisor)
Assistant Professor and Director of Global Public Health Graduate Program
Institute of Global Health and Human Ecology (IGHHE)
The American University in Cairo (AUC)

Prof. Dr. Hassan A. N. El-Fawal (Co-advisor)
Professor and Chairman
Institute of Global Health and Human Ecology (IGHHE)
The American University of Cairo (AUC)

Dr. Mohamed Salama (Co-advisor)
Associate Professor
Institute of Global Health and Human Ecology (IGHHE)
The American University of Cairo (AUC)
Senior Atlantic Fellow for the GBHI, TCD, Dublin, Ireland

Fall 2021

ACKNOWLEDGEMENTS

First and foremost, I would like to express my deepest gratitude to my supervisor, Dr. Anwar Abdelnaser, whose support was invaluable in seeing this bit of work through. His insightful feedback and pedagogical approach pushed me to sharpen my thinking and brought my technical know-how to a higher level. Moreover, his trust in my capabilities fundamentally helped build my confidence, my problem-solving abilities and my research competence. Dr. Abdelnaser has always thought of me when a new scientific endeavor or a growth opportunity came about; for this and for every bit of support he afforded me, I'm ever so indebted.

I would like to thank Dr. Hassan El-Fawal for being the ultimate father figure. Not only did Dr. El-Fawal champion my desire to venture into the realm of neuroscience, he also generously afforded me the opportunity to work in the newly inaugurated labs of the Institute of Global Health and Human Ecology, giving me access to some of the most advanced facilities at the AUC. Moreover, despite Dr. El-Fawal's busy schedule as the school's dean, he never turned down a request to meet and strove to fit me into his ever-tight schedule.

I count myself lucky to have made the acquaintance of Dr. Mohamed Salama, who – beyond his tremendous scientific standing – is one of the friendliest, most helpful, and most approachable professors I have ever known. Dr. Salama literally inspired this project. I will never forget the friendly brainstorming session, where Dr. Salama first introduced me to the notion of Nrf2 activation in neurodegenerative diseases. Dr. Salama never failed to support and for this unconditional backing, I'm profoundly grateful.

I would like to acknowledge our collaborating team at Broad Institute Inc. for providing me with the experimental compounds. I owe special thanks to Dr. Florence F. Wagner and certainly the very outstandingly cooperative and accommodating Dr. Joshua Sacher.

I am most appreciative of all my professors at the AUC and everyone else who – in one way or another – had a role to play in facilitating this otherwise arduous journey. I would like to thank my

colleagues who made the undertaking a lot easier than it could have been. I can't think of any other group of people in my life with whom I would want to celebrate the conclusion of this piece of work.

I am eternally indebted to my mother. All the words in the English language fail me as I attempt to express my gratitude for the gift of her. My mother has been the only mainstay, the truest emotional support, and my sturdy backbone, not only throughout this journey, but my entire life. If I am presenting a thesis to earn a degree in a biomedical discipline, she should definitely be receiving a doctorate with distinction in the discipline of motherhood. Any bit of achievement I realize – and indeed this is one – is a testament to the impeccability of her lifelong work. Thank you, mom.

I also need to thank my old man for championing my academic pursuits, despite the grandness of the enterprise. I know how burdensome this has been on different levels and his buying into the undertaking is simply heartwarming. Not only did he advocate my desire to go into grad school, but my father also countenanced my scarcity for the better part of four years with not so much as a scolding remark. Your pride and investment in this endeavor has been enough incentive to get me where I am today. Thank you for having my back, dad.

Last but certainly not least, I owe a good deal of thanks to my family and friends for putting up with my absence and being there for me despite the many, many downs I've been through. Their support, tolerance and understanding speak volumes of how true these people are to their names.

ABSTRACT

Neuroinflammatory glial responses have been an increasingly recognized component of neurodegenerative diseases. Of the various glial subsets within the CNS, microglia come at the forefront of the neural innate immunity and their dysregulation is fundamental to degenerative neuropathologies. Agreeing with the oxidative paradigm of aging, both neuronal and glial subsets undergo prolonged oxidative stress, which is ultimately conducive to cellular senescence, neuroinflammatory and neurodegenerative changes. Nuclear factor erythroid 2-related factor 2 (Nrf2), the cellular master regulator of redox homeostasis is often deregulated in neurodegenerative diseases and its transcriptional activation has been a prominent disease-modifying approach. Glycogen Synthase Kinase 3 (GSK3) is the primary mediator of tau hyperphosphorylation and aberrant amyloid deposition and dysregulation of its activity is a major contributor to CNS proteopathy. GSK3 is also associated with the proinflammatory phenotype of microglia and has been shown to act in concert with NF-κB, a key inflammatory molecule. Moreover, GSK3 is a negative regulator of Nrf2 and its inhibition is among postulated strategies of anti-oxidative Nrf2 activation. Only one of the two isoforms of GSK3 (GSK3β) has been thoroughly studied and mostly its role in proteopathies of neuronal origin has been the focus of previous research. In this study, we aimed to explore the multimodal disease-modifying utility of GSK3 beyond neuronal proteopathologies, particularly in microglia, whereby its inhibition was surmised to simultaneously activate the Nrf2-orchestrated antioxidant response, discourage NF-κB-driven inflammatory events, over and above its tried and tested utility in modulating protein pathology. Furthermore, we aimed to underscore the difference in therapeutic value between the two GSK3 paralogs by isoform-selective chemical inhibition.

The anti-inflammatory effects of BRD0705 (GSK3α-selective inhibitor), BRD3731 (GSK3β-selective inhibitor), and BRD0320 (GSK3α/β inhibitor) were preliminarily determined as a function of the reductive capacity of each to mitigate LPS-induced proinflammatory activation of SIM-A9 microglia, as demonstrated by downscaling of the levels of secreted nitrite. Building upon this, post-treatment downregulation of LPS-elevated mRNA expression of several inflammatory markers (CD11b, Iba1, iNOS, IL-1β, IL-6, and TNF-α) was evaluated by real-time qPCR. Transcriptional targets of Nrf2 (HO-1 and Osgin1) were also analyzed by qPCR to determine the

competency of selective GSK3 inhibition at mediating Nrf2 transcriptional activation. Additionally, post-treatment concentrations of the secretory proinflammatory cytokines IL-1β, IL-6, and TNF-α in supernatant of LPS-stimulated SIM-A9 microglia were estimated by sandwich ELISA. To deduce whether the regulatory action of the GSK3 inhibitor compounds may be mediated via the nuclear translocation of NF-κB and Nrf2, nuclear lysates of LPS-stimulated and GSK3 inhibitor-treated SIM-A9 cells were analyzed for NF-κB and Nrf2 expression by western immunoblotting. β-catenin was similarly appraised to circumstantiate the projected discrepancy between BRD0705 (GSK3α inhibitor) and BRD3731 (GSK3β inhibitor) as to their β-catenin-destabilizing influence. Finally, to infer whether the counter-inflammatory activity of the GSK3 inhibitor compounds was Nrf2-dependent, DsiRNA-mediated knockdown of Nrf2 was attempted. The mRNA expression of the Nrf2 target genes HO-1 and Osgin1 as well as the proinflammatory markers iNOS, IL-1β, IL-6, and TNF-α in LPS-activated SIM-A9 DsiNrf2 cells treated with GSK3 inhibitors was reassessed by real-time qPCR to monitor post-knockdown modulatory trends.

Results from our experiments reveal a superior anti-inflammatory and anti-oxidative efficacy for GSK3β-selective inhibition, compared to GSK3α-selective and non-selective pan-inhibition, suggesting that inhibition of GSK3β is more crucial to a significant disease-modifying outcome than GSK3α; hence use of selective GSK3β inhibitors is likely to be more propitious than non-selective dual inhibitors administered at comparable doses. Not incongruous with the above, GSK3α-selective inhibition remains a worthy recourse in pro-oncogenic contexts, given its mild to moderate anti-inflammatory and anti-oxidative potential in addition to its impotency at activating the tumorigenic β-catenin-driven transcriptional program. Moreover, our results suggest that the anti-inflammatory effects of GSK3 inhibition is not Nrf2 dependent.

GRAPHICAL ABSTRACT

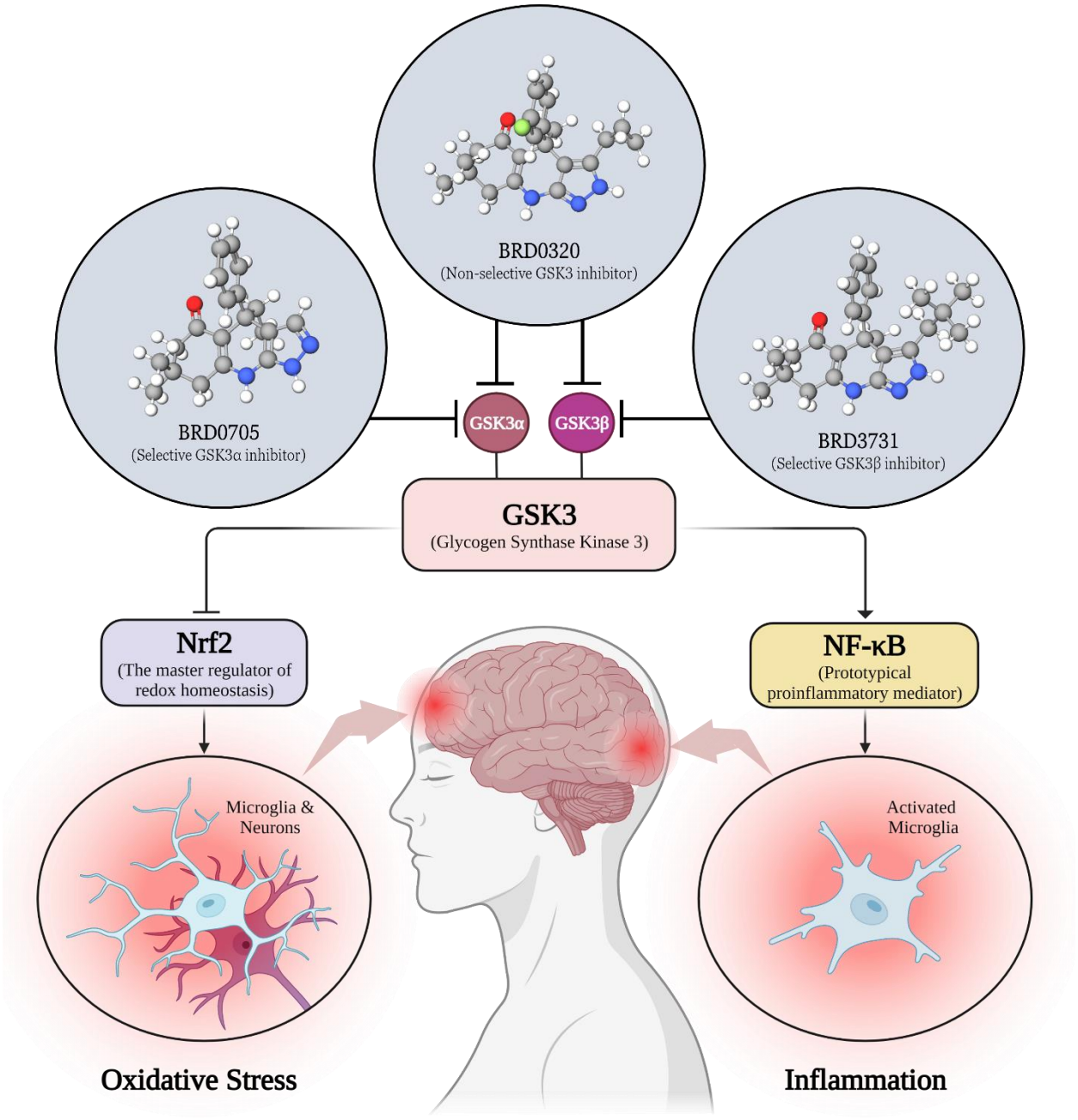

Table of Contents

LIST OF TABLES

LIST OF FIGURES

LIST OF ABBREVIATIONS

6-OHDA	6-hydroxydopamine
AD	Alzheimer's disease
Akt	Protein kinase B
ALS	Amyotrophic lateral sclerosis
AML	Acute myeloid leukemia
ARE	Antioxidant response element
ARG1	Arginase 1
Aβ	Amyloid-β
BACE1	Beta-secretase 1
BBB	Blood-brain barrier
BDNF	Brain-derived neurotrophic factor
β-TrCP	β-transducing repeat-containing protein
bZIP	Basic-region leucine zipper
CBP	CREB-binding protein
CCL22	C-C motif chemokine 22
CDK3	Cyclin-dependent kinase 3
CNC	Cap "n" collar
CNS	Central nervous system
COX-2	Cyclooxygenase-2
CSF1	Colony stimulating factor 1
CUL3/RBX1	Cullin 3 and RING-box protein 1
CycE1	Cyclin E1
DMF	Dimethyl fumarate
EMP	Erythromyeloid precursor
FIZZ1	Found in inflammatory zone 1
FTD	Frontotemporal lobar dementia
GDNF	Glial cell-derived neurotrophic factor
GSK3	Glycogen synthase kinase 3

HD	Huntington's disease
HDAC3	Histone Deacetylase 3
HGPS	Hutchinson-Gilford progeria syndrome
IFN-γ	Interferon-gamma
IGF-1	Insulin-like growth factor 1
IKKβ	Inhibitor of nuclear factor kappa-B kinase subunit beta
IL-10	Interleukin-10
IL-1β	Interleukin-1 beta
IL-6	Interleukin-6
iNOS	Inducible nitric oxide synthase
IκBα	NF-kappa-B inhibitor alpha
JNK	c-Jun N-terminal kinase 3
Keap1	Kelch-like ECH-associated protein 1
LPS	Lipopolysaccharide
MAPK	Mitogen-activated protein kinase
MCI	Mild cognitive impairment
MHC-II	Major histocompatibility complex II
MLK3	Mixed lineage kinase 3
NDs	Neurodegenerative diseases
Neh	Nrf2-ECH homology
NF-κB	Nuclear factor kappa-light-chain-enhancer of activated B cells
NLRP3	NLR Family Pyrin Domain Containing 3
NO	Nitric oxide
Nrf2	Nuclear factor erythroid 2-related factor 2
PD	Parkinson’s disease
PI3K	Phosphoinositide 3-kinase
P-tau	Hyperphosphorylated tau
RNS	Reactive nitrogen species
ROS	Reactive oxygen species
SIM-A9	Spontaneously immortalized microglia, clone A9
sMaf	Small masculoaponeurotic fibrosarcoma

SOD1	Cu/Zn superoxide dismutase
STAT3/5	Signal transducer and activator of transcription 3/5
TGFBR1	Transforming growth factor beta receptor 1
TLR	Toll-like receptor
Tmem119	Transmembrane Protein 119
TNF-α	Tumor necrosis factor-α
Ym1	Chitinase-like protein 3

1. INTRODUCTION AND LITERATURE REVIEW

1.1. Neuroinflammation: what's in a name?

Neuroinflammation is the inflammatory response occurring in the central nervous system (CNS) following any number of stimuli, benign or pernicious (DiSabato et al., 2016). Primarily mediated by CNS-resident glia, inflammation within the brain or spinal cord is fundamentally beneficial and essential to homeostatic neurophysiology. However, uncontrolled chronic inflammatory responses are essentially maladaptive and conducive to extensive CNS damage that can very well go as far as engendering neuronal degeneration (Chitnis & Weiner, 2017; DiSabato et al., 2016). Physiological changes associated with old age such as cellular senescence and build-up of cellular debris result in age-linked parainflammation, a chronic inflammatory phenomenon that has been recognized well enough to receive its own name, "inflammaging" (M. Chen & Xu, 2015; Walker, 2019). A growing body of evidence suggests that neuroinflammation is an integral component of neurodegenerative diseases (NDs) such as Alzheimer's disease (AD), Parkinson's disease (PD), amyotrophic lateral sclerosis (ALS), and frontotemporal lobar dementia (FTD) (Guzman-Martinez et al., 2019; H. S. Kwon & Koh, 2020; Ransohoff, 2016). According to a news feature published in Nature in 2018 (Abbott, 2018), four of eight drug-discovery projects sponsored by the British Dementia Consortium sought to tackle neuroinflammation. Moreover, several patents relating to CNS inflammation-targeting pharmaceuticals have been filed and it is anticipated that an upswing of clinical trials will soon be seen, according to Martin Hofmann-Apitius of the Fraunhofer Institute, who specializes in pharmaceutical research (Abbott, 2018). It is as early as the 1990s that inflammation was being linked to neurodegeneration; epidemiological data even showed that individuals on anti-inflammatory therapy for conditions such as rheumatoid arthritis were less likely to develop Alzheimer's disease than was the general population (Chou et al., 2016; Judge et al., 2017; Newby et al., 2020). According to Streit and associates, "*The term neuroinflammation has come to denote chronic, CNS-specific, inflammation-like glial responses that do not reproduce the classic characteristics of inflammation in the periphery but that may engender neurodegenerative events; including plaque formation, dystrophic neurite growth, and excessive tau phosphorylation*" (Streit et al., 2004). As such, neuroinflammation is increasingly becoming acknowledged as intrinsic to NDs, a group of pathologies that had not been previously thought of

as essentially inflammatory. Moreover, emerging evidence suggests that neuroinflammation has a causal role in neurodegenerative pathophysiology (Guzman-Martinez et al., 2019; Morales et al., 2016). Such departure from classical views was occasioned by a better-informed understanding of microglial neurobiology and awareness of the fact that the events accompanying microglial activation rise above the classical notion of "reactive gliosis", which entails a passive glial response rather than the "take-charge" role microglia assume and which is inherent to the activation paradigm hereunder explained. Presently, microglia constitute the focus of neuroimmunology as corroborated by Graebera and colleagues, who thought that "*microglia are of greatest interest in the context of neuroimmunology*" (Manuel B. Graeber et al., 2011), and in turn, neuroinflammation (Streit et al., 2004).

1.2. Microglia: the brain's front battalion

Microglia are immunocompetent cells of the monocyte lineage and the resident macrophages of the CNS (Streit, 2002). Microglia arise from yolk-sac-derived erythromyeloid precursors (EMPs) during primitive hematopoiesis, as demonstrated by fate-mapping studies (Perdiguero et al., 2015). EMPs colonize the brain *in utero,* around 8.5 days post-fertilization in mice and as early as 13 weeks of gestation in humans, before the completion of vasculature arborization and the formation of the blood-brain barrier (BBB) (Z. Chen & Trapp, 2016; Perdiguero et al., 2015). EMPs then differentiate into microglia, which maintain their population by self-renewal throughout an individual's lifespan (Ajami et al., 2007); such self-maintenance without any hematopoietic input may suggest that microglia are particularly vulnerable to aging and degeneration (Ginhoux et al., 2010; Lenz & Nelson, 2018), which has enormous bearing on the thesis of this study. Microglia make up to 16% of the total cellular population in the CNS in humans and up to 12% in rodents (Norden & Godbout, 2013).

Microglia, the only true parenchymal macrophages, serve as the front line of defense in the face of any incursion against the CNS (Q. Li & Barres, 2017). Through a repertoire of specialized surface receptors, they recognize potential insults to the CNS and initiate an immune response for the elimination of the causative noxious agent (Yin et al., 2017). Beyond their immunoregulatory role, microglia are integral to normal development of the CNS and its lifelong maintenance

thereafter (Erblich et al., 2011; Hoshiko et al., 2012; Michell-Robinson et al., 2015; Schafer et al., 2012; Squarzoni et al., 2014; Ueno et al., 2013). During development, microglia keep neurogenesis in check by phagocytosing neural precursor cells to prevent the overproduction of neurons beyond the requirement of the cerebral cortex (Cunningham et al., 2013). They also postnatally carry out synaptic pruning to clear superfluous excitatory synapses (Hong et al., 2016; Paolicelli et al., 2011). Their housekeeping role also involves synaptic remodeling (Y. Wu et al., 2015), maintenance of myelin homeostasis (Hagemeyer et al., 2017), and clearing up of debris and dead cells (Herzog et al., 2019; Neumann et al., 2009; Petersen & Dailey, 2004). Dysregulation of these housekeeping functions may thus have neurodegenerative implications.

Microglia populate the brain in microdomains forming a mosaic, grid-like network, which makes them ideally distributed to effectively carry out their functions (Beggs & Salter, 2016). Microglia have been thought to be idle bystanders in health. This postulation has long been invalidated. In their "surveillance" state, microglia project numerous ramified and highly motile processes that constantly extend and retract at a rate of 2.5 μm-1.5 mm/min, continuously sampling their local microenvironment to monitor for and promptly combat any dyshomeostasis (Nimmerjahn et al., 2005; Peri & Nüsslein-Volhard, 2008; Svahn et al., 2013). Therefore, the common terminologies of "resting microglia" or "quiescent microglia" for this microglial subset should be recognized as misnomers (Hanisch & Kettenmann, 2007; Thompson & Tsirka, 2017). These glial sentinels have an elaborate sensome, made up of around 100 genes thanks to which, such surveillant role is possible (Lively & Schlichter, 2018). If and when an aggravating stimulus is encountered, microglia assume an "activated state", which is characterized by several phenotypic changes (Leyh et al., 2021). Activated microglia undergo cytoskeletal rearrangements and exhibit an amoeboid morphology with a hypertrophic cyton and retracted processes (Doorn et al., 2014). Activated microglia have also been demonstrated to display multi-nucleated, rod, epithelioid and dystrophic morphologies (Boche et al., 2013). Microglia have a very low threshold of activation and such activation occurs within only a few min of exposure to the noxious stimulus (Shinozaki et al., 2014). Microglial activation is normally transient and the cells revert back to the surveillant state once the inciting stimulus has been resolved (Perry & Teeling, 2013).

A model describing macrophage activation as distinctive polarization states has been adopted over two decades ago (Mills et al., 2000). Such polarization paradigm recognizes a proinflammatory state of macrophages that has been labelled “M1” and an anti-inflammatory state known as “M2” (Yunna et al., 2020). According to this paradigm, proinflammatory M1 macrophages can be induced by bacterial lipopolysaccharide (LPS), peptidoglycan or interferon-gamma (IFN-γ) (K. Ma et al., 2019). They exhibit increased expression of integrins (CD11b, CD11c) (Kamphuis et al., 2016; Ladeby et al., 2005; A Roy et al., 2008), major histocompatibility complex II (MHC-II) (Jurga et al., 2020), Fc receptors (Okun et al., 2010; Peress et al., 1993; Song et al., 2002, 2004) as well as co-stimulatory molecules (CD68, CD86, CD36) and are characterized by the production of nitric oxide through stimulation of inducible nitric oxide synthase (iNOS) (Brown, 2007). Microglia generate reactive oxygen and nitrogen species in addition to a range of chemokines such as C-C motif chemokine 22 (CCL22) and proinflammatory cytokines, e.g., tumor necrosis factor-α (TNF-α), interleukin-1 beta (IL-1β), and interleukin-6 (IL-6) (Akiyama et al., 2000; Varnum & Ikezu, 2012). M2 macrophages, on the other hand, work to counteract inflammation. They manifest an upregulation of arginase 1 (ARG1) (Akiyama et al., 2000), produce growth factors such as colony stimulating factor 1 (CSF1), anti-inflammatory mediators viz. interleukin-4 (IL-4), interleukin-10 (IL-10) (Lyons et al., 2007; Nolan et al., 2005), found in inflammatory zone 1 (FIZZ1), extracellular matrix-binding lectins, namely chitinase-like protein 3 (Ym1) (Raes, Baetselier, et al., 2002; Raes, Noël, et al., 2002) and neurotrophic factors like glial cell-derived neurotrophic factor (GDNF), and brain-derived neurotrophic factor (BDNF). Under the M1/M2 paradigm, microglia are surmised to exist in a neutral M0 state to physiologically maintain a balance between both activation states. However, in disease, this balance is conjectured to be skewed, favoring one activation state over the other. That being said, attempts to define a clear-cut M1 or M2 signature have failed and, recently, the M1/M2 dichotomy – which may stand *in vitro* – has been widely debunked and rejected as way too simplistic to describe a much more complex and graded spectrum of microglial phenotypes *in vivo* (Bachiller et al., 2018; Biase et al., 2017; Keren-Shaul et al., 2017).

To bring the above into perspective, the heterogeneity of microglial phenotypes can be observed with any single anatomical brain region; even in very close proximity, microglia can show disparate transcriptomic signatures which weighs in on their functional role and characteristics

(Bachiller et al., 2018; Jiang-Shieh et al., 2003; C. H. Wu et al., 1997). Such heterogeneity of activation profiles is especially significant in NDs, where variegation of the transcriptional landscape proportionally correlate with disease progression (Bachiller et al., 2018). This *in vivo* complexity partially derives from the perpetual and reciprocal interaction of microglia with other components of the CNS (Colton, 2009; D. Morgan et al., 2005). Additionally, M1/M2 assumptions made about peripheral macrophages may not translate to microglia, given their distinctive developmental origin and the versatility of their function compared to peripheral macrophages (Jurga et al., 2020; Q. Li & Barres, 2017). Microglial phenotypes are thus plastic and the use of the M1/M2 nomenclature will therefore be limited throughout the remainder of the text.

Drawing on the neuroinflammatory nature of dementias, it is worth mentioning that dysregulated activation of microglia is indeed a common pathological feature of NDs. Even in the early depictions sketched by Alois Alzheimer, microglia feature abundantly alongside neurons, proximal to regions were the prototypical plaques and tangles were depicted (M.B. Graeber et al., 1997; Hemonnot et al., 2019; Stelzmann et al., 1995). Post-mortem reports provided credence to these early sketches by showing microglia gathering around plaques and in degenerating brain regions (Hemonnot et al., 2019). Moreover, proinflammatory cytokines were found in the cerebrospinal fluid of AD patients (X. Chen et al., 2018; Llano et al., 2012).

In the context of their study of AD pathophysiology, Heneka and colleagues found that activated microglia eliminate remnants of inflammasomes (cytosolic protein oligomers of innate immunity orchestrating the activation of the inflammatory response) in the form of minuscule lumps (Venegas et al., 2017). These flecks go on to seed further amyloidopathy, spreading the disease across the brain. Heneka labelled this phenomenon as “the perfect storm”, given the findings proving that toxic amyloid-β (Aβ) incites inflammation, which foments the formation of further toxic Aβ. Surprisingly, knocking out NLR Family Pyrin Domain Containing 3 (NLRP3) – the gene encoding the NLRP3 protein, a major component of inflammasomes – was neuroprotective in AD murine models (Heneka et al., 2012).

Therefore, contrary to linear models suggesting precedence of neuroinflammation to neuronal degeneration – on grounds of its detrimental effects and the disease-spreading capacity of

microglial cells – and to simple “cause and effect” constructs attesting to the initiation of neuroinflammation subsequent of neurodegeneration, the chronic nature of neurodegenerative proteopathies entails intricate feedback loops and complex, bilateral neuron-glia interactions .

Notwithstanding evidence supporting a pathophysiological non-linearity, there still exist other likewise well-grounded views that support a more directional progress of events. To provide an instance, one accepted model outlining a sequence of events for AD gives precedence to Aβ accumulation, which in turn instigates microglial activation (Hickman et al., 2018). Activated microglia subsequently engender the hyperphosphorylation of tau and the consequent emergence of neurofibrillary tangles (D. C. Lee et al., 2010; Yoshiyama et al., 2007), which eventually leads to neurodegeneration and ensuing cognitive impairment (Hickman et al., 2018).

For all the above-outlined, whether microglia should be triggered or subdued for a beneficial clinical outcome remains debatable. It is true that microglia can go rogue, overreacting to proteopathic stimuli in desperate attempts to up their game. These subsets overproduce inflammatory signals, regurgitate phagocytosed toxic proteins that seed new plaques and tangles and mistakenly flag synapses for destruction, which altogether contribute to furthering neurodegeneration. Nonetheless, given the heterogeneity of microglial phenotypes, the diverse roles they play in different stages of disease and the slew of studies showing microglia clearing away toxic protein forms and protecting neurites from destruction; finetuning the microglial response and working to enrich innocuous subsets is increasingly being pursued and regarded as meritorious. As a general framework, while neuroprotective in the earlier stages of disease, microglia shift to a neurotoxic phenotype as the disease progresses (Onuska, 2020).

1.3. The GSK3/Nrf2/NF-κB signaling network in neuroinflammation

Within a fairly complex signaling circuitry, glycogen synthase kinase 3 (GSK3), nuclear factor erythroid 2-related factor 2 (Nrf2) and nuclear factor kappa-light-chain-enhancer of activated B cells (NF-κB) constitute a particularly important regulatory loop in neuroinflammation and NDs (Bianca Marchetti, 2020). In the context of Parkinson’s disease for instance, one group put forth

multiple reports suggesting a signaling cooperativity between the Nrf2/ARE pathway and the Wnt/β-catenin pathway, of which GSK3 is a central regulator. The convergence of these two axes was recognized as consequential to glial-mediated inflammation, aging and neuronal degeneration and – when properly regulated – conducive to promoting cellular survival, regenerative and anti-aging molecular programs (Harvey & Marchetti, 2014; L'episcopo et al., 2011; L'Episcopo et al., 2010, 2012, 2013, 2014; B Marchetti & Pluchino, 2013). Crosstalk between GSK3 and NF-κB as well as NF-κB and Nrf2 has been corroborated and evinced to actively affect cellular inflammatory programs and modulate degenerative subcellular events. To outline the framework of the study at hand and present the molecular paradigm after which this work was designed, each of the above mediators shall be hereunder discussed in detail in relation to the other players.

1.3.1. Nuclear factor erythroid 2-related factor 2 (Nrf2)

Nuclear factor erythroid 2 [NF-E2]-Related Factor 2 (Nfe2l2 or Nrf2) is a basic-region leucine zipper (bZIP) transcription factor discovered in 1994, belonging to the cap "n" collar (CNC) subfamily (Moi et al., 1994). Nrf2 is the principal regulator of the cellular response against oxidative stress by oxidants, electrophiles, and inflammatory agents (Q. Ma, 2013; Silva-Islas & Maldonado, 2018; Tummala et al., 2016). More than 250 cytoprotective genes are regulated by Nrf2 (Hayes & Dinkova-Kostova, 2014); these genes encode a myriad of vital enzymes involved in biotransformation of endo- and xenobiotics, NADPH regeneration, lipid and heme catabolism, detoxification of reactive oxygen species (ROS), among others (Cuadrado, Manda, et al., 2018; Tonelli et al., 2018). Beyond its role in regulating antioxidant responses, Nrf2 has also been reported to modulate mitochondrial bioenergetics (Holmström et al., 2013) and mitigate the unfolded protein response (Meakin et al., 2014; M. Wang & Kaufman, 2014).

Nrf2 is a multidomain protein comprised of seven Nrf2-ECH homology modules (Neh1–Neh7), each with distinctive features and functions (Itoh et al., 1999; H. Wang et al., 2013) (Figure 1.1). The DNA-binding CNC-bZIP domain is represented in the Neh1 module of the protein (Itoh et al., 1999). The sequence of this domain, particularly its basic region, is evolutionarily conserved, signifying its importance to the transcriptional activity of Nrf2 (Fuse & Kobayashi, 2017). The DLG and ETGE motifs, nested within the Neh2 domain, are two other largely conserved stretches

of the protein (Tong et al., 2006). These motifs are essential for the interaction of Nrf2 with its primary negative regulator, Kelch-like ECH-associated protein 1 (Keap1) (Itoh et al., 1999; McMahon et al., 2003; Tong et al., 2006). The Neh2 module also contains seven lysine residues between the DLG and ETGE motifs, which also have important regulatory roles (D. D. Zhang et al., 2004). The Neh3 module at the C-terminus, along with Neh4 and Neh5, constitute the transactivation domains of Nrf2 and cooperatively function to mediate the transcription of its target genes (Katoh et al., 2001; Nioi et al., 2005). The Neh6 module harbors two serine-rich motifs, DSGIS and DSAPGS, which play a central role in GSK3-mediated Keap1-independent regulation of Nrf2 (Chowdhry et al., 2012).

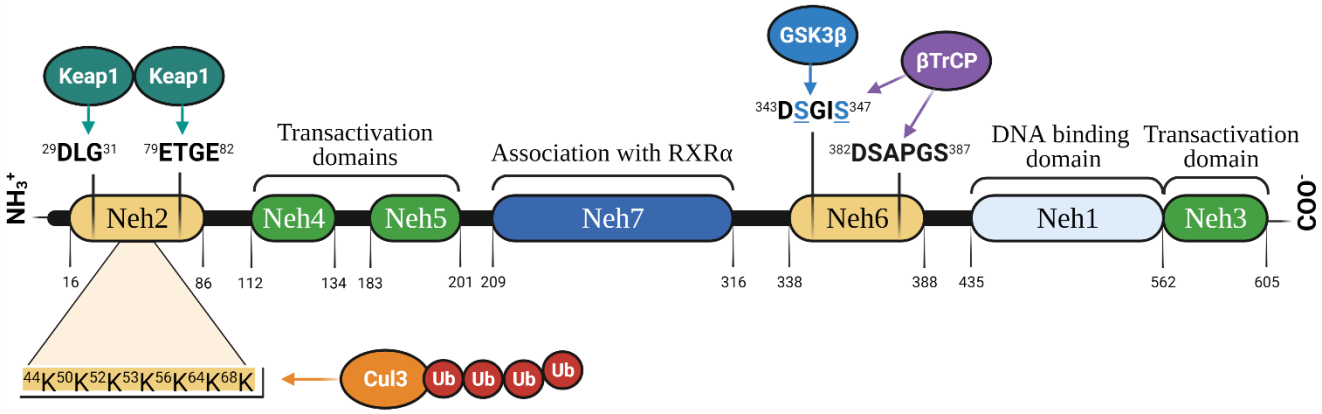

Figure 1.1. Structure of Nrf2 protein. The Nrf2 protein is composed of 7 Nrf2-ECH homolog (Neh) domains (Neh1-Neh7). Both Neh2 and Neh6 are degron domains. The Neh2 domain is located at the N-terminus of the Nrf2 protein; it harbors the DLG and ETGE motifs that are recognized by the E3 ligase adaptor, Keap1. The Nrf2-bound Keap1 homodimer presents Nrf2 to the CUL3/RBX1 complex which ubiquitinates seven lysine residues between the DLG and ETGE motifs (K44, K50, K52, K53, K56, K64, K68) marking the protein for proteosomal degradation. The Neh6 domain features the DSGIS and DSAPGS motifs which are recognized by the E3 ligase adaptor β-TrCP and, once bound, the CUL1/RBX1 complex is recruited for ubiquitination of Nrf2 and its degradation by the proteosome. Nrf2 recognition by β-TrCP requires prior phosphorylation by GSK3β at S344 and S347 residues (colored in blue) of the DSGIS motif. Neh3, Neh4 and Neh5 are all transactivation domains. The Neh1 module is the DNA-binding domain; it associates with small Maf proteins and other transcription factors to initiate the transcription of ARE genes. Direct interaction between the retinoid X receptor and the Neh7 domain mediates the repression of Nrf2 transcriptional activity. Created with BioRender.com.

The abundance and transcriptional activity of Nrf2 are rigorously regulated on the DNA, RNA and protein levels. Herein, only regulation by protein stabilization is outlined, given its relevance to the premise of the proposed work.

Nrf2 is primarily stabilized in the cytoplasm by Keap1, an adaptor for substrates of the E3 ubiquitin ligase complex, Cullin 3 and RING-box protein 1 (CUL3/RBX1) (A. Kobayashi et al., 2004).

Keap1 is a redox sensor and functions as a negative regulator of Nrf2 in absence of electrophilic stimuli (Cullinan et al., 2004; Furukawa & Xiong, 2005; A. Kobayashi et al., 2004; D. D. Zhang et al., 2004). In absence of such stimuli, Keap1 binds the DLG and ETGE motifs of Neh2 through the Kelch motif in its beta propeller domain, whereby Nrf2 is marked for ubiquitination by CUL3/RBX1 and its proteasomal degradation is subsequently initiated (Baird et al., 2014; Dinkova-Kostova et al., 2002; Itoh et al., 2003; Levonen et al., 2004). Given the short half-life of Nrf2 (10-30 min) and its rapid turnover by Keap1, the basal levels of Nrf2 are minimal (Tonelli et al., 2018). Oxidative stress stimulates the detachment of Keap1 from Nrf2, where reactive cysteines in the former are particularly sensitive to oxidation by free radicals/electrophiles and their modification lends to a conformational change of the negative regulator and its dissociation from Nrf2 (Cuadrado, Manda, et al., 2018; Silva-Islas & Maldonado, 2018; Tonelli et al., 2018; D. D. Zhang & Hannink, 2003). Consequently, Nrf2 is free to translocate to the nucleus, where it heterodimerizes with small masculoaponeurotic fibrosarcoma (sMaf) proteins (MafF, MafG and MafK) (W. Li et al., 2008; Motohashi et al., 2002), binds to the antioxidant response element (ARE; 5′-TGACXXXGC-3′) within the promoter regions of its target antioxidant genes and initiates their transcription (Friling et al., 1992; Rushmore et al., 1991; Telakowski-Hopkins et al., 1988).

An alternative ubiquitination-dependent regulatory mechanism hinges on the phosphorylation of serine residues within the DSGIS motif of Neh6 by GSK3β, which presents Nrf2 to the substrate recognition adaptor, β-transducing repeat-containing protein (β-TrCP) (Rada et al., 2011). CUL1/RBX1 ubiquitin ligase complex is recruited to β-TrCP-bound Nrf2, initiating a Keap1-independent mode of Nrf2 proteosomal degradation (Rada et al., 2011). Both canonical and non-canonical Nrf2 regulatory pathways are illustrated in Figure 1.2.

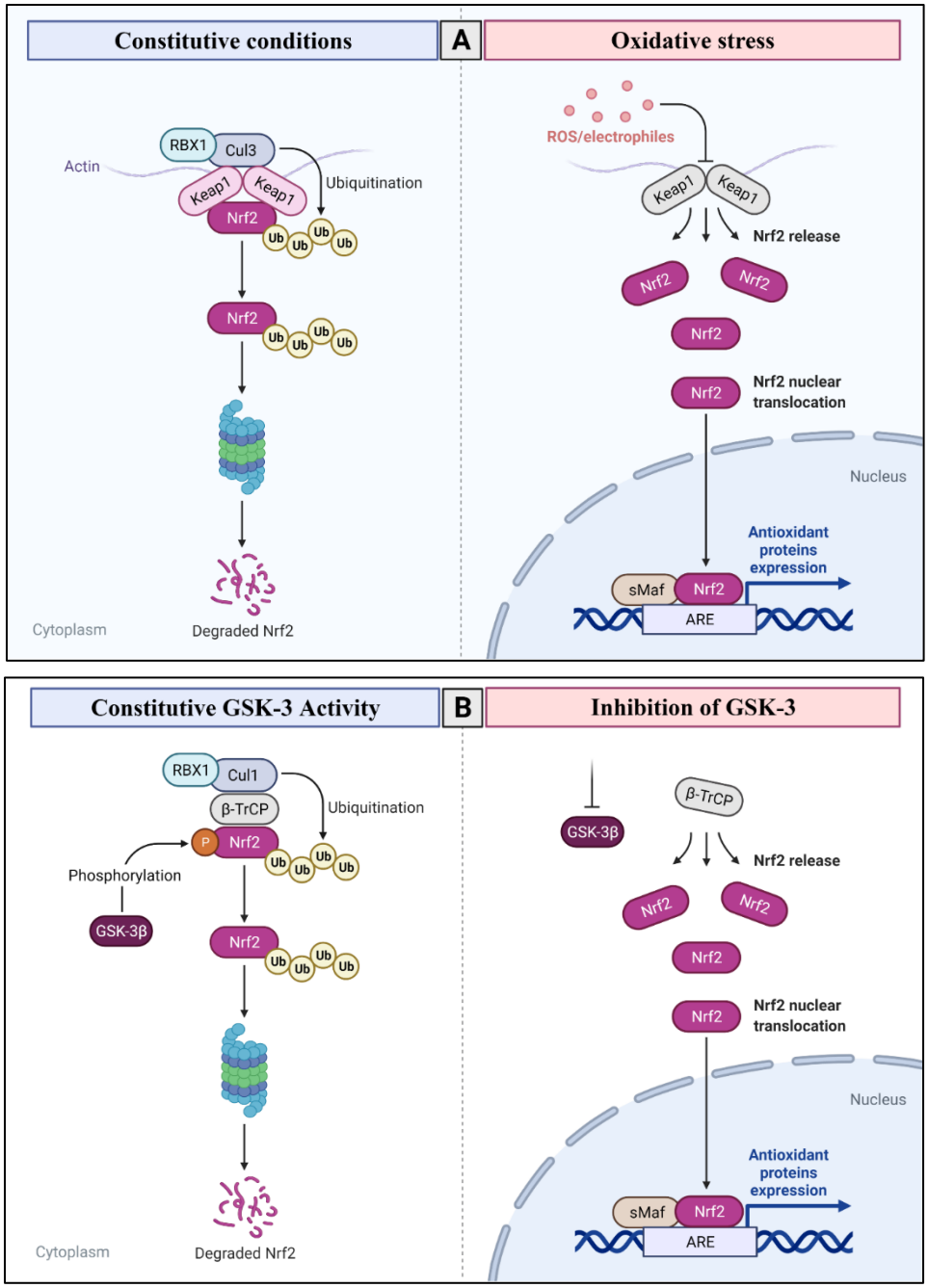

Figure 1.2. Regulation of Nrf2 activity: *A. Canonical Nrf2/ARE pathway*: In resting conditions, Nrf2 is kept in the cytosolic compartment by the homodimeric adaptor protein Keap1, which binds the DLG and the ETGE motifs of the Neh2 domain of Nrf2. As a result, Nrf2 is recognized by the Cul3/RX1 complex, which ubiquitinates several ubiquitin acceptor lysine residues in between the Keap1-interfacing motifs, marking Nrf2 for proteosomal degradation. In conditions of oxidative stress, free radicals or electrophilic agents oxidize reactive cysteine residues within the BTB domain of Keap1, causing its detachment from Nrf2, which then becomes free to translocate to the nuclear compartment, where it binds sMAF proteins, initiating the transcription of ARE genes. *B. Non-canonical regulation*: GSK3β constitutively phosphorylates key serine residues within the DSGIS motif of the Nrf2 Neh6 module, priming its recognition by β-TrCP. Once bound by β-TrCP, Nrf2 can be ubiquitinated by the Cul1/RBX1 complex and shipped off to the proteosome for degradation. Inhibition of GSK3β precludes the priming phosphorylation event that initiates the degradative cascade, ultimately resulting in enhanced nuclear entry. Created with BioRender.com.

1.2.1.1. Nrf2 in neuronal degeneration

Dysregulation of Nrf2 has been linked to NDs such as AD, PD, ALS, multiple sclerosis, Huntington's disease (HD), and Friedreich's ataxia (Dinkova-Kostova et al., 2018; Johnson & Johnson, 2015; Yang et al., 2015). Generally, chronic and aging-related diseases often entail low-grade cellular stress (Calder et al., 2017; Sanada et al., 2018), which is distinctly characterized by the formation of free radicals and ROS as byproducts of cellular processes in the mitochondria, endoplasmic reticulum and peroxisomes and occurs as a consequence of dysregulated homeostatic mechanisms (Zuo et al., 2019). At exaggerated levels, these oxidative/electrophilic entities can seriously damage vital biomolecules (Rahal et al., 2014). Conforming to the oxidative paradigm of aging, an age-associated exacerbation of cerebral oxidative damage has been recurrently demonstrated (Kumar et al., 2012; Yamazaki et al., 2015).

A study of the fatal Hutchinson-Gilford progeria syndrome (HGPS), which is essentially a premature aging condition, embroiled mislocalized Nrf2 in the HGPS-characteristic accelerated cellular senescence that was consequent of persistent oxidative stress. Progerin, a mutant structural protein of the nucleus, was found to sequestrate Nrf2 resulting in the latter's subnuclear localization and failure to initiate its antioxidative transcriptional program. These events were reiterated in HGPS progeroid fibroblasts in which Nrf2 was silenced, whereas gain-of-function experiments abrogated these changes (Kubben et al., 2016).

Several accounts convey the finding that Nrf2 is downregulated in AD brains (Carvalho et al., 2015; Kanninen et al., 2008; Y. Liu et al., 2016; Manczak et al., 2018). Indeed, Nrf2 ablation aggravated AD-like pathology in APP/PS1 transgenic (AT) mice (Ren et al., 2020). Of pertinence to the current report, a study published in *Alzheimer's Research & Therapy* last year suggests that Nrf2 activation through the PI3K/Akt/GSK3 axis checks the Aβ-mediated neuronal damage, ameliorates mitochondrial function and reverses deleterious amyloidopathy-associated metabolic changes (Sotolongo et al., 2020). Another study published earlier also presented evidence that the GSK3β/Nrf2 signaling loop is integral to salvaging hippocampal cultures against Aβ detrimental effects (Zou et al., 2012). A direct connection between Nrf2 and Aβ was elsewhere underscored, directly implicating Aβ in the dysregulation of the Nrf2/ARE pathway and the dysfunction of the

antioxidant response to pathogenic amyloid deposition (Simoni et al., 2017). Further evidence showed that Nrf2 suppresses Beta-secretase 1 (BACE1), the rate-limiting enzyme catalyzing the formation of Aβ (Bahn et al., 2019). As a matter of fact, quite a few studies reported a modulation of amyloidopathy via increased Nrf2 transcriptional activity (Dong et al., 2020; S. Kwon et al., 2015; H. Yu et al., 2019).

Protective Nrf2 upregulation correlated with synucleinopathy in PD patients (Petrillo et al., 2020), while stereotactic delivery of a Nrf2 activator rescued nigral dopaminergic neurons and relieved gliosis in mice (Lastres-BeckerIsabel et al., 2016). Additionally, activation of the Nrf2/ARE signaling blocked neurotoxicity induced by 6-hydroxydopamine (6-OHDA) in SH-SY5Y neuroblastoma cells (Lou et al., 2014) and rat organotypic nigrostriatal cocultures (Siebert et al., 2009) and mitigated striatal oxidative stress as well as degeneration of dopaminergic neurons in a 6-OHDA murine model of PD (Lou et al., 2014). Elsewhere, a meta-analysis utilizing microarray data from PD and AD patients identified 31 ARE transcriptionally repressed genes (Q. Wang et al., 2017). Moreover, the murine AT-Nrf2 knockout model, which lacks Nrf2 while featuring coincident tauopathy and amyloidopathy exhibited upregulated markers of neuroinflammation and oxidative stress when compared to AT-Nrf2 wild type mice (Rojo et al., 2017).

A murine model of ALS bearing the H46R mutant of the Cu/Zn superoxide dismutase (SOD1) gene retained locomotive functions and displayed a protracted post-onset disease evolvement, following pharmacologically induced Nrf2 activation (Kanno et al., 2012). NSC-34 cells harboring an exogenously introduced G93A mutation of the SOD1 gene displayed shorter and fewer neurites and rounded soma; these changes were correlated with the dysregulation of Nrf2/ARE signaling (F. Wang et al., 2014). Furthermore, *in vivo* overexpression of Nrf2 in astrocytes carrying a SOD1 mutation rescued these cells and resulted in increased production of glutathione, which protected motor neurons, deferred disease onset and made for better survival rates (Vargas et al., 2008). What's more, Nrf2 activation is a well-established modulatory therapy in MS. Dimethyl fumarate (DMF), marketed under the brand name Tecfidera®, has been a licensed oral therapy for relapsing remitting MS since 2013 (Brandes & Gray, 2020).

Overall, and taking the collective body of literature into account, the multitude of evidence that support a neuroprotective role for Nrf2 in Alzheimer's disease (Bahn et al., 2019; Dong et al., 2020; Kerr et al., 2017; Ren et al., 2020; Uruno et al., 2020), Parkinson's disease (Alarcón-Aguilar et al., 2014; Barone et al., 2011; P.-C. Chen et al., 2009; Jazwa et al., 2011; Williamson et al., 2012), Huntington's disease (Jimenez-Sanchez et al., 2017; Prasad & Bondy, 2016; Quinti et al., 2017; van Roon-Mom et al., 2008), multiple sclerosis (Gopal et al., 2017; Owyang et al., 2016), among others can hardly be refuted.

1.2.1.1. Nrf2 in neuroinflammation

Not only does Nrf2 contribute to shielding against degenerative events of neuronal origin, but it also mediates a similar homeostatic function to sustain a balanced microglial activation profile, which – as thoroughly explained above – is essential to the overall neural harmony and imperative for foreclosing neuroinflammatory events associated with both pro-neurodegenerative and post-neurodegeneration pathologenic processes. Attenuation of LPS-stimulated microglial inflammatory response has been observed following phytochemically induced Nrf2 activation, as evident by the diminution of the levels of proinflammatory cytokines (IL-1β, IL-6, TNF-α) and other inflammatory mediators (NO and COX-2) (Townsend & Johnson, 2016; Velagapudi et al., 2017, 2018; Zheng et al., 2019; Y. Zhou et al., 2019). Nrf2 modulation by a panel of small molecules produced similar outcomes (Foresti et al., 2013). Additionally, the Nrf2/PI3K/Akt signaling circuit – noted in neurons and above acknowledged for its relevance to this study – was replicated in microglia following treatment with sulforaphane, a bona fide Nrf2 activator (Townsend & Johnson, 2016). Further drawing on the liaison between Nrf2/ARE and the PI3K/Akt pathways, transactivation of ARE genes by Nrf2 was reported to repress microgliosis via inhibition of GSK3 in an *in vivo* model of tauopathy (Lastres-Becker et al., 2014), a condition in which GSK3 is a key player. These results suggest that Nrf2 is mobilized to the nucleus and checks microglial overactivation induced by aberrant tau forms. In other pathological contexts, microglial dynamics were determined to be significantly influenced by Nrf2 modulation, where Nrf2 homozygous knockout mice displayed cognitive impairment coinciding with an augmentation of proinflammatory cytokines, curtailment of anti-inflammatory mediators and deregulation of homeostatic signatures viz. TMEM119 and TGFBR1 (Rojo et al., 2010; I.-C. I. Yu et al., 2019).

Chronic oxidative stress by prolonged cerebral hypoperfusion compromised the integrity of the BBB in white matter tracts and correlated with higher densities of microglial subsets, which was evident in $Nrf2^{+/-}$ knockouts yet extensively more significant in the loss-of-function phenotype (Sigfridsson et al., 2020).

1.3.2. Nuclear factor κ-light-chain enhancer of activated B cells (NF-κB)

Nrf2 is well integrated into a complex regulatory network with modulatory effects on many signaling cascades, as evidenced by transcription pattern analyses. One particularly relevant component of the Nrf2 interactome is nuclear factor κ-light-chain enhancer of activated B cells (NF-κB) (Ahmed et al., 2017). Inflammatory responses are aggravated by ROS and reactive nitrogen species (RNS) and involve the activation of the canonical subunit of NF-κB, p65 (M. J. Morgan & Liu, 2010; Wardyn et al., 2015). Interestingly, IKKβ, like Nrf2, also has an ETGE motif, which – under basal conditions – is recognized by Keap1 and results in the ultimate ubiquitination of IKKβ and its subsequent degradation by the proteasome (Jiang et al., 2013). An unphosphorylated IκBα inhibits NF-κB. As is the case with Nrf2, ROS mediate the deactivation of the regulatory function of Keap1, whereby IKKβ is stabilized and IκBα is phosphorylated and hence degraded, leading to an upswing of NF-κB (Napetschnig & Wu, 2013). Being the master coordinator of redox homeostasis, Nrf2 indirectly orchestrates the regulation of NF-κB; the two transcription factors crosstalk through feedback and feedforward mechanisms. To elaborate, LPS concomitantly stimulates an acute NF-κB proinflammatory response and a steady, counteracting Nrf2 response (Cuadrado et al., 2014). NF-κB induces the transcription of Nrf2 thanks to shared promoter elements (Rushworth et al., 2012). However, when Nrf2 reaches maximal levels, NF-κB is inhibited (Cuadrado et al., 2014). As such, the anti-inflammatory activity of Nrf2 was suggested to be partially attributed to its inhibition of NF-κB, as well as its transcriptional inhibition of proinflammatory genes such as the interleukins IL-1β and IL-6 (E. H. Kobayashi et al., 2016).

According to published reports, NF-κB has been implicated in the regulation of Nrf2-mediated transcription of ARE genes, although such a role has been reckoned complex and contingent on the cellular context. A number of mechanisms has been described by which the p65 subunit of NF-κB may suppress expression of ARE genes (Wardyn et al., 2015). Overexpression of p65 was

evinced to repress Nrf2/ARE signaling, where it was demonstrated to hinder the binding of Nrf2 to its cognate DNA sequence. Moreover, p65 was found to physically interact with Keap1 and mediate its nuclear translocation, which in turn facilitates Keap1-orchestrated post-induction reversal of Nrf2 activity by exporting it back to the cytosol (Sun et al., 2007; M. Yu et al., 2011). A more established mechanism by which p65 checks Nrf2 transcriptional activity entails the competition of both for the transcriptional coactivator, CREB-binding protein–p300 complex (CBP) (Wardyn et al., 2015). In a groundbreaking work by Liu and colleagues, CBP was shown to associate with the Neh4 and Neh5 transactivation domains of Nrf2. Once bound to Nrf2, CBP catalyzes the acetylation of the DNA-binding module that is Neh1, which is overall conducive to enhanced transcriptional activity. Meanwhile, CBP displays an affinity to p65 bearing a phosphorylated S276. Thereon, overabundance of p65 seems to favor the expression of NF-κB−transcribed genes and limits CBP availability to Nrf2, translating into the transcriptional arrest of ARE genes (G. H. Liu et al., 2008). The authors also indicated that p65 works to couple Histone deacetylase 3 (HDAC3) with MafK, which occasions the failure of dimerization with Nrf2 and abortion of ARE genes transcription. Beyond CBP, other modulators of Nrf2 viz. β-TrCP (Rada et al., 2011; Winston et al., 1999) and the ubiquitin-binding protein p62 (Ichimura et al., 2013; Wooten et al., 2005) seem to crosstalk with p65 as well. Perhaps most interesting is the fact that p65 is also a substrate for GSK3, which is the third player in the mechanistic loop under investigation. GSK3 is postulated to affect the DNA-binding affinity of p65 (Hoffmeister et al., 2020; Chandi C. Kandar et al., 2021; Medunjanin et al., 2016; J.-S. Zhang et al., 2014), which supports the notion that GSK3 activity translates to an inflammatory phenotype, especially when concomitantly considering its negative regulation of Nrf2. Below, GSK3, the final cog in this mechanistic machinery is discussed.

1.3.3. Glycogen Synthase Kinase 3 (GSK3)

Many kinases demonstrate an increased activity in neurological disorders; one of these especially notorious enzymes is GSK3 (Duda et al., 2018). GSK3 is a pleiotropic serine/threonine kinase that was discovered in the 1980s. It was first identified as a regulator of the enzymatic activity of the eponymous *Glycogen Synthase* (Chandi Charan Kandar et al., 2021). Almost 100 proteins have been recognized as GSK3 substrates and well beyond 500 others are being considered as putative

targets (Calum Sutherland, 2011), which in effect means that – through phosphorylation of key residues in its cognate substrates – GSK3 is entrenched in orchestrating normal cellular function and its dysregulation is invariably linked to pathophysiological events (Eleonore Beurel et al., 2015).

Of all kinases that have been shown to mediate neuropathogenic protein modifications, GSK3 is acknowledged as the principal tau-phosphorylating kinase, which led to a growing interest in GSK3 as a therapeutic target in neurodegenerative tauopathies (Avila et al., 2012; Cuadrado, Kügler, et al., 2018; G. Lee & Leugers, 2012), beyond its above-described neuroinflammatory role. GSK3 was found to mediate the phosphorylation of the majority of abnormally phosphorylated residues in AD (Hanger et al., 2009; Ramkumar et al., 2018). Seeing as tau primarily functions to stabilize the microtubule network to regulate neuronal dynamics, such anomalous hyperphosphorylation leads to tau self-assembly (Toral-Rios et al., 2020); this consequently results in lowered interaction of tau with dynein and kinesin. The ensuing destabilization of the microtubule network and the cytoskeletal instability within neuronal cells culminates in the genesis of the characteristic neurofibrillary tangles (Avila et al., 2012; Toral-Rios et al., 2020).

Back in 2005, a team from the University of Alabama in Birmingham first shed light on the proinflammatory role GSK3 plays in monocytes, where elevated GSK3 activity correlated with an upsurge of the proinflammatory cytokines TNF-α, IL-6, and IL-1β (Martin et al., 2005). Henceforth, GSK3 has been recognized as a pivotal regulator of Toll-like receptor (TLR) signaling, maintaining the balance between proinflammatory and anti-inflammatory responses, whether within the CNS or beyond (Ajmone-Cat et al., 2016). GSK3 was also proven to encourage the microglial inflammatory program, mirroring the effects observed in monocytes. GSK3 incites microglial activation and provokes overproduction of proinflammatory cytokines, chemokines and nitric oxide (NO) (Ajmone-Cat et al., 2016; Eléonore Beurel et al., 2009; Cheng et al., 2009; Yuskaitis et al., 2009). Moreover, GSK3 was found to promote microglial migration, reportedly via upregulating the complement receptor, the integrin αMβ2 and CD11b, a marker of microglial activation (Solovjov et al., 2005; Yuskaitis et al., 2009). By the same token, inhibition of GSK3 in microglia was found to correlate with attenuated NF-κB, signal transducer and activator of

transcription 3/5 (STAT3/5), p44/p42 mitogen-activated protein kinase (p44/p42 MAPK) and mixed lineage kinase 3/c-Jun N-terminal kinase 3 (MLK3/JNK) signaling (Eléonore Beurel & Jope, 2009; Koistinaho et al., 2011; M.-J. Wang et al., 2010). Such modulation of deregulated signaling is reflected in a marked drop in LPS-stimulated proinflammatory mediators (Il-1β, IL-6, TNF-α, NO), enhanced production of counteracting anti-inflammatory cytokines (e.g., IL-10), downregulation of activation markers (e.g., CD11b), and decreased *in vitro* and *in situ* microglial migration, both random and directed, by 50%-70% (Eléonore Beurel et al., 2009; Koistinaho et al., 2011; Nahman et al., 2011; Nassar & Azab, 2014; M.-J. Wang et al., 2010; Yuskaitis et al., 2009). It has been conjectured that GSK3 is mixed up in the above-described crosstalk between activated microglia and injured neurons, exacerbating neuronal loss. Some studies have gone as far as to conclude that GSK3 overactivity is a primary driver in neuroinflammation-mediated neuronal loss (D. Li et al., 2014; Yuskaitis et al., 2009), which is on top of the long-established, inflammation-independent role of GSK3 in neurodegeneration.

GSK3 is one of many kinases that require "priming" before it can carry out its function; that is, it requires its substrate to have been phosphorylated by another kinase at specific positions, namely four C-terminal residues away from the phosphorylation site (Frame & Cohen, 2001). Thus, a general consensus sequence for GSK3-mediated substrate phosphorylation is (S/T-X_1-X_2-X_3-pS/pT), where X is any amino acid (Cole et al., 2004). Despite the fact that some unprimed substrates were reported to be subject of GSK3 regulation, lack of priming is associated with 90% reduction in GSK3 activity (Calum Sutherland, 2011).

Thanks to evolutionary gene duplication events, multiple paralogs of many genes were generated. GSK3 is no exception. With a variant on chromosome 19 (GSK3A) and another on chromosome 3 (GSK3B), two protein isoforms (GSK3α and GSK3β) account for GSK3 activity in all mammals (Woodgett, 1991). Moreover, owing to alternative splicing, GSK3β may exist in two different mRNA transcripts, GSKβ1 and GSK3β2 (Wood-Kaczmar et al., 2009). The encoded kinase enzymes have overlapping yet distinct catalytic roles (Soutar et al., 2010). The catalytic domain is conserved between the two GSK3 isoforms with 98% homology (Calum Sutherland, 2011; Terwel et al., 2008). The N-terminal region is significantly different, though, with GSK3α boasting a glycine-rich extension at the N-terminus, resulting in a higher molecular weight of 51 kDa, as opposed to 47 kDa for GSK3β1 and 49 kDa for GSK3β2 (Calum Sutherland, 2011).

GSK3 activation is mediated by autophosphorylation of Y279 in GSK3α and Y216 in GSK3β (Eleonore Beurel et al., 2015), which lends to better substrate accessibility and is purportedly requisite for optimal assembly of the catalytic site during protein folding (roughly 5-fold improvement of the catalytic capacity) (Lochhead et al., 2006). A reduced GSK3 activity can sometimes be subsequent of dephosphorylation of Y279/216. The principal counteractive influence, however, is played out by inhibitory phosphorylation (Calum Sutherland, 2011). Most prominently, inhibition occurs by phosphorylation at S21 in GSK3α and S9 in GSK3β, by several kinases (Cross et al., 1995; Fang et al., 2000; Stambolic & Woodgett, 1994; C Sutherland et al., 1993). Dephosphorylation of such deactivated GSK3 is carried out by protein phosphatase PP2A, which catalyzes the removal of the deactivating phosphate groups from the abovementioned serine residues (Lauretti et al., 2020; Wagner et al., 2018).

The N-terminus of GSK3 features a negative regulatory domain as does its C-terminus; its kinase domain features the catalytic site as well as the ATP-binding domain (Calum Sutherland, 2011). Conserved lysine residues (GSK3α: K148 and K149; GSK3β: K85 and K86) within the active site were determined to mediate ATP binding and catalysis of γ-phosphate transfer to the interfacing substrate (Hoffmeister et al., 2020). However, within the hinge region of GSK3, the ATP-binding domain features a single switch of the amino acid glutamate (E196) in GSK3α to the amino acid aspartate (D133) in GSK3β, resulting in significant topological and structural disparity between the two paralogs, due to an alteration of hydrogen bonding between the enzyme domains (Wagner et al., 2018) (Figure 1.3).

A

```
GSK-3α MSGGGPSGGGPGGSGRARTSSFAEPGGGGGGGGGGGPGGSASGPGGTGGGKASVGAMGGGV  60
GSK-3β MSG------------RPRTTSFAESCK----------PVQQPSAFGSMKVS--------  29

GSK-3α GASSSGGGPSGSGGGGSGGPGAGTSFPPPGVKLGRDSGKVTTVVATVGQGPERSQEVAYT 120
GSK-3β --------------------------------RDKDGSKVTTVVATPGQGPDRPQEVSYT  57

GSK-3α DIKVIGNGSFGVVYQARLAETRELVAIKKVLQDKRFKNRELQIMRKLDHCNIVRLRYFFY 180
GSK-3β DTKVIGNGSFGVVYQAKLCDSGELVAIKKVLQDKRFKNRELQIMRKLDHCNIVRLRYFFY 117

GSK-3α SSGEKKDELYLNLVLEYVPETVYRVARHFTKAKLITPIIYIKVYMYQLFRSLAYIHSQGV 240
GSK-3β SSGEKKDEVYLNLVLDYVPETVYRVARHYSRAKQTLPVIYVKLYMYQLFRSLAYIHSFGI 177

GSK-3α CHRDIKPQNLLVDPDTAVLKLCDFGSAKQLVRGEPNVSYICSRYYRAPELIFGATDYTSS 300
GSK-3β CHRDIKPQNLLLDPDTAVLKLCDFGSAKQLVRGEPNVSYICSRYYRAPELIFGATDYTSS 237

GSK-3α IDVWSAGCVLAELLLGQPIFPGDSGVDQLVEIIKVLGTPTREQIREMNPNYTEFKFPQIK 360
GSK-3β IDVWSAGCVLAELLLGQPIFPGDSGVDQLVEIIKVLGTPTREQIREMNPNYTEFKFPQIK 297

GSK-3α AHPWTKVFKSSKTPPEAIALCSSLLEYTPSSRLSPLEACAHSFFDELRRLGAQLPNDRPL 420
GSK-3β AHPWTKVFRP-RTPPEAIALCSRLLEYTPTARLTPLEACAHSFFDELRDPNVKLPNGRDT 369

GSK-3α PPLFNFSPGELSIQPSLNAILIPPHLRSPAGPASPLTTSYNPSSQALTEAQTGQDWQPSD 480
GSK-3β PALFNFTTQELSSNPPLATILIPPHARIQAAASPPANAT------AASDTNAGDRGQTNN 423

GSK-3α ATTATLASSS 490
GSK-3β AASASASNST 433
```

B

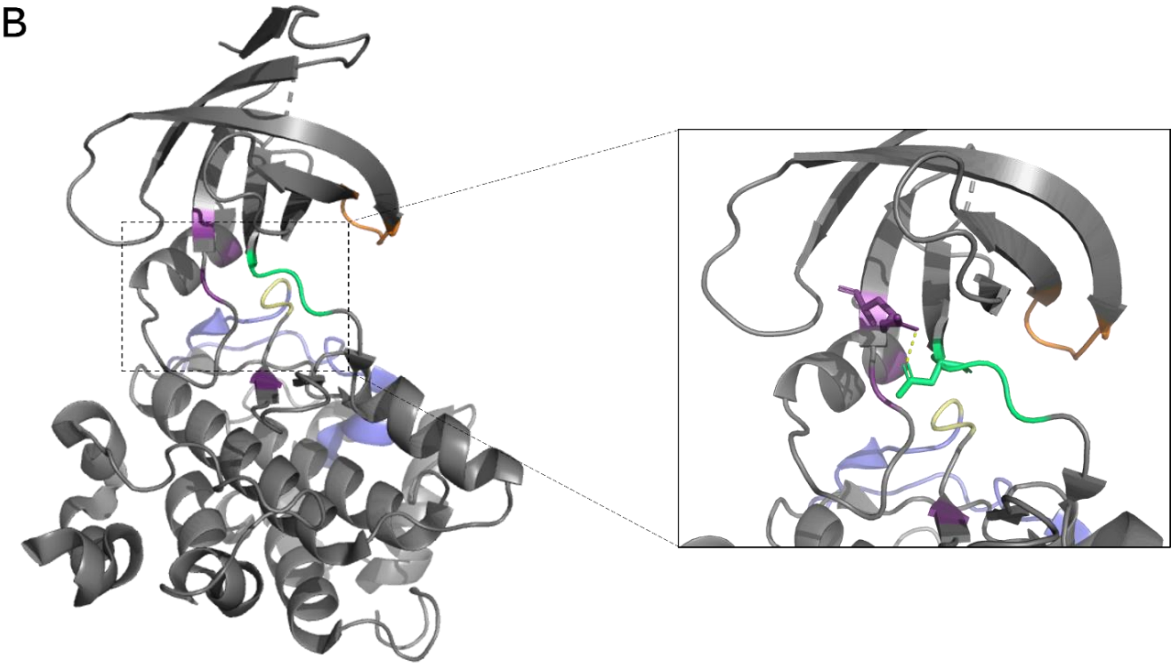

Figure 1.3. Structure of GSK3. (A) Global alignment of murine GSK3α (NP_001026837.1) and GSK3β (NP_001334161.1) proteins by the Needleman–Wunsch algorithm of NCBI Blast® online tool. Mismatches are highlighted in red. Key motifs and regions are color-coded as follows: activation loop (blue), hinge region (green), DFG motif (yellow), backend region (purple), and P-loop (orange). (B) 3D representation of GSK3β protein (PDB ID: 1I09), highlighting the different color-coded regions. In the inset, the hydrogen bonding between D133 and R113 is highlighted. The images were rendered on the PyMOL Molecular Graphics System, Version 2.5.2 Schrödinger, LLC.

Unraveling such a subtle difference between GSK3 paralogs, Wagner et al., a team from Broad Institute at Massachusetts Institute of Technology set out to exploit this single amino acid substitution and the resulting topological dissimilitude between the isoforms with the purpose of developing paralog-selective GSK3 inhibitors (Wagner et al., 2018). In context of their work on acute myeloid leukemia (AML), paralog selectivity was surmised to be a promising approach on account of the fact that GSK3α inhibition was not associated with stabilization of β-catenin as was GSK3β inhibition; the pro-malignant transcriptional activity of β-catenin is of concern in AML patients. The team thereupon developed a set of compounds with remarkable selectivity profiles. BRD0705, BRD3731 and BRD0320 (pyrazolo-tetrahydroquinolinone ATP competitive GSK3 inhibitors) were presented as GSK3α selective, GSK3β selective and GSK3α/β non-selective inhibitors, respectively. Below, each of these inhibitors is briefly introduced.

— *BRD0705*

BRD0705 (CAS No.: 2056261-41-5; Figure 1.4A) is a potent, selective GSK3α inhibitor protected in the patent US20160375006A1 held by Massachusetts Institute of Technology, Broad Institute Inc. BRD0705 displays an 8-fold selectivity for GSK3α over GSK3β, and an outstanding selectivity in a panel of 311 kinases (Scolnick et al., 2016; Wagner et al., 2018). Within a dosing range of (10-40 μM), BRD0705 hindered the kinase-activating Tyr279 autophosphorylation of GSK3α in a time-dependent manner, without affecting autophosphorylation of GSK3β at Tyr216 (Wagner et al., 2018). Inability of BRD0705 to stabilize β-catenin was confirmed by a TCF/LEF luciferase reporter assay, as communicated by Wagner and consociates at the Broad Institute.

— *BRD3731*

BRD3731 (CAS No.: 2056262-08-7; Figure 1.4B) is a potent, selective inhibitor of GSK3β, also patented by Massachusetts Institute of Technology, Broad Institute Inc, under the forenamed patent number. BRD3731 exhibits 14-fold selectivity for GSK3β versus GSK3α, as well as superb selectivity the same kinome of 311 kinases (Scolnick et al., 2016; Wagner et al., 2018). BRD3731 was shown to stabilize β-catenin in the HL-60 AML cell line, starting at a concentration of 20 uM.

It restricted the S33/37/T41 phosphorylation of β-catenin and promoted its phosphorylation at S675, resulting in its improved nuclear accumulation (Scolnick et al., 2016).

— *BRD0320*

BRD0320 (Figure 1.4C) is a non-selective pan-inhibitor of GSK3. BRD0320 displays 46-fold selectivity for GSK3 over CDK3/CycE1, the kinase to which BRD0320 exhibits highest affinity beyond GSK3, as revealed by kinome selectivity assays (Wagner et al., 2018).

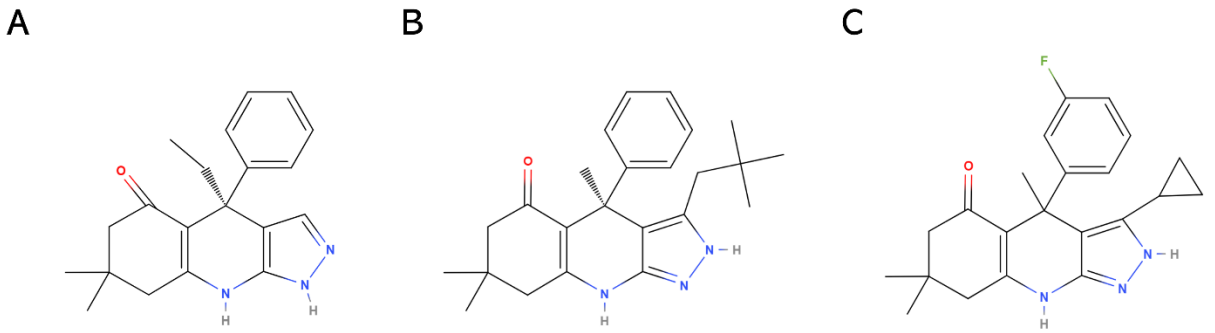

Figure 1.4. Chemical structure of BRD0705 (GSK3α inhibitor) (A), BRD3731 (GSK3β inhibitor) (B), and BRD0320 (GSK3α/β non-selective inhibitor) (C). Structures were drawn using MolView.

1.4. Rationale

In the current study, we utilize these GSK3 inhibitors to selectively inhibit GSK3 paralogs in the context of microglial activation. As hereinabove explained, GSK3 is multimodally inculpated in mediating both neuronal (proteopathic) and glial (inflammatory) etiopathogenic processes in NDs, especially tauopathies, in which GSK3 dysregulation is a primary pathophysiological feature. Given the oxidative nature of this disease group in all neural subsets, inhibition of GSK3 can entail a multimodal modulatory utility by simultaneously targeting the oxidative, inflammatory and proteopathogenic underpinnings of neurodegenerative disorders; whereby GSK3 inhibition would stunt pathological phosphorylation events associated with injurious misfolded proteins, alleviate glia-mediated neuroinflammatory processes, and mitigate oxidative damage in both neurons and neuroglia. Moreover, given its inability to initiate the pro-malignant β-catenin−driven transcriptional program, selective inhibition of GSK3α is conjectured to be particularly useful in individuals with a predisposition to developing neoplasms or actual cancer patients who are at concomitant risk of age-related proteopathies and/or neuroinflammation by dint of a family history or, for instance, patients early in the neurodegenerative disease continuum like those scoring suboptimal scores on mild cognitive impairment (MCI) tests.

1.5. Hypothesis

In light of the numerous reports outlined above, we hypothesized that inhibition of GSK3 in microglial cells should confer anti-inflammatory and antioxidant effects in microglial cells and that these effects are likely to be – at least partially – paralog-dependent. Additionally, given the corroborated crosstalk between GSK3, NF-κB and Nrf2, dysregulation of their interplay was surmised to occur under proinflammatory conditions, which was conjectured to be favorably modulated via GSK3 inhibition.

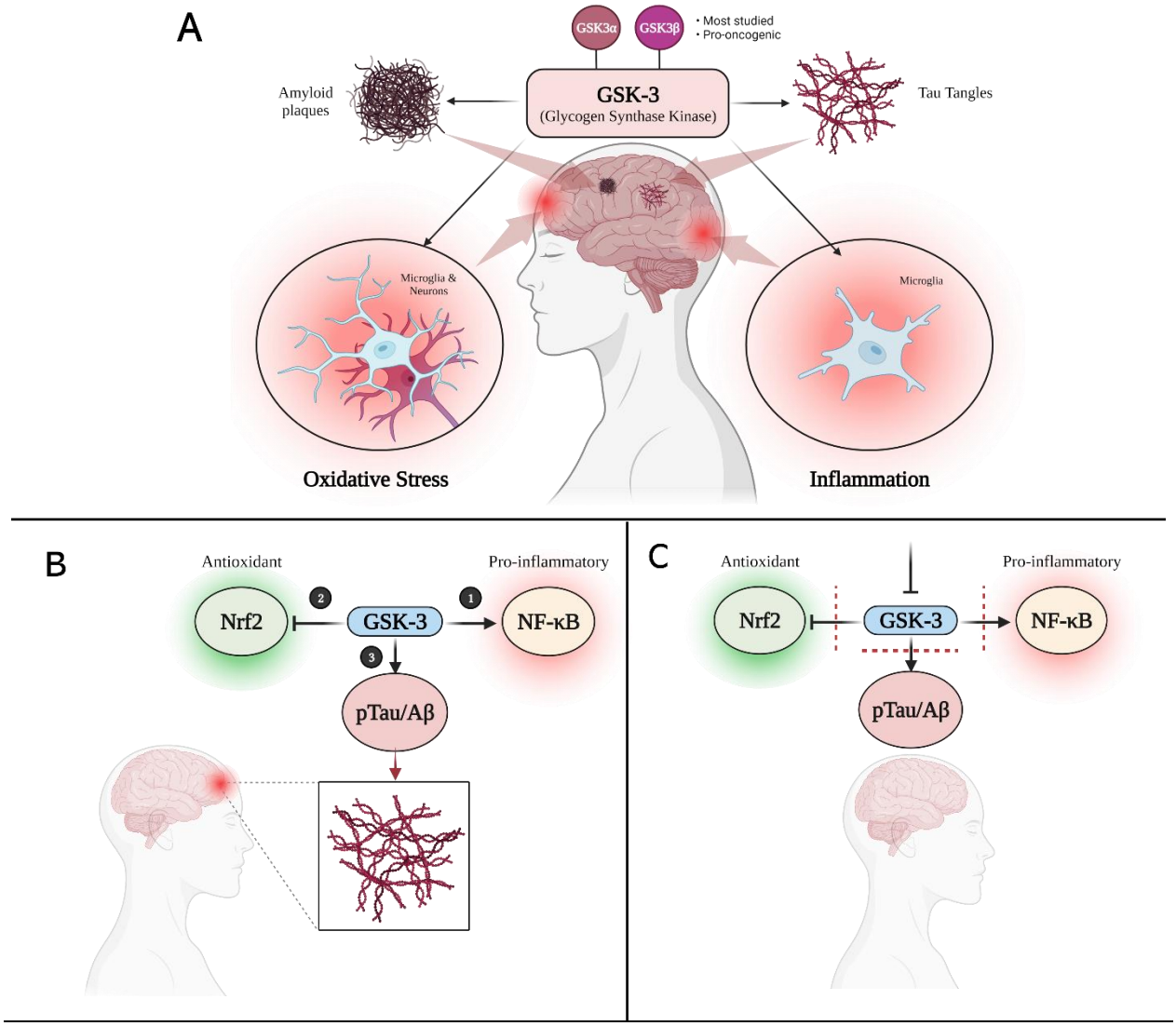

Figure 1.5. Exploiting the multimodal disease-modifying potential of the GSK3/Nrf2/NF-κB network in inflammatory degenerative disorders of the CNS. (A) GSK3 mediates several neuropathological events that converge to trigger degenerative changes in the CNS. It is involved in glial proinflammatory responses and promotes oxidative stress in disparate neural subpopulations, over and above to its infamous engagement in incentivizing proteopathologies such as tauopathy and amyloidopathy. (B) GSK3 actuates NF-κB signaling and prompts the proteosomal degradation of Nrf2. In protein pathologies characteristic of neurodegenerative diseases, GSK3 is notorious for orchestrating the pathological hyperphosphorylation of tau and encouraging the deposition of amyloid plaques. (C) Under our investigational paradigm, inhibition of GSK3 is rationalized to target multiple pathological pathways at once. On account of NF-κB suppression resultant of GSK3 inhibition, microglial activation is surmised to be mitigated. Additionally, blocking GSK3 activity is proposed to have anti-oxidative reverberations in various neural subsets, on grounds of subsequent Nrf2 activation, which should ultimately dampen the associated parainflammation. Moreover, the attenuation of GSK3 catalytic activity should preclude hyperphosphorylation of proteins and their subsequent misfolding, aggregation and deposition. Created with BioRender.com.

1.6. Objectives and aims

The overarching objective of this study is to compare the anti-inflammatory and antioxidant potential of paralog-selective inhibition of GSK3 in activated microglial cells. In order to accomplish this, a number of specific aims, outlined below, were set for experimental investigation and validation or disproval of related hypotheses.

Specific aims:

1. Comparatively examine the effects of BRD0705 (GSK3α inhibitor), BRD3731 (GSK3β inhibitor), and BRD0320 (GSK3α/β inhibitor) on modulation of the mRNA expression of the microglial activation markers CD11b and Iba1 and the proinflammatory mediators IL-1β, IL-6, TNF-α, and iNOS in LPS-activated SIM-A9 microglia via real-time qPCR.
2. Establish the ability of BRD0705 (GSK3α inhibitor), BRD3731 (GSK3β inhibitor), and BRD0320 (GSK3α/β inhibitor) to induce the mRNA expression of the Nrf2 target genes, HO-1 and Osgin1 in LPS-activated SIM-A9 microglia and discriminately evaluate the extent to which paralog-selective GSK3 inhibition correlates with Nrf2 activation.
3. Assess the effects of BRD0705 (GSK3α inhibitor), BRD3731 (GSK3β inhibitor), and BRD0320 (GSK3α/β inhibitor) on LPS-mediated induction of nitric oxide in SIM-A9 cells using the Griess method and the expression levels of the secretory proteins IL-1β, IL-6, and TNF-α using ELISA.
4. Determine the effects of BRD0705 (GSK3α inhibitor), BRD3731 (GSK3β inhibitor), and BRD0320 (GSK3α/β inhibitor) on the nuclear translocation of Nrf2, NF-κB, and β-catenin by immunoblotting of post-treatment SIM-A9 nuclear lysates.
5. Investigate whether the observed effects of BRD0705 (GSK3α inhibitor), BRD3731 (GSK3β inhibitor), and BRD0320 (GSK3α/β inhibitor) are Nrf2-dependent by employing small interfering RNA-mediated knockdown of Nrf2, followed by real-time qPCR of the abovementioned mRNA targets.

▪ *Novelty of this research*

The novelty of the proposed work can be realized in its precedence in exploring the differences between the two GSK3 isoforms. As far as we are aware, this is the first study to compare the effects of paralog-selective inhibition of GSK3. Adding another dimension to the study is the exploration of such paralog-selectivity in context of mechanistic characterization of the oxidative/microglia-mediated neuroinflammatory paradigm of neurodegenerative diseases. Moreover, this work is the first investigating these regulatory loops in SIM-A9 cells, which – as will be discussed – the closest cell line to recapitulate characteristics of primary microglial cells.

2. MATERIALS AND METHODS

2.1. Materials

The SIM-A9 murine microglial cell line (CRL-3265™) was purchased from the American Type Culture Collection (ATCC). BRD0705 (GSK3α inhibitor), BRD3731 (GSK3β inhibitor) and BRD0320 (GSK3α/β) were kindly provided by the Broad Institute, Inc (Cambridge, MA, USA) in accordance with a material transfer agreement. Sulforaphane (SFN; 10496) was purchased from Cayman Europe OÜ (Tallinn, Estonia). LPS (*Escherichia coli* O111:B4; L2630) was purchased from Sigma Chemical Co. (MO, USA). Dulbecco's Modified Eagle Medium/Nutrient Mixture F-12 Gibco™ DMEM/F-12, HEPES (31330038), Gibco™ Fetal Bovine Serum (10270106), Gibco™ Horse Serum, heat inactivated (26050070), Gibco™ DPBS, no calcium, no magnesium (14190094), Dimethyl sulfoxide DMSO (67-68-5), Chloroform (HPLC grade; C607SK-1), Isopropanol (HPLC grade; BP26324), Ethanol (HPLC grade; 64-17-5), RevertAid cDNA kit (K1621), PowerUp™ SYBR™ Green (2X) Master Mix (A25741), mRNA (CD11b, IL-6, iNOS, TNF-α, GAPDH) primers (10629186; designed by NCBI primer blast tool), Pierce™ BCA Protein Assay Kit (23225) and Pierce™ ECL Western Blotting Substrate (32106) were all acquired from ThermoFisher Scientific (MA, USA). MTT (M6494), Griess Reagent Kit (G7921), NuPAGE™ LDS Sample Buffer (NP0007), NuPAGE™ Reducing Agent (NP0009), NuPAGE™ 10%, Bis-Tris, 1.0 mm, Mini Protein Gels, 10-well (NP0301), 20X NuPAGE™ MES Running Buffer (NP0002), NF-κB p65 polyclonal antibody (PA1-186) and Blocker™ BSA (10%) in PBS (37525) were obtained from Invitrogen (CA, USA). Penicillin-Streptomycin Mixture Pen/Strep (09-757F), Phosphate Buffered Saline (10X) PBS (17-516Q) were supplied by Lonza-Bioscience (Basel, Switzerland). QiAzol lysis buffer (79306) and nuclease-free water (129114) were procured from Qiagen (Hilden, Germany). Protease Inhibitor Cocktail (5871), Phosphatase Inhibitor Cocktail (5870), Prestained Protein Marker, Broad Range (11-190 kDa) (13953), Nrf2 monoclonal antibody (12721T), β-Catenin (D10A8) XP® Rabbit mAb (8480) and Secondary goat anti-rabbit HRP-conjugated antibody (7074P2) were all requisitioned from Cell Signaling (Danvers, MA, USA). 10X Towbin Buffer (42558.02), 10X TBS Buffer (42596.01), Tween 20 (39796.01) and Methanol (45631.02) were from SERVA Electrophoresis GmbH (Heidelberg, Germany). Mouse IL-1β ELISA Kit (E-EL-M0037), Mouse IL-6 ELISA Kit (E-EL-M0044), Mouse TNF-α ELISA Kit (E-

EL-M0049) and Lamin B1 Polyclonal Antibody (E-AB-40257) were obtained from Elabscience (Houston, TX, USA). HERA^{PLUS} SYBR® Green qPCR Kit (WF10308001) was purchased from Willowfort (Birmingham, UK) and primers IL-1β, Iba1, c-Myc, HO-1 and Osgin1 (S015950; designed by NCBI primer blast tool) were ordered from Synbio Technologies (Monmouth Junction, NJ, USA). TriFECTa RNAi Kit and PrimeTime Assays for Nrf2 (Mm.PT.58.29108649) and HPRT (Mm.PT.39a.22214828) were supplied by Integrated DNA Technologies (Coralville, IA, USA), and the Minute™ Cytoplasmic & Nuclear Extraction Kit for Cells (SC-003) was bought from Invent Biotechnologies (Plymouth, MN, USA).

2.2. Cell culture

According to recommendations by the ATCC, SIM-A9 cells (CRL-3265™) (Figure 2.1) were maintained in Dulbecco's Modified Eagle Medium/Nutrient Mixture F-12 (DMEM/F12) medium supplemented with 10% heat-inactivated fetal bovine serum, 5% heat-inactivated donor horse serum and 1% Pen-Strep (100 units/mL penicillin, and 100 µg/mL streptomycin) in a 5% CO_2 humidified incubator at 37 °C. On reaching a confluence of 80-90% (a cell density averaging about 1.2×10^6 cells/mL), cells were non-enzymatically harvested either by scrapping or a brief (10 min) incubation with a dissociation solution of 1 mM EDTA, 1 mM EGTA and 1 mg/mL glucose in calcium/magnesium-free Dulbecco's phosphate-buffered saline. Cells were seeded at densities ranging from 2×10^4 cells/mL to 1×10^6 cells/mL, depending on the experimental procedure. For all experiments aiming to assess the efficacy of treatments in LPS-activated microglia, SIM-A9 cells were pretreated with GSK3 inhibitors (or SFN) for 2 h before the cells were treated with *E. coli* LPS for 24 h, in continued presence of the treatment compounds. SIM-A9 cell line information as specified by the ATCC is outlined in Table 2.1.

Table 2.1: SIM-A9 cell line information

SIM-A9 (CRL-3265™)	
Organism	*Mus musculus*
Strain	C57BL/6
Cell type	Microglial cell
Morphology	Neuronal-like
Tissue	Brain; Cerebral cortex
Biosafety Safety Level	1
Growth properties	Mixed: adherent and suspension
Immortalization method	Spontaneous immortalization
Antigen expression	$CD68^+$; ionizing calcium-binding adaptor molecule 1 $(Iba1)^+$
Growth Medium	Base medium: DMEM/F12 Complete medium: DMEM/F12 supplemented with heat-inactivated horse serum to a final concentration of 5% and heat-inactivated fetal bovine serum to a final concentration of 10%.
Culture Conditions	37 °C, 5% CO_2 in air atmosphere
Subcultivation Ratio	1:3 to 1:6
Medium renewal	every 2 to 3 days
Reagents for cryopreservation	Complete growth medium supplemented with 10% (v/v) DMSO

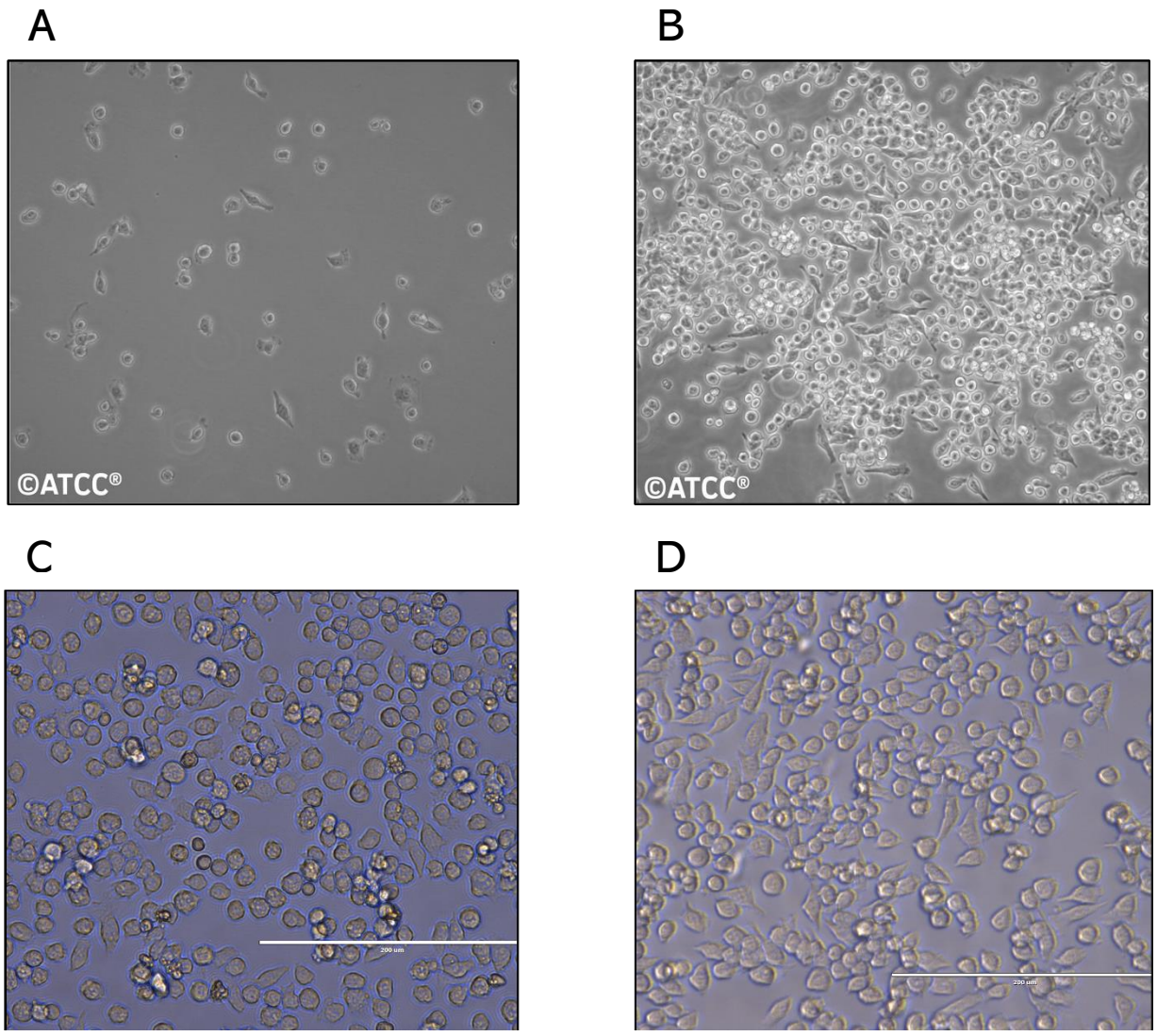

Figure 2.1. SIM-A9 cells ATCC® CRL-3265. Reference 10X micrographs of the SIM-A9 cell line at a low density (A) and a high density (B). Micrographs captured at 20X magnification on reaching confluency (C) and (D).

2.3. Cell Viability: MTT Assay

SIM-A9 cells were seeded in 96-well microtiter plates at a density of 1×10^5 cells/mL and allowed to acclimate overnight. To determine non-cytotoxic concentrations of the experimental compounds, the cells were then treated with different concentrations (10 μM, 20 μM, 40 μM and 80 μM) of GSK3 inhibitors for 24 h. Sulforaphane (SFN), used as a positive control for countering inflammation and Nrf2 activation, was also evaluated for its cytotoxicity at different molarities (1 μM, 5 μM, 10 μM). Additionally, varying concentrations (10 ng/mL, 100 ng/mL and 1 μg/mL) of *E. coli* LPS (O111:B4) were similarly evaluated.

Based on the results from these preliminary experiments and informed by the results of the Griess assay, concomitant treatment with LPS at a concentration of 100 ng/mL and GSK3 inhibitors at the concentrations 10 μM, 20 μM, and 40 μM, or SFN at 5 μM were also evaluated for their cytotoxic effects to simulate subsequent experimental conditions. For these experiments, the cells were seeded at a density of 5×10^5 cells/mL, given that this cellular concentration produced the optimal response to stimulation by LPS in the Griess experiment. All treatments were prepared in serum-free DMEM/F12 medium.

Cell viability following treatments was determined using the MTT colorimetric assay. The cellular metabolic activity was used as an indicator for cell viability, where only viable and metabolically active cells are capable of reducing the MTT tetrazolium dye to chromogenic formazan crystals. Following a 24 h incubation of the treatments with the cells, the culture medium was aspirated off and replaced with 100 μL of (1 mg/mL) MTT solution prepared in serum-free DMEM/F12 medium. Subsequent to a further 2 h incubation, the MTT solution was discarded, and the insoluble formazan crystals formed were dissolved in 100 uL DMSO. Absorbance was measured at 540 nm using NanoSPECTROstar microplate reader (BMG LABTECH, Ortenberg, Germany) and cell viability was calculated relative to untreated controls.

2.4. Determination of Nitrite: Griess Method

To preliminarily evaluate the anti-inflammatory capacity of the experimental compounds, the concentration of nitrite in the culture medium was determined using the Griess method. Nitrite concentration serves as an indicator for the levels of NO produced in the course of the LPS-initiated inflammatory response. The Griess reaction was performed following a treatment protocol in which cells were pretreated with the GSK3 inhibitors (10 μM, 20 μM, and 40 μM) or SFN (5 μM) for 2 h and then stimulated with 100 ng/mL LPS for 24 h, with continued exposure to the compounds. Thereafter, 150 μL of cell culture media were diluted with 130 μL of deionized water and 20 μL of the Griess reagent (1:1 mixture of 1% sulfanilamide in 5% phosphoric acid and 0.1% naphthylethylenediamine dihydrochloride in water) were added to the diluted supernatant. Following a 30 min incubation in the dark to permit the diazotization reaction, the color of the formed azo chromophore was spectrophotometrically measured at 548 nm using Nano SPECTROstar microplate reader, where the optical density of the nitrite-azo dye commensurately corresponds to the concentration of nitrite in the sample. The concentration of nitrite in each sample was computed using the linear equation generated from a standard curve, which was plotted using the recorded absorbance values for various concentrations of a nitrite standard.

2.5. Treatment and isolation of total RNA

SIM-A9 cells were seeded in 6-well plates at a density of 1×10^6 cells/mL and allowed to acclimate overnight. The cells were then treated with GSK3 inhibitors at the concentrations 10 μM and 20 μM, or SFN at 5 μM for 2 h. Afterwards, the media were aspirated off and the cells treated with a mixture preserving the same abovementioned concentrations of the compounds with the addition of LPS at a concentration of 100 ng/mL to induce microglial activation in the presence of the GSK3 inhibitors or SFN. Following a 6 h incubation, total RNA was extracted by lysing the cells using the phenol/guanidine-based QIAzol Lysis Reagent as per the manufacturer's instructions. To lyse the cells, 1 mL of the QIAzol reagent was added to each well and – following a brief trituration – the cell lysates were incubated at room temperature for 5 min before collection into separate microcentrifuge tubes. To each tube, 200 μL chloroform were added and vigorously shaken with the lysate for 15 sec. The homogenate was allowed to rest for 2-3 min at room

temperature and then centrifuged at 12,000 ×g for 15 min at 4 ℃ for phase separation. The upper aqueous phase from each sample, where the RNA partitions, was transferred into a new tube and the DNA/protein-containing organic layer was discarded. To salt the RNA out of the aqueous isolate, 500 µL isopropanol were added to each tube. The solution was then thoroughly vortexed for optimal mixing and maximal RNA recovery and thereafter centrifuged at 12,000 ×g for 10 min at 4 ℃, following a 10 min benchtop incubation. The supernatant was carefully aspirated off and the pelleted RNA was briefly vortexed in a 75% ethanol wash before a final centrifugation at 7,500 ×g for 5 min at 4 ℃. Finally, the supernatant was discarded, and the RNA pellet was allowed to air-dry before being resuspended in 25 µL nuclease-free water. The RNA isolates were quantified and checked for purity by recording their optical densities at 260 nm (ng/µL) and the A_{260}/A_{280} ratio (indication of absence or presence of protein and DNA contaminants) using the NanoDrop™ One/OneC Microvolume UV-Vis spectrophotometer. The RNA samples were stored at -80 ℃ for downstream experiments.

2.6. cDNA Synthesis

First strand cDNA was synthesized using the RevertAid First Strand cDNA Synthesis Kit in line with the manufacturer's instructions. In brief, 1 µg of RNA* from each sample was watered down to 10 µL with nuclease-free water. Next, 10 µL of the cDNA mastermix (Table 2.2) were added to each RNA sample for a total reaction volume of 20 µL. The cDNA reactions were amplified in a 96-well Thermal Cycler (Applied Biosystems™, CA, USA) according to the following cycling conditions: 25 ℃ for 5 min (necessary for extension by random hexamer primers), followed by 42 ℃ for 60 min (for extension primed by both random hexamers and oligo(dT)18 primers), and then 70 ℃ for 5 min to terminate the reaction. Finally, the reactions were cooled down to 4 ℃ and then stored at -20 ℃ until further use. Prior to gene quantitation by qPCR, the cDNA reactions were diluted by nuclease-free water in a 1:3 ratio (40 µL nuclease-free water added to the final cDNA

* For synthesizing cDNA from post-knockdown RNA templates, 500 ng RNA were used to synthesize cDNA, instead of 1 µg (given lower RNA concentrations). cDNA reactions were diluted in a 1:5 ratio (80 µL nuclease-free water added to the final cDNA reaction volume of 20 µL) to produce enough template for the intended qPCR runs and avoid inconsistency issues secondary to using cDNA from different knockdown experiments. For qPCR, 2 µL of cDNA were used, amounting to 10 ng cDNA/reaction.

reaction volume of 20 µL). For qPCR, 3 µL of cDNA were used as a template, amounting to 50 ng cDNA/reaction.

Table 2.2. RevertAid cDNA Reaction Composition

Reaction Component	Volume per reaction (µL)
5X Reaction Buffer	4
Oligo $(dT)_{18}$ primer	1
Random Hexamer Primer	1
RiboLock RNase Inhibitor (20 U/µL)	1
10 mM dNTP Mix	2
RevertAid M-MuLV RT (200 U/µL)	1
Total volume	10

2.7. Quantification of mRNA using real-time PCR (qPCR)

The mRNA expression levels of microglial activation markers (CD11b and Iba1), inflammation-related genes (iNOS, IL-1β, IL-6, TNF-α), Nrf2 target genes (HO-1 and Osgin1) and the β-catenin-driven c-Myc were quantified by real-time quantitative polymerase chain reaction using the ABI Prism 7500 real-time PCR system (Applied Biosystems, CA, USA). Expression was normalized to GAPDH, and relative fold gene expression was computed using the comparative CT (ΔΔCT) method. Specific primer pairs were generated via the NCBI Primer-Blast tool* and purchased from ThermoFisher or Synbio Technologies; primer sequences are shown in Table 2.4. For primer reconstitution, the lyophilized primers were briefly centrifuged and hydrated in 10 times their molecular weight (expressed in nanomoles) in nuclease-free water to yield a 100 µM primer stock solution, from which 10 µM working stocks were prepared. A melting curve was generated at the end of each qPCR run to exclude any instances of primer dimer formation and confirm primer specificity (amplicon purity). The qPCR master mix comprised 6.25 µL of PowerUp™ SYBR™

* (https://www.ncbi.nlm.nih.gov/tools/primer-blast/)

Green (2X) Master Mix or HERA^{PLUS} SYBR® Green qPCR master mix, 0.375 µL of 10 µM forward primer and 0.375 µL of 10 µM reverse primer (equivalent to a final primer concentration of 300 nM) in addition to 2.5 µL of nuclease-free water to make up a final volume of 9 µL added to 3 µL cDNA (50 ng of template/reaction) (Table 2.3). The reactions were prepared in MicroAmp™ Optical 8-Tube Strip, 0.2 mL (Applied Biosystems™; CAT# 4316567), carefully capped using MicroAmp™ Optical 8-Cap Strips (Applied Biosystems™; CAT# 4323032) and subjected to the following thermocycling conditions: an initial holding stage run at 95 ℃ for 10 min, followed by 40 2-step cycles of denaturation at 95 ℃ for 15 sec then annealing/extension for 60 sec at 60 ℃; data collection was set to occur during step 2.

Table 2.3. SYBR green mRNA qPCR reaction

Component	Volume per reaction (µL)
PowerUp™ SYBR™ Green (2X) Master Mix	6.25
Forward Primer (0.3 µM)	0.375
Reverse Primer (0.3 µM)	0.375
Nuclease-free water	2.5
cDNA	3
Total volume	12.5

For post-knockdown qPCR experiments, variations to the above protocol are hereunder summarized. PrimeTime™ qPCR primers for Nrf2 and HPRT were purchased from Integrated DNA Technologies (Coralville, IA, United States) as predesigned primer assays. As per the manufacturer's guidelines, the primer tubes were centrifuged, and the primers resuspended in 500 µL nuclease-free water to make a 20X stock solution. The composition of the qPCR master mix was modified as follows: 5 µL of HERA^{PLUS} SYBR® Green qPCR master mix, 0.5 µL of 20X PrimeTime qPCR primer assay (equivalent to a final primer concentration of 500 nM) in addition to 2 µL of nuclease-free water to make up a final volume of 8 µL added to 2 µL cDNA (10 ng of template/reaction).

Table 2.4. List of primers used for qPCR

Target mRNA	Sequence (5'-3')		Tm (°C)
CD11b	*Forward Primer:*	AAGCAGCTGAATGGAGGAC	55
	Reverse Primer:	GGGCCCCATTGGTTTTGTGAA	55
Iba1	*Forward Primer:*	CCTGCAGACTTCATCCTCTC	57
	Reverse Primer:	AGGCATCACTTCCACATCAG	55
IL-6	*Forward Primer:*	GATGCTACCAAACTGGATATAATCAG	55
	Reverse Primer:	CTCTGAAGGACTCTGGCTTTG	58
IL-1β	*Forward Primer:*	AAAGCTCTCCACCTCAATGG	55
	Reverse Primer:	TTGGGATCCACACTCTCCAG	57
iNOS	*Forward Primer:*	GGAACCTACCAGCTCACTCTGG	63
	Reverse Primer:	TGCTGAAACATTTCCTGTGCTGT	60
TNF-α	*Forward Primer:*	GAACTCCAGGCGGTGCCTAT	63
	Reverse Primer:	TGAGAGGGAGGCCATTTGGG	63
Nfe2l2	*Forward Primer:*	TGATGGACTTGGAGTTGCC	55
	Reverse Primer:	TCAAACACTTCTCGACTTACTCC	54
HO-1	*Forward Primer:*	CACAGATGGCGTCACTTCGTC	60
	Reverse Primer:	GTGAGGACCCACTGGAGGAG	62
Osgin1	*Forward Primer:*	CGGTGACATCGCCCACTAC	62
	Reverse Primer:	GCTCGGACTTAGCCCACTC	62
c-Myc	*Forward Primer:*	AGCTGTTTGAAGGCTGGATT	53
	Reverse Primer:	CTGCTGTTGCTGGTGATAGA	55
GAPDH	*Forward Primer:*	CTTTGTCAAGCTCATTTCCTGG	57
	Reverse Primer:	TCTTGCTCAGTGTCCTTGC	58
HPRT	Forward Primer:	CCCCAAAATGGTTAAGGTTGC	55
	Reverse Primer:	AACAAAGTCTGGCCTGTATCC	55

For analysis of the generated real-time PCR amplification output and as per the User Bulletin 2 of Applied Biosystems (User Bulletin #2 ABI PRISM 7700 Sequence Detection System), the second-derivative algorithm "$2^{-\Delta\Delta CT}$" was employed to determine gene expression relative to a housekeeping reporter gene in treated samples versus untreated controls (comparative CT or ΔΔCT method). For every gene of interest, ΔCT values were determined for each sample as the difference between the CT values obtained for the target gene and the reporter gene in the same sample ($CT_{\text{gene of interest}} - CT_{\text{housekeeping gene}}$), where GAPDH (or HPRT in post-knockdown qPCR assessment of proinflammatory markers) was used as the housekeeping reporter gene. Relative changes in

expression of any given gene (ΔΔCT) were then calculated as the difference between the ΔCT of each treatment group and the average ΔCT of the untreated control group. Finally, fold change of expression was determined as $2^{-\Delta\Delta CT}$, individually calculated for each group. The values are expressed in the figures as ($2^{-\Delta\Delta CT}$ ± SE), where SE is the standard error of the mean of the $2^{-\Delta\Delta CT}$ values.

2.8. Quantification of secretory proinflammatory cytokines using ELISA

Pre-coated micro-ELISA plates from Elabscience® were used to quantify the protein expression of the proinflammatory cytokines IL-1β, IL-6 and TNF-α in the supernatant of SIM-A9 cells stimulated with LPS in the presence of GSK3 inhibitors or SFN, following the treatment protocol above. In short, the cells were seeded in 6-well plates at a density of 1×10^6 cells/mL. Following overnight incubation, the cells were pretreated with GSK3 inhibitors at the 20 μM concentration or SFN at 5 μM for 2 h. The media were then removed and replaced with fresh media containing 100 ng/mL of LPS, while maintaining the concentration of GSK3 inhibitors at 20 μM and SFN at 5 μM. The culture media were collected 24 h later, centrifuged at 1,000 ×g for 20 min at 4 °C and the supernatant transferred to clean microcentrifuge tubes.

2.8.1. Sample preparation

For IL-6 and TNF-α, the supernatant was diluted in a ratio of 1:20 in the kit-provided Reference Standard and Sample Diluent, whereas undiluted samples were used for detection of IL-1β.

2.8.2. Reagent preparation

2.8.2.1. Wash buffer

As per the manufacturer's recommendations, 30 mL of concentrated (25X) wash buffer were diluted in 720 mL of deionized water to give 750 mL of a 1X working solution, for each plate.

2.8.2.2. Standard working solution

Vials containing the reference standard were centrifuged at 10,000 ×g for 1 min and then reconstituted in 1 mL of the Reference Standard and Sample Diluent to give 2000 pg/mL (IL-6

and TNF-α) and 500 pg/mL (IL-1β) working solutions. Serial dilutions were prepared following the recommended dilution gradient for each standard.

2.8.2.3. Biotinylated detection antibody working solution

A vial containing 120 µL of (100X) biotinylated detection antibody was centrifuged at 800 ×g for 1 min and then diluted in 11.88 mL of the included Biotinylated Detection Antibody Diluent to make 12 mL of a 1X working solution, for each plate.

2.8.2.4. HRP conjugate working solution

A 1X working solution was prepared from a 100X concentrated stock exactly as outlined for the biotinylated detection antibody working solution.

2.8.3. Assay

Following the sandwich ELISA principle, 100 µL of each sample or standard dilution were pipetted into their assigned wells to bind the well-coating antibody that captures its cognate antigen in the added sample or standard. Samples were assayed in triplicates and each standard concentration in duplicates. The plate was then covered with a plate sealer and incubated at 37 ℃ for 90 min. Afterwards, the plate was decanted and 100 µL of the (1X) biotinylated detection antibody working solution (also specific to the antigen of interest) were added immediately, without washing. The plate was covered with a new sealer and again incubated at 37 ℃ for 1 h. By the end of this incubation, the antigen of interest should be sandwiched between the well-coating antibody and the biotinylated antibody. Subsequently, the antibody solution was removed and 350 uL of wash buffer were added to each well and the plate allowed to soak for 1 min before the wash solution was removed. Following two more washes, 100 µL of the 1X HRP working solution were added to each well and the cover-sealed plates incubated at 37 ℃ for 30 min; this Avidin-HRP conjugate binds the biotin-tagged antibody that is now bound to the protein of interest. The plate was thereafter decanted and washed five times as outlined hereabove, before 90 µL of 3,3'5,5'-Tetramethylbenzidine (TMB) HRP-substrate were added to each well. For one last time, the sealed plate was incubated at 37 ℃ for 20 min. Only wells containing the antigen should have formed the antigen-antibody-HRP complex and bound the substrate, producing a blue color.

To terminate the enzymatic reaction, 50 µL of stop solution were added to each well in the same order the substrate was added; the developed blue color immediately shifts to yellow on adding the acidic stop solution. Optical density was measured at 450 nm using NanoSPECTROstar microplate reader (BMG LABTECH, Ortenberg, Germany). A standard curve was obtained by plotting the recorded OD values from reference standard wells against their respective concentrations. The linear equation generated from the standard curve was used to compute the protein concentration within each sample. The concentrations calculated for diluted samples were multiplied by the dilution factor to give the actual concentration of the original protein prep.

2.9. Fractionation of total cell lysates into nuclear and cytoplasmic extracts

In order to evaluate the effect of inhibition of GSK3 paralogs on the transcriptional activity of Nrf2 and NF-κB p65, nuclear lysates of treated SIM-A9 cells were extracted using the Minute™ Cytoplasmic and Nuclear Extraction Kit for Cells to assess the translocation of these transcription factors to the nucleus following treatment. SIM-A9 cells seeded at a density of 1×10^6 cells/mL in 6-well plates were pretreated with GSK3 inhibitors at the concentration 20 µM or SFN at 5 µM for 2 h. Following an additional 24 h incubation with 100 ng/mL LPS in the presence of the test compounds, the cells were washed in ice-cold PBS buffer and then 300 µL cytoplasmic extraction buffer, containing 1X Protease Inhibitor Cocktail and 1X Phosphatase Inhibitor Cocktail, were added to each well. The plates were placed on ice for 5 min before the lysed cells were scraped off and the cell lysates were transferred to pre-chilled microcentrifuge tubes and vortexed vigorously for 15 sec. The tubes were then centrifuged at 12,000 ×g for 5 min at 4 ℃. The supernatant (cytosolic fraction) was transferred to a clean tube and stored at -80 ℃ for future use. As per the manufacturer-recommended buffer volume to culture container ratio, 150 µL nuclear extraction buffer, also containing 1X Protease Inhibitor Cocktail and 1X Phosphatase Inhibitor Cocktail, were added to the pelleted nuclei and the mixture forcefully vortexed for 15 sec then incubated on ice for 1 min. The last step was repeated 4 times alternating between vigorous vortexing for 15 sec and 1 min incubation on ice. The nuclear extracts were then transferred to pre-chilled filter cartridges mounted onto collection tubes and centrifuged at 16,000 ×g for 30 sec. The filter cartridges were then discarded, and the collected nuclear extracts were stored at -80 ℃ until future use.

2.10. Quantification of cytoplasmic and nuclear proteins

The concentrations of total cytoplasmic and nuclear proteins were determined using the Pierce™ BCA Protein Assay Kit, which employs a colorimetric method for protein quantification based on the two-step biuret reaction. The first step of the reaction involves the reduction of Cu^{+2} from Copper(II) sulfate to Cu^{+1} by proteins in the sample. The amount of Cu^{+2} ions reduced is thus proportional to the amount of protein in the sample. Two molecules of bicinchoninic acid (BCA) then chelate the newly formed Cu^{+1} ions giving a purple water-soluble complex that can be optically measured.

2.10.1. Reagent Preparation

2.10.1.1. Preparation of diluted albumin (BSA) standards

An ampule of 2 mg/mL bovine serum albumin standard (BSA) was used to prepare eight standard concentrations within the range of 25-2000 μg/mL, according to the dilution scheme recommended by the manufacturer. Standard dilutions were prepared using the same lysis buffer in which the samples were prepared, and each dilution was assayed in triplicates.

2.10.1.2. Preparation of the BCA working reagent

The BCA working reagent was prepared by mixing 50 parts of BCA Reagent A to 1 part of BCA Reagent B, giving a clear, green-colored working reagent.

2.10.2. Assay

In a 96-well microtiter plate, 25 μL of each sample and standard dilution were added to the designated wells. For blanking, 25 μL of lysis buffer were added to the respective wells. Every sample or standard dilution was assayed in triplicates. In each well, 200 μL working BCA reagent were added, the plate was thoroughly mixed on an orbital shaker for 30 sec and then incubated at 37 ℃ for 30 min. The plate was then cooled down and the absorbance of the formed colored

complexes measured at 562 nm using NanoSPECTROstar microplate reader (BMG LABTECH, Ortenberg, Germany). Sample concentrations were computed from the line equation generated by plotting OD values for varying concentrations of a bovine serum albumin standard.

2.11. Western Blotting

Western blotting for nuclear Nrf2, NF-κB p65, and β-catenin was carried out in denaturing and reducing conditions. Samples were prepared such that the loading volume of 25 µL would contain 15 µg of protein per well. Each sample was prepared in 1X NuPAGE™ LDS Sample Buffer and 1X NuPAGE™ Reducing Agent and completed to volume with deionized water. The samples were briefly vortexed, spun down and heated at 70 ℃ for 10 min. The samples were then run on NuPAGE™ 10%, Bis-Tris, 1.0 mm, Mini Protein Gels (10-wells) in an XCell SureLock™ Mini-Cell containing 600 mL running buffer in its lower chamber and 200 mL in its upper chamber. To prepare 1X SDS running buffer, 50 mL of 20X NuPAGE™ MES Running Buffer were added to 950 mL deionized water. In each well, 25 µL sample (containing 15 ug protein) were loaded; 5 µL of a pre-stained protein marker, were introduced into wells assigned for molecular weight reference. Gels were run at 200 V for 35 min, using the PowerEase® 90W Power Supply (Invitrogen™, CAT# PS0091). For blotting the gels, 1X transfer buffer was prepared by adding 50 mL of 10X Towbin buffer and 100 mL methanol to 850 mL deionized water to yield 1X transfer buffer containing 10% methanol, for blotting one gel. In case two gels were blotted simultaneously, the transfer buffer was prepared so as to contain 20% methanol. Blotting pads and filter papers were presoaked in around 700 mL of the prepared transfer buffer. Polyvinylidene fluoride (PVDF) membranes were activated in methanol for 30 sec and then washed in deionized water before soaking in transfer buffer. The blotting sandwich was prepared in an XCell II™ Blot Module (Invitrogen™, CAT# EI9051) The blotting module was then clamped, inserted into the XCell SureLock™ Mini-Cell and filled with 200 mL transfer buffer; the outer chamber was filled with 650 mL deionized water to prevent overheating. Blotting was set to run for 1 hour at 30 V. Following completion of transfer, membranes were briefly washed in 1X TBST buffer and blocked using 5% BSA in 1X TBST for 1 h on an orbital shaker. Subsequently, the membranes were washed 3 times in 1X TBST for 5 min, after which, primary anti-mouse Nrf2 monoclonal antibody (1:1,000), anti-mouse β-catenin monoclonal antibody (1:1000), anti-mouse NF-κB p65 polyclonal

antibody (1:2,000) or anti-mouse Lamin B1 polyclonal antibody (1:1,000) were added to the membranes and incubated at 4 ℃ overnight, on a shaker. Next, the primary antibodies were removed, and the membranes washed 3 times in 1X TBST. Secondary goat anti-rabbit HRP-conjugated antibody (1:2,500) was then added to the membranes and incubated on a shaker for an hour at room temperature. After removal of the secondary antibody and five repeated 5 min washes with 1X TBST, Pierce™ ECL Western Blotting Substrate was added to the membranes in a 1:1 ratio of peroxide solution to luminol enhancer. Chemiluminescence was measured using the ChemiDoc™ Imaging System (Bio-Rad®, CAT# 12003153); densitometric analysis of the bands was carried out using the Image Lab 6.1 software, using Lamin B1 as a loading control.

2.12. Transfection of SIM-A9 cells with Nrf2-targeting siRNAs

For transfection of SIM-A9 cells, the TriFECTa RNAi Kit from Integrated DNA Technologies was used; this kit utilizes 27mer duplex RNAs optimized for processing by Dicer (DsiRNAs), instead of the conventional 21mer siRNAs. The kit contains 3 different predesigned Nrf2-targeting DsiRNAs (Table 2.5) in addition to a non-targeting negative control DsiRNA, an HPRT-targeting positive control DsiRNA and a TYE 563 Transfection Control DsiRNA. Lipofectamine™ 3000 was used as the transfection reagent.

Tubes containing the dried annealed oligos were briefly spun down in a microcentrifuge and then the duplexed oligos were resuspended in nuclease-free buffer to make 100 μM stock solution from which 20 μM working stocks were prepared. To prepare a 20 μM working stock of Nrf2-targeting DsiRNA pool from the 3 DsiRNAs, equal volumes from the 100 μM stock of each DsiRNA were mixed to yield a DsiRNA cocktail of a concentration one-third the original of each individual DsiRNA. A 20 μM working stock of this DsiRNA pool was then prepared and used to make a 10 nM treatment solution of pooled Nrf2-targeting DsiRNAs in DMEM/F12 basal medium. Lipofectamine™ 3000 was similarly diluted in basal DMEM/F12 such that 3.75 μL are added to each well of a 6-well plate.

Table 2.5. Nrf2-targeting DsiRNAs

DsiRNA (IDT Duplex Name)	*Strand*	*Duplex Sequences*	*IDT Ref. No.*	*Targeted Transcript (NCBI Reference Sequence; bp range)*
Nrf2 dsiRNA 1 (mm.Ri.Nfe2l2.13.1)	5'-3'	AAAGUCUCAAUGUUGAAUCAGUUTC	228168776	Nrf2 transcript variant 1 (NM_010902.4; bp range: 2201-2227)
	3'-5'	AAUUUCAGAGUUACAACUUAGUCAAAG		
Nrf2 dsiRNA 2 (mm.Ri.Nfe2l2.13.2)	5'-3'	GCGAUGAAUUUUAUUCUGCUUUCAT	228168779	Nrf2 transcript variant 1 (NM_010902.4; bp range: 1071-1097)
	3'-5'	ACCGCUACUUAAAAUAAGACGAAAGUA		
Nrf2 dsiRNA 3 (mm.Ri.Nfe2l2.13.3)	5'-3'	AUAUACGCAGGAGAGGUAAGAAUAA	228168782	Nrf2 transcript variant 1 (NM_010902.4; bp range: 1728-1754)
	3'-5'	UCUAUAUGCGUCCUCUCCAUUCUUAUU		

Given the notoriety of macrophages for being difficult-to-transfect cells and driven by the fact that reverse transfection is often more conducive to a higher transfection efficiency, SIM-A9 cells were reverse-transfected. For complexing, Lipofectamine™ 3000 and DsiRNAs, both diluted in basal DMEM/F12 medium, were added to each other in a 1:1 ratio, such that the manufacturer-recommended volume of transfection reagent/well is maintained at 3.75 μL and the formed lipid complex encapsulates 10 nM DsiRNA. The mixture was incubated for 20 min for complete complexing. Afterwards, 750 μL cell suspension (equivalent to 6×10^5 cells/well) and 250 μL of the DsiRNA-lipid complex were added to each well. The plates were thoroughly mixed and incubated in a 5% CO_2 humidified incubator at 37 °C for 24 h. Fluorescence in cells transfected with the TYE 563-labeled Transfection Control DsiRNA (Absorbance Maximum: 549 nm – Emission Maximum: 563 nm) was checked under the Olympus IX70 Inverted Fluorescent Light Microscope at 6 h and 24 h. The next day, the media containing the transfection complex was discarded and the treatment protocol commenced as hereabove outlined. Following a 6 h incubation with LPS and GSK3 inhibitors (20 uM) or SFN (5 uM), the cells were lysed in QIAzol Lysis Reagent. Total RNA was thereafter extracted and processed for qPCR experiments as previously described.

2.13. Statistical Analysis

One way Analysis of variance (ANOVA) followed by Student–Newman–Keuls post hoc test was applied to determine the statistical significance among the various study groups. A threshold value of 0.5 was set for the probability value (*P*-value), with $P < 0.05$ considered statistically significant. The data are presented as the means ± standard error of the mean (SE) for the designated number of independently executed experiments. Comparative analysis among study groups was carried out via SigmaPlot (Version 14.0; Systat Software, Chicago, IL, USA) and GraphPad Prism (Version 9.0.0; San Diego, CA, USA). Data was graphically rendered in GraphPad Prism.

3. RESULTS

3.1. Interaction enrichment of the Nrf2/NF-kB/GSK3/β-catenin network

To preliminarily validate the robustness of the inferred functional association network involving the key protein players (Nrf2, NF-κB, GSK3, and β-catenin) under study, the STRING database was interrogated for interactions between these molecular targets. The analysis returned 4 nodes, 1 for each protein and 6 edges, representing the interactions between them (Figure 3.1). The network was determined to have significantly more interactions than expected, with a protein-protein interaction enrichment *P*-value totaling 0.0097. As indicated by the STRING database, this interaction enrichment means that our proteins have more interactions among themselves than what would be expected for any random set of proteins of the same size and degree distribution drawn from the genome; it entails that these proteins are at least partially biologically connected as a group. Full functional enrichments for this association network can be found at the following permalink:
https://version-11-5.string-db.org/cgi/network?networkId=bJ9KyjAgorhs.

This enrichment analysis was withdrawn from 9920 publications, 33 KEGG pathways, and 16 Wikipathways, assuming the whole *Mus musculus* genome (NCBI taxonomy ID: 10090) for statistical background.

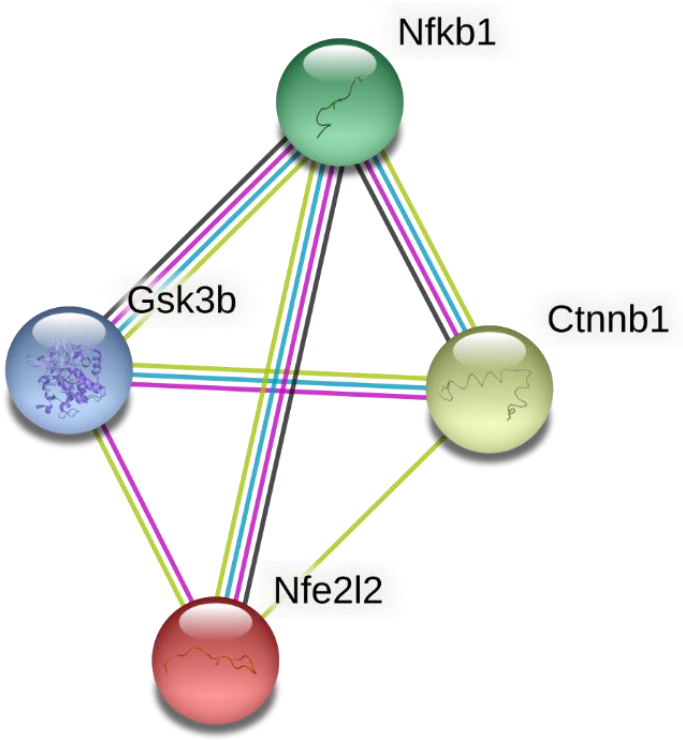

Figure 3.1. A simplified representation of the interaction enrichment of the Nrf2/NF-kB/GSK3/β-catenin association network. This network can be expanded for higher complexity associations from the permalink hereabove provided. Each node represents a protein within the network. Splice isoforms and post-translational modifications are collapsed; each node represents all forms of a protein encoded by a single protein-coding gene locus (details can be viewed at the above permalink). The internodal edges represent protein-protein interactions; an edge represents a functional interaction and does not necessarily mean a physical association between any two proteins. Cyan-colored edges represent known interactions from curated databases, violet-colored edges represent experimentally determined interactions, black edges indicate co-expression tendencies and lime-colored edges represent interactions derived from text mining.

3.2. Effect of LPS on viability of SIM-A9 cells

For the purposes of this study, LPS is used to stimulate a proinflammatory program in SIM-A9 microglia. The MTT assay and the Griess method were conjointly employed to determine the optimal concentration of LPS at which maximal microglial activation can be achieved, without compromising cell viability (Figure 3.2 and Figure 3.4). To that end, SIM-A9 seeded at varying densities were treated with LPS at the following concentrations: 10 ng/mL, 100 ng/mL and 1 μg/mL. Subsequent of measuring nitrite levels in the culture media from each group to determine the LPS concentration/cell density combination of the strongest proinflammatory response, the metabolic activity of the cells was assayed using the MTT reagent as outlined above. Lower seeding densities were associated with increased cytotoxicity at the 100 ng/mL and the 1 μg/mL concentrations; where viability of cells seeded at a density of 0.5×10^5 cells/mL (1×10^4 cells/well of a 96-well microplate) was reduced by 33.89% at the 100 ng/mL concentration and by 44.61% at the 1 μg/mL concentration. Cells seeded at a density of 1×10^5 cells/mL (2×10^4 cells/well of a 96-well microplate) fared considerably better with only a 5.72% reduction of cell viability at the 100 ng/mL concentration and a further decline by 18.3% at the 1 μg/mL concentration. On the other hand, seeding densities of 2.5×10^5 cells/mL (5×10^4 cells/well of a 96-well microplate) and 5×10^5 cells/mL (10×10^4 cells/well of a 96-well microplate) only exhibited a significant drop of viability at the 1 μg/mL LPS concentration, with 46.75% and 37.46% decline in viability, respectively. However, cells seeded at both these densities maintained acceptable rates of viability for downstream experimentation when treated with 100 ng/mL LPS, with only 7.27% and 6.51% decrease in viability at the 2.5×10^5 cells/mL and 5×10^5 cells/mL cellular concentrations, respectively. LPS administered at 10 ng/mL was not associated with significant cytotoxicity across all cell densities. Given that treatment of cells seeded at 5×10^5 cells/mL with LPS at the 100 ng/mL concentration was associated with the highest nitrite levels (as will be shown), while maintaining a good viability profile (Figure 3.2), these conditions were adopted for subsequent experiments.

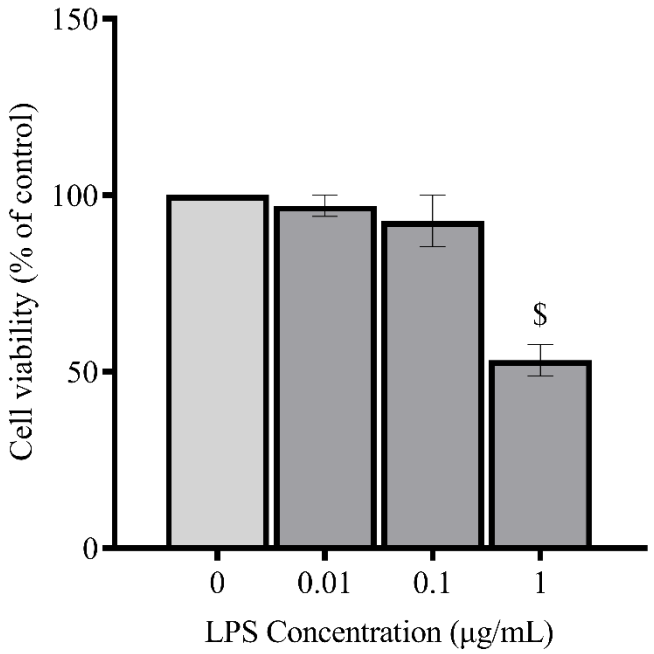

Figure 3.2. Effect of LPS on viability of SIM-A9 cells. Cell viability/LPS cytotoxicity was assessed using the MTT assay following treatment of SIM-A9 cells (5×10^5 cells/mL) with 10 ng/mL, 100 ng/mL and 1 μg/mL LPS. Data is expressed as means ± SEM. Group comparisons were drawn using one-way ANOVA, followed by the Student-Newman-Keuls post-hoc test; $ *P*-value < 0.05 (relative to negative [untreated] controls).

3.3. Effect of BRD0705, BRD3731, BRD0320, and SFN on viability of SIM-A9 cells

As mentioned in the "Materials and Methods" section, the experimental GSK3 inhibitors were evaluated for their cytotoxicity in SIM-A9 cells via the MTT assay, following the hereinabove outlined treatment protocol, which uses 10, 20, 40 and 80 micromolar concentrations of each compound alone or in conjunction with 100 ng/mL LPS. As is evident in Figure 3.3, none of the compounds was significantly cytotoxic at any of the treatment concentrations, either alone or in conjunction with LPS. SFN, used as a positive control for countervailing inflammation and Nrf2 activation, was also assayed for its cytotoxicity at the treatment concentrations of 0.5 μM, 1 μM, 5 μM, and 10 μM. Again, cellular viability was sustained across all treatment concentrations.

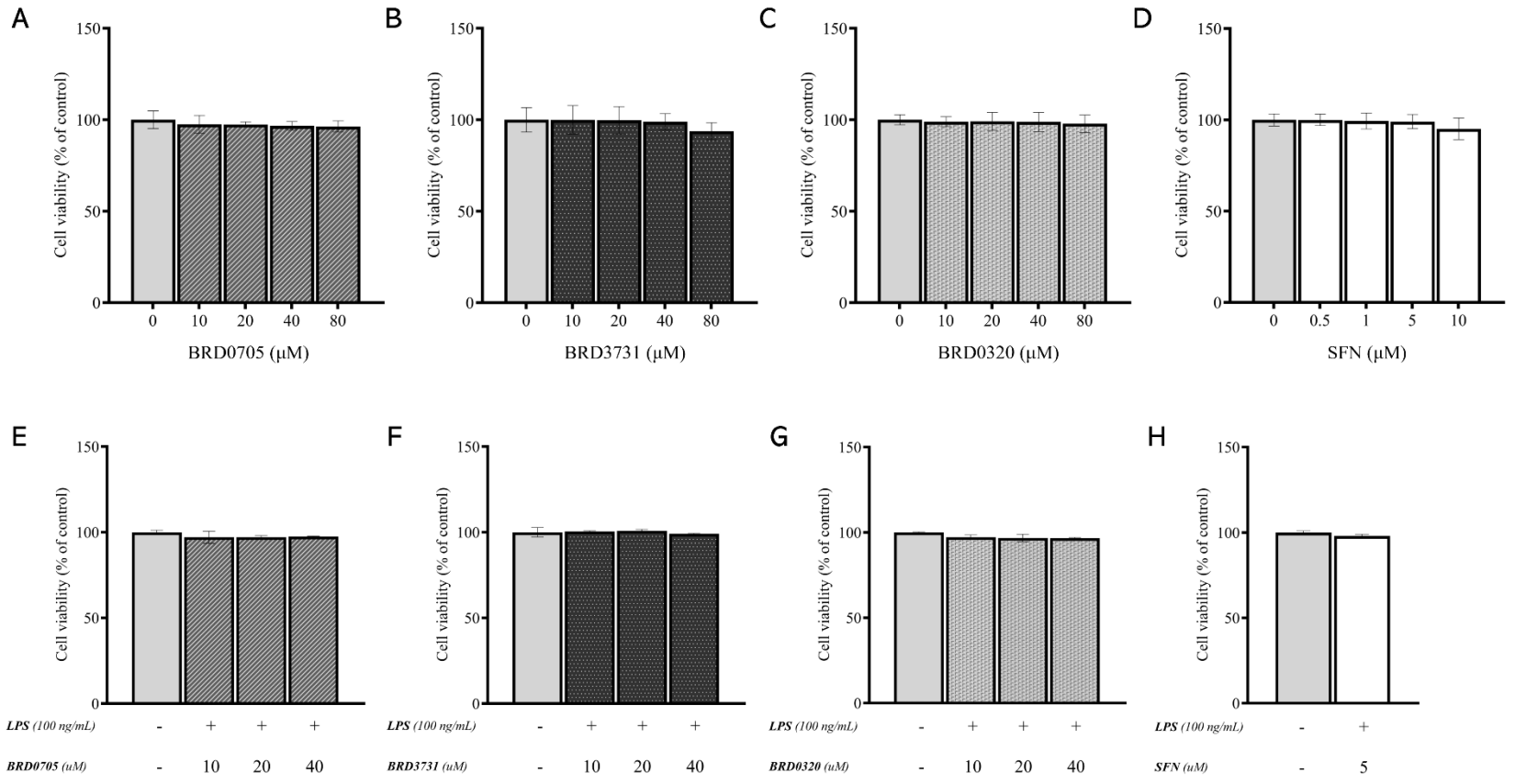

Figure 3.3. Effect of BRD0705, BRD3731, BRD0320, and SFN on viability of SIM-A9 cells. Cell viability was assessed using the MTT assay following treatment of SIM-A9 cells with BRD0705 (GSK3α inhibitor; A), BRD3731 (GSK3β inhibitor; B), BRD0320 (GSK3α/β inhibitor; C), and SFN (D). All experimental compounds were then reassessed in presence of 100 ng/mL LPS (E-H). Data is expressed as means ± SEM. Group comparisons were drawn using one-way ANOVA, followed by the Student-Newman-Keuls post-hoc test.

3.4. Effect of different concentrations of LPS on nitrite production in SIM-A9 cells

In order to instigate an inflammatory response in microglial cells, LPS-induced increase of nitric oxide was evaluated by the Griess method using 3 incrementally increasing concentrations of LPS of the *E. coli* O111:B4 strain (10 ng/mL, 100 ng/mL and 1 μg/mL). None of the tested LPS concentrations was able to induce a significantly observable rise in nitrite production from cells seeded at densities of 0.5×10^5 cells/mL or 1×10^5 cells/mL. However, an obvious and dose-dependent rise in nitrite concentration was observed in cells plated at 2.5×10^5 cells/mL and 5×10^5 cells/mL seeding densities, which was statistically significant (*P*-value < 0.05) across all concentrations. Considering that exposure to LPS at the 1 μg/mL concentrations correlated with extensive cell death as evidenced by the MTT assay, only the 10 ng/mL and the 100 ng/mL concentrations were to be comparatively considered for ensuing experiments. LPS at the concentration 10 ng/mL incited a 1.89-fold (188.65%) and a 3.44-fold (344.39%) upsurge in nitrite levels in cells plated at the concentrations 2.5×10^5 cells/mL and 5×10^5 cells/mL, respectively; whereas 100 ng/mL LPS increased nitrite production by 3.78-fold (378.38%) and 5.6-fold (560.43%) in the cellular densities 2.5×10^5 cells/mL and 5×10^5 cells/mL, respectively (Figure 3.4). Taken together, these results along with those obtained from experiments of cell viability demanded that subsequent experiments be run using LPS at the 100 ng/mL concentration for stimulation of SIM-A9 cells seeded at a concentration of 5×10^5 cells/mL.

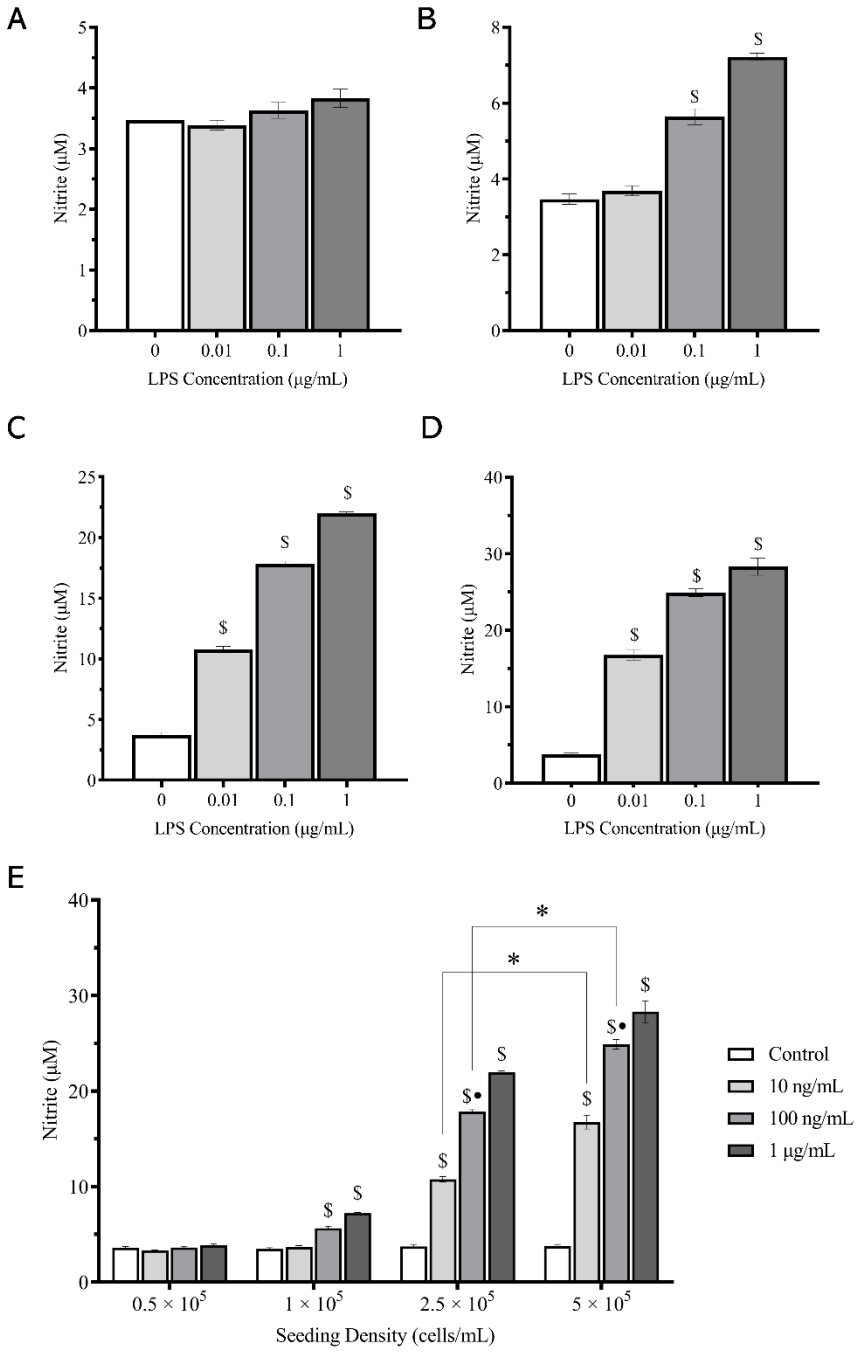

Figure 3.4. Effect of different concentrations of LPS on SIM-A9 cells with varying cellular densities. Effect of different LPS concentrations on nitrite production in SIM-A9 cells seeded at a density of 0.5×10^5 cells/mL (A), 1×10^5 cells/mL (B), 2.5×10^5 cells/mL (C), and 5×10^5 cells/mL (D). (E) Combined representation of LPS-mediated increase in nitrite production in SIM-A9 cells seeded at varying densities. Data is expressed as means ± SEM. Comparison of different LPS concentrations for a given seeding density was drawn using one-way ANOVA, followed by the Student-Newman-Keuls post-hoc test. To measure interactivity of LPS concentrations with varying seeding densities, group comparisons were drawn using two-way ANOVA, followed by the Student-Newman-Keuls post-hoc test; $ *P*-value < 0.05 (relative to negative [untreated] controls); * *P*-value < 0.05 (LPS concentration at seeding density of 2.5×10^5 vs same LPS concentration at seeding density of 5×10^5); • *P*-value < 0.05 (100 ng/mL LPS vs 10 ng/mL LPS at the same seeding density)

3.5. Effect of GSK3 inhibitors on nitrite production in LPS-activated SIM-A9 cells

To initially evaluate any potential anti-inflammatory effect associated with the tested GSK3 inhibitors on a functional level, nitrite production was again measured in the cell culture media of SIM-A9 cells treated with LPS and the GSK3 inhibitor compounds, according to the protocol previously outlined. In this experiment, LPS significantly increased nitrite levels compared to control (Figure 3.5). BRD0705 (GSK3α inhibitor) significantly inhibited the LPS-stimulated production of nitrites by 18.39%, 34.09%, and 35.43% at 10 μM, 20 μM, and 40 μM, respectively. The GSK3β inhibitor, BRD3731, also significantly inhibited LPS-stimulated nitrite production by 20.12%, 52.78%, and 59.44% at 10 μM, 20 μM, and 40 μM, respectively. The anti-nitrosative efficacy of the lowest concentration of the GSK3α/β inhibitor BRD0320 (10 μM) surpassed the highest of BRD0705 (GSK3α inhibitor; 40 μM) as it significantly inhibited the LPS-stimulated production of nitrites by 34.36%. Furthermore, BRD0320 (GSK3α/β inhibitor) significantly inhibited the LPS-stimulated production of nitrites by 48.41% and 56.11% at 20 μM and 40 μM, respectively. Differences between the nitrite-lowering efficacy of the 20 μM and 40 μM concentrations of BRD0705 (GSK3α inhibitor) and BRD3731 (GSK3β inhibitor) were statistically significant, while only at the highest concentration did BRD0705 (GSK3α inhibitor) and BRD0320 (GSK3α/β inhibitor) exhibit any significant differences. Variations between BRD3731 (GSK3β inhibitor) and BRD0320 (GSK3α/β inhibitor) were insignificant across all concentrations. Lastly, SFN significantly inhibited the LPS-stimulated production of nitrites by 98.65% at 5 μM.

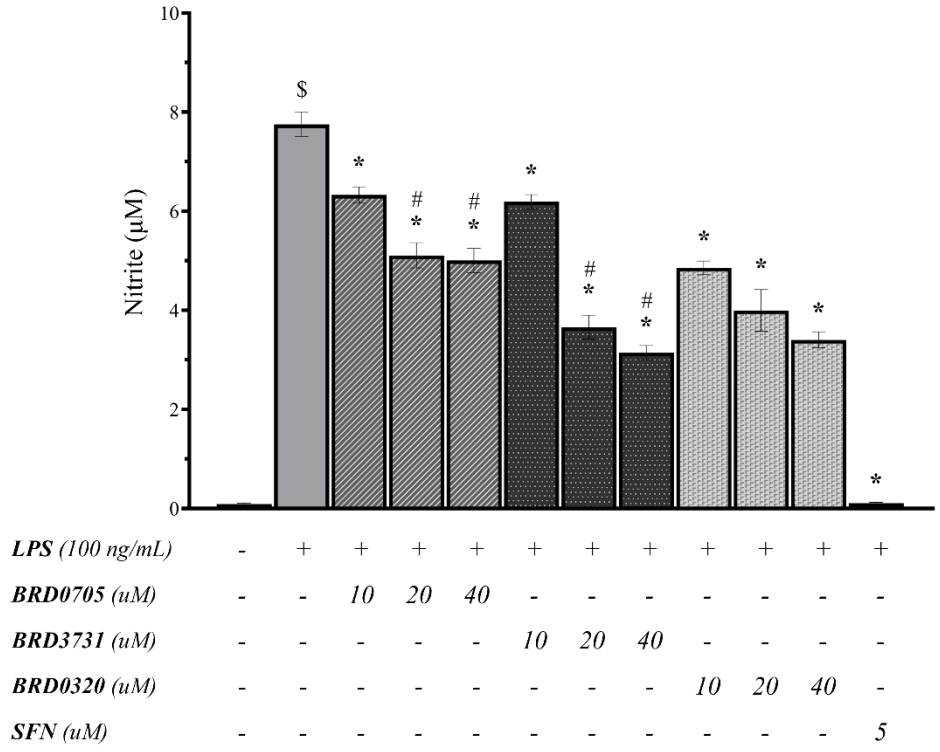

Figure 3.5. Effect of GSK3 inhibitors on nitrite production in LPS-activated SIM-A9 cells. SIM-A9 cell (5×10^5 cells/mL cell density) were stimulated with 100 ng/mL LPS for 24 h, in presence of the GSK3 inhibitors (BRD0705, BRD3731, and BRD0320) and SFN. Nitrite production was measured in the cell culture media using the Griess method. Data is expressed as means ± SEM. Group comparisons were drawn using one-way ANOVA, followed by the Student-Newman-Keuls post-hoc test; * *P*-value < 0.05 (relative to the LPS-activated group); $ *P*-value < 0.05 (relative to negative [untreated] controls); # *P*-value < 0.05 (BRD0705 at any given concentration relative to BRD3731 at the corresponding concentration).

3.6. Effect of GSK3 inhibitors on the mRNA expression of the microglial activation markers CD11b and Iba1 in LPS-activated SIM-A9 cells

To further investigate the putative anti-inflammatory effects of selective and non-selective pharmacological GSK3 inhibition, gene expression analysis via quantitative real-time PCR was performed to assess the mRNA levels of principal proinflammatory genes. First, mRNA levels of the commonly assessed surface markers of microglial activation CD11b (Ladeby et al., 2005; Yuskaitis et al., 2009) and Iba1 (Ohsawa et al., 2004) were quantitatively assessed in treatment-naïve controls and LPS-activated cells, in presence and absence of GSK3 inhibitors, following the above-described treatment protocol. As shown in Figure 3.6, activation of SIM-A9 microglia by 100 ng/mL LPS resulted in a significant upregulation of CD11b and Iba1. Selective inhibition of GSK3α by 10 μM and 20 μM BRD0705 lowered the mRNA levels of CD11b by 11.22% and 26.2%, and those of Iba1 by 76.37% and 84.53%, respectively. Non-selective inhibition of GSK3 by BRD0320 correlated with an improved reduction of CD11b and Iba1, compared to GSK3α-selective inhibition. CD11b and Iba1 mRNA levels were significantly inhibited by 33.53% and 73.41%, respectively at 10 μM, and by 45.13% and 80.78%, respectively at 20 μM BRD0320 (GSK3α/β inhibitor). GSK3β-selective inhibition by BRD3731 was the most potent suppressor of the mRNA expression of these microglial activation markers. As such, CD11b mRNA levels were significantly decreased by 38.11% and 53.23% at 10 μM and 20 μM, respectively. Additionally, Iba1 mRNA levels were significantly inhibited by 88.58% and 95.48% at 10 μM and 20 μM, respectively. The dose-dependent amelioration of function was statistically significant for all three compounds, and at 20 μM, the functional differences between all treatments were statistically meaningful, with the exception of Iba1 modulation by BRD3731 (GSK3β inhibitor) and BRD0320 (GSK3α/β inhibitor). Finally, SFN at 5 μM significantly inhibited CD11b and Iba1 mRNA levels by 43.11% and 99.72%, respectively.

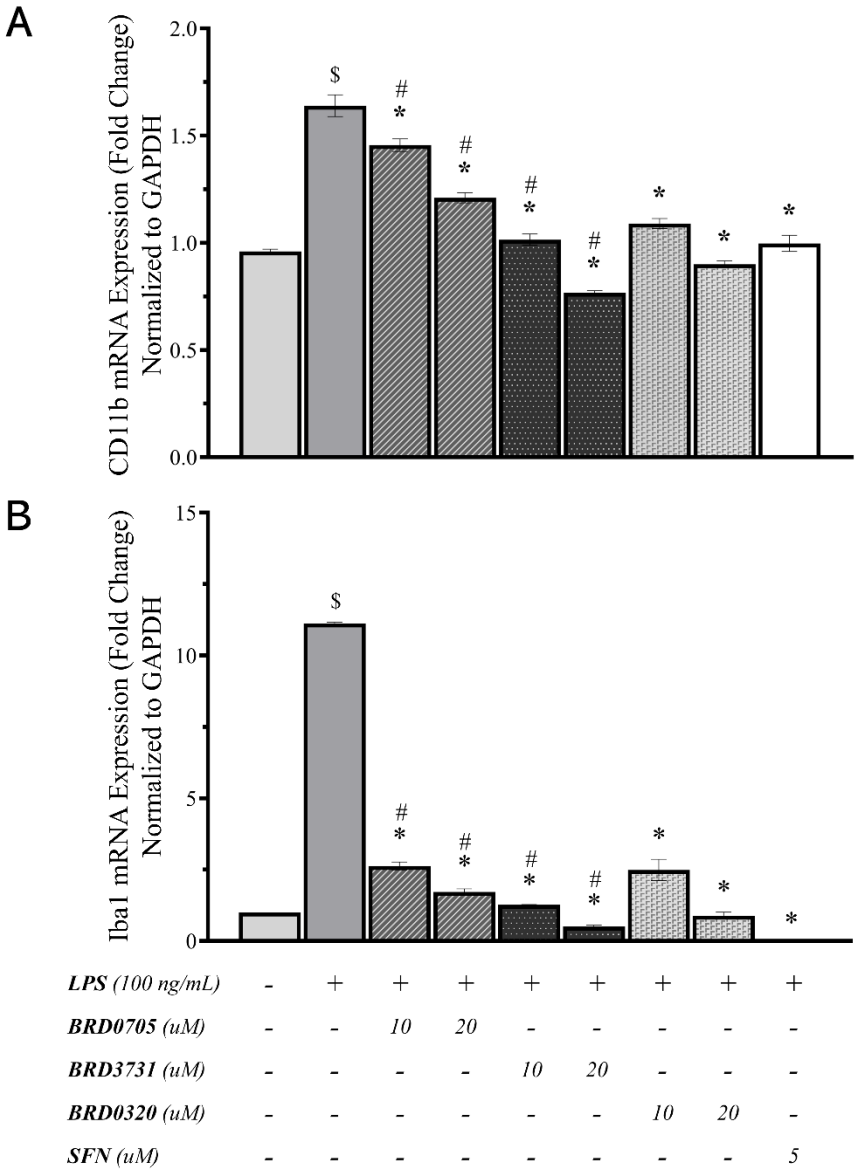

Figure 3.6. Effect of GSK-3 inhibitors on the mRNA expression of the microglial activation markers CD11b and Iba1 in LPS-activated SIM-A9 cells. Target mRNA expression was quantified by real-time qPCR and normalized to GAPDH. All compounds show a dose-dependent decrease of the LPS-triggered upregulation of the microglial activation markers CD11b (A) and Iba1 (B). Data is expressed as means ± SEM. Group comparisons were drawn using one-way ANOVA, followed by the Student-Newman-Keuls post-hoc test; * *P*-value < 0.05 (relative to the LPS-activated group); $ *P*-value < 0.05 (relative to negative [untreated] controls); # *P*-value < 0.05 (BRD0705 at any given concentration relative to BRD3731 at the corresponding concentration).

3.7. Effect of GSK3 inhibitors on the mRNA expression of iNOS in LPS-activated SIM-A9 cells

In verification of results obtained from the Griess assay, iNOS, a major player in inflammatory and para-inflammatory disorders (Suschek et al., 2004; Xue et al., 2018) was evaluated for its transcriptional rates in the different treatment groups versus untreated controls. The results are shown in Figure 3.7. BRD0705 (GSK3α inhibitor) insignificantly inhibited LPS-stimulated iNOS mRNA levels by 4.82% at 10 μM, and it significantly inhibited iNOS mRNA levels by 28.8% at 20 μM. Dual inhibition of the two GSK3 isoforms by BRD0320 resulted in significant inhibition of LPS-stimulated iNOS mRNA levels by 23.99% at 10 μM and 31.4% at 20 μM, whereas GSK3β-selective inhibition by BRD3731 significantly inhibited iNOS mRNA levels by 26.4% at 10 μM and 34.38% at 20 μM. As evident in Figure 7, SFN at 5 μM significantly inhibited iNOS mRNA levels by 97.77%.

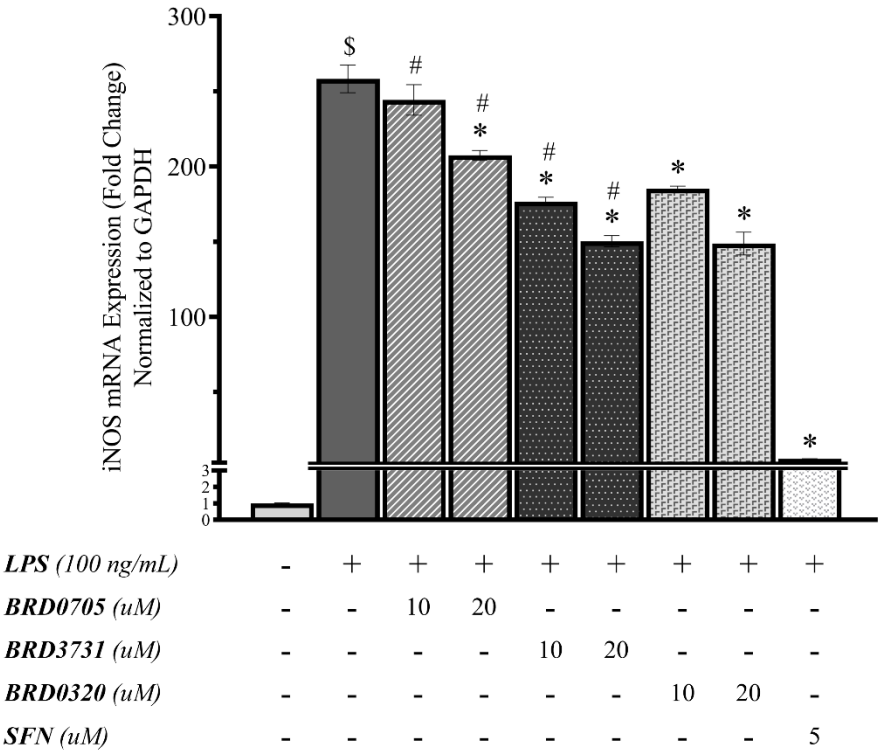

Figure 3.7. Effect of GSK3 inhibitors on the mRNA expression of iNOS in LPS-activated SIM-A9 cells. Target mRNA expression was quantified by real-time qPCR and normalized to GAPDH. All compounds show a dose-dependent reduction of the LPS-stimulated upregulation of iNOS. Data is presented as means ± SEM. Group comparisons were drawn using one-way ANOVA, followed by the Student-Newman-Keuls post-hoc test; * *P*-value < 0.05 (relative to the LPS-activated group); $ *P*-value < 0.05 (relative to negative [untreated] controls); # *P*-value < 0.05 (BRD0705 at any given concentration relative to BRD3731 at the corresponding concentration).

3.8. Effect of GSK3 inhibitors on the mRNA expression of the proinflammatory cytokines IL-1β, IL-6 and TNF-α in LPS-activated SIM-A9 cells

Stimulated proinflammatory cytokine signaling is typical of activated microglia and is associated with neuroinflammation and neurodegenerative proteopathy (W.-Y. Wang et al., 2015). mRNA expression of the secretory proinflammatory cytokines IL-1β, IL-6, and TNF-α was therefore performed and echoed the results obtained for CD11b, Iba1, and iNOS. LPS significantly increased IL-1β, IL-6, and TNF-α mRNA levels. BRD0705 (GSK3α inhibitor) significantly inhibited IL-1β mRNA levels by 48.09% and 59.22% at 10 μM and 20 μM, respectively. Importantly, BRD3731 (GSK3β inhibitor) significantly inhibited IL-1β mRNA levels by 75.67% and 92.75% at 10 μM and 20 μM, respectively. Additionally, BRD0320 (GSK3α/β inhibitor) significantly inhibited IL-1β mRNA levels by 73.41% and 80.78% at 10 μM and 20 μM, respectively. SFN significantly inhibited IL-1β mRNA levels by 97.17% at 5 μM. The same trend was observed for IL-6; BRD0705 (GSK3α inhibitor) significantly inhibited IL-6 mRNA levels by 14.26% and 26.69% at 10 μM and 20 μM, respectively. BRD3731 (GSK3β inhibitor) significantly inhibited IL-6 mRNA levels by 42.14% and 54.57% at 10 μM and 20 μM, respectively. BRD0320 (GSK3α/β inhibitor) significantly inhibited IL-6 mRNA levels by 32.29% and 43.06% at 10 μM and 20 μM, respectively, whereas SFN significantly inhibited IL-6 mRNA levels by 91.92% at 5 μM.

Post-treatment TNF-α transcriptional modulation followed a similar course. TNF-α levels dropped by 40.8% and 62.87% following BRD3731 (GSK3β inhibitor) treatment at 10 μM and 20 μM, respectively. BRD0320 (GSK3α/β inhibitor) lowered LPS-exacerbated TNF-α levels by 34.55% at 10 μM and by 52.66% at 20 μM, while BRD0705 (GSK3α inhibitor) brought on a 17.94% decline in TNF-α transcripts at 10 μM, almost doubling to 37.6% at 20 μM. A 70.51% reduction in TNF-α levels was registered for SFN (5 μM). The evident dose-dependency was statistically powerful as relayed by the analysis of data retrieved for the 10 μM and 20 μM concentrations. The functional differences between BRD0705 (GSK3α inhibitor) and BRD3731 (GSK3β inhibitor) were also significant, from a statistical standpoint. Only for TNF-α, the modulatory variance between BRD0705 (GSK3α inhibitor) and BRD0320 (GSK3α/β inhibitor) was, however, not statistically significant (Figure 3.8).

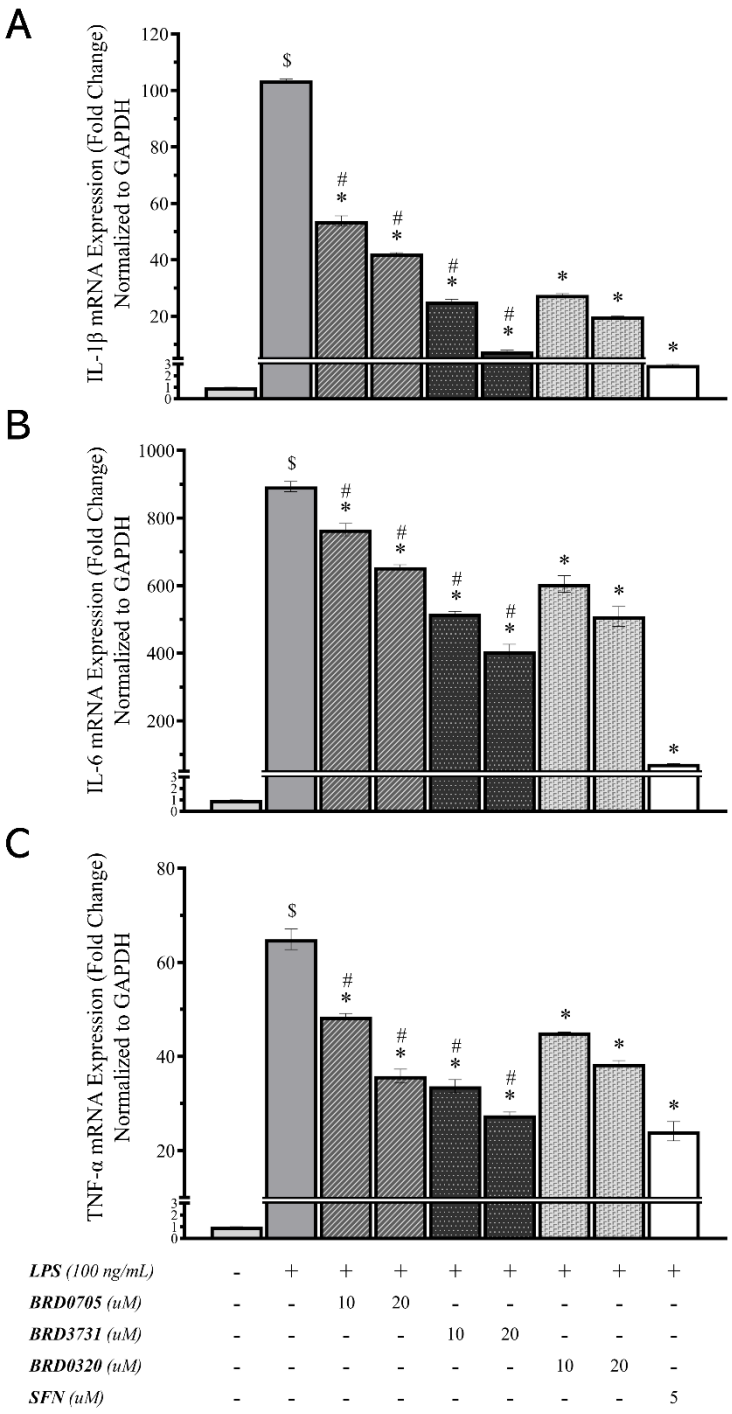

Figure 3.8. Effect of GSK3 inhibitors on the mRNA expression of the proinflammatory cytokines IL-1β, IL-6 and TNF-α in LPS-activated SIM-A9 cells. Target mRNA expression was quantified by real-time qPCR and normalized to GAPDH. All compounds manifest a dose-dependent moderation of the LPS-induced escalation of the proinflammatory cytokines IL-1β (A), IL-6 (B), and TNF-α (C). Results shown are represented as means ± SEM. Group comparisons were drawn using one-way ANOVA, followed by the Student-Newman-Keuls post-hoc test; * *P*-value < 0.05 (relative to the LPS-activated group); $ *P*-value < 0.05 (relative to negative [untreated] controls); # *P*-value < 0.05 (BRD0705 at any given concentration relative to BRD3731 at the corresponding concentration).

3.9. Effect of GSK3 inhibitors on the mRNA expression of Nrf2-driven ARE genes HO-1 and Osgin1 in LPS-activated SIM-A9 cells

In order to evaluate the effects of selective suppression of the individual GSK3 paralogs on mediating Nrf2 transcriptional activation, the mRNA expression of two ARE genes, HO-1 and Osgin1, was quantified by real-time PCR, following treatment with the GSK3 inhibitors, under the supposition that Nrf2 destabilization and nuclear localization should translate to enhanced transcription of its target genes. The results are shown in Figure 3.9. BRD3731 (GSK3β inhibitor) was the most potent Nrf2 activator; it induced a 36.56% enhancement of HO-1 expression at 10 μM and 73.99% at 20 μM, compared to untreated LPS-stimulated microglia. Osgin1 mRNA expression was similarly enhanced by 125.69% at 10 μM BRD3731 (GSK3β inhibitor) and by 237.19% at 20 μM. BRD0320 (GSK3 α/β inhibitor) increased HO-1 mRNA expression by 38.21% and 43.86% at 10 μM and 20 μM, respectively, whereas these concentrations brought about a 144.52% and a 175.08% increase in Osgin1 mRNA levels. BRD0705 (GSK3α inhibitor) at 10 μM treatment stimulated HO-1 transcription by 10.89% and by 22.66% at 20 μM. Osgin1 expression was upraised by 58.56% at the 10 μM concentration and by 67.87% at the 20 μM concentration. With BRD0705 (GSK3α inhibitor), dose variations were of no statistical import for either target, neither were the differences in functional competency with BRD0320 (GSK3α/β inhibitor) for HO-1.

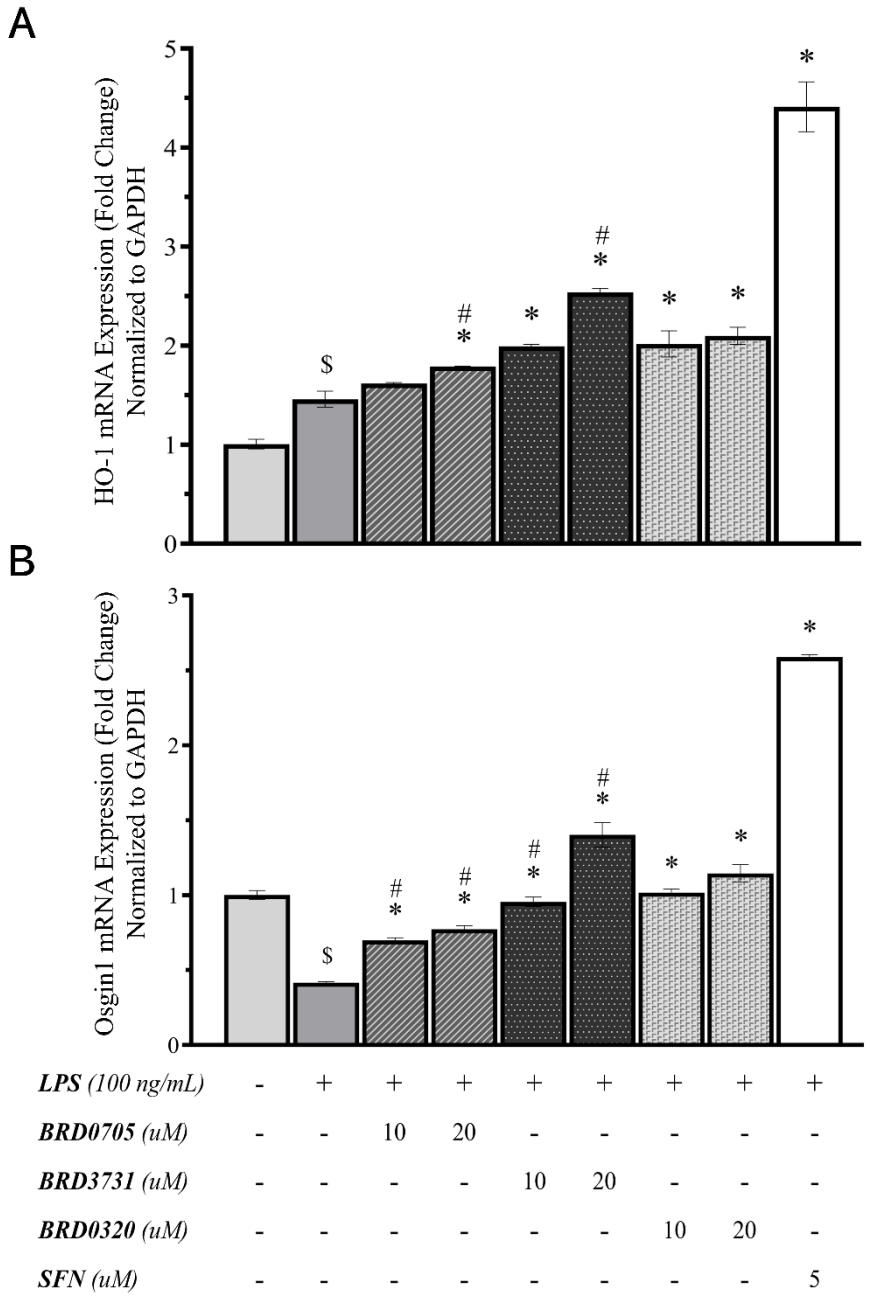

Figure 3.9. Effect of GSK3 inhibitors on the mRNA expression of the Nrf2-driven ARE genes HO-1 and Osgin1 in LPS-activated SIM-A9 cells. Target mRNA expression was quantified by real-time qPCR and normalized to GAPDH. All GSK3 inhibitor treatments – except for BRD0705 (GSK3α inhibitor) at 10 μM – show a statistically significant upregulation of the Nrf2-driven ARE gene HO-1 (A) and all treatments – without exceptions – correlate with a rise in Osgin1 mRNA levels (B). BRD3731 (GSK3β inhibitor) displays the greatest Nrf2-inducing activity after the positive control (SFN; 5 μM), followed by BRD0320 (GSK3α/ β inhibitor), then BRD0705 (GSK3α inhibitor). Data is expressed as means ± SEM. Group comparisons were drawn using one-way ANOVA, followed by the Student-Newman-Keuls post-hoc test; * *P*-value < 0.05 (relative to the LPS-activated group); $ *P*-value < 0.05 (relative to negative [untreated] controls); # *P*-value < 0.05 (BRD0705 at any given concentration relative to BRD3731 at the corresponding concentration).

3.10. Effect of GSK3 inhibitors on the mRNA expression of the β-catenin-transcribed c-Myc in LPS-activated SIM-A9 cells

Given empirical evidence suggesting isoform-distinctive β-catenin regulatory profiles (Wagner et al., 2018) and other data herein cited (see Discussion) that pinpoints the involvement of β-catenin in our pathophysiological context of interest, we set out to evaluate c-Myc mRNA levels, a transcriptional target of Wnt/β-catenin signaling pathway (Herbst et al., 2014). LPS alone incited a 404.79% rise in c-Myc levels. BRD0705 (GSK3α inhibitor) elaborated on this increase by 8.29% (446.61% overall increase relative to untreated controls) at 10 μM and by 12.81% (469.46% overall increase relative to untreated controls) at 20 μM. Selective inhibition of GSK3β by BRD3731 displayed the most β-catenin destabilization, as shown by the elevated c-Myc mRNA levels; BRD3731 (GSK3β inhibitor) upregulated c-Myc by 1,399.93% at 10 μM and by 2,086.86% at 20 μM, relative to untreated controls. This trend translates to a 197.14% and a 333.22% increase in c-Myc expression at 10 and 20 μM, respectively, compared to cells solely treated with LPS. Non-selective GSK3 inhibition by BRD0320 promoted c-Myc transcription by 1,031.67% at 10 μM and 1,376.07% at 20 μM, compared to untreated controls (124.19% and 192.41% relative to LPS-stimulated cells). Coupling the insignificance of dose-dependent biological outcome, no statistical significance was demonstrable between the two concentrations of BRD0705 (GSK3α inhibitor). Nonetheless, variations in the pattern of c-Myc mRNA expression were significant statistically across all three compounds, wherever comparisons between matched concentrations were made. Results are shown in Figure 3.10.

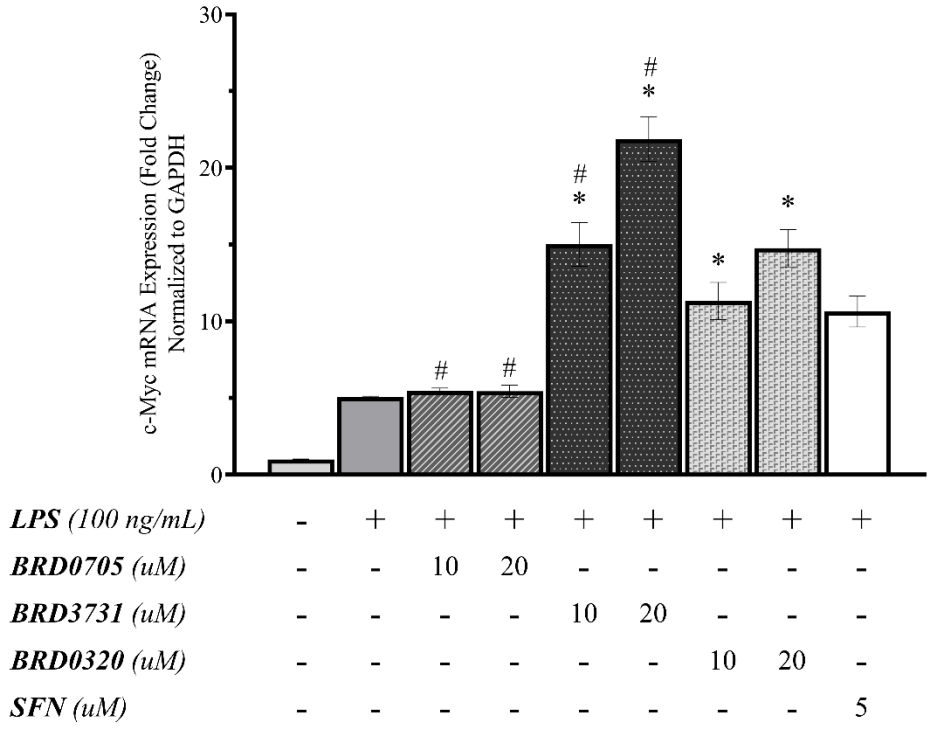

Figure 3.10. Effect of GSK3 inhibitors on the mRNA expression of the β-catenin−transcribed c-Myc in LPS-activated SIM-A9 cells. Target mRNA expression was quantified by real-time qPCR and normalized to GAPDH. Only BRD3731 and BRD0320 show a statistically significant augmentation of c-Myc transcription. BRD3731 (GSK3β inhibitor) displays the most β-catenin−inducing activity followed by BRD0320 (GSK3α/β inhibitor). BRD0705 (GSK3α inhibitor) does not induce any considerable change in c-Myc expression beyond that which is already occasioned by LPS alone. Data is expressed as means ± SEM. Group comparisons were drawn using one-way ANOVA, followed by the Student-Newman-Keuls post-hoc test; * *P*-value < 0.05 (relative to the LPS-activated group); # *P*-value < 0.05 (BRD0705 at any given concentration relative to BRD3731 at the corresponding concentration).

3.11. Effect of GSK3 inhibitors on the protein levels of the proinflammatory cytokines IL-1β, IL-6 and TNF-α in LPS-activated SIM-A9 cells

To confirm that the anti-inflammatory responses observed on the mRNA level carried through to the protein level, the protein concentrations of the secretory proinflammatory cytokines IL-1β, IL-6 and TNF-α were evaluated by ELISA in the cell culture supernatant. LPS (100 ng/mL) promoted the proinflammatory profile of SIM-A9 cells as reflected by the elevated protein levels of the evaluated cytokines (Figure 3.11). At 20 μM, BRD0705 (GSK3α inhibitor) reduced the LPS-mediated increase of IL-1β by 24.33%, IL-6 by 34.67%, and TNF-α by 14.9%. At the same concentration, BRD3731 (GSK3β inhibitor) reduced IL-1β by 89.57%, IL-6 by 47.85% and TNF-α by 74.62%. Dual inhibition of the two GSK3 isoforms by BRD0320 at 20 μM corresponded with 59.27%, 39.33%, and 54.01% reduction in LPS-elevated IL-1β, IL-6, and TNF-α proteins, respectively. Statistical analysis inferred the significance of all changes noted between the compounds, excepting the instance of comparing BRD0705 (GSK3α inhibitor) and BRD0320 (GSK3α/β inhibitor) within the IL-6 assay.

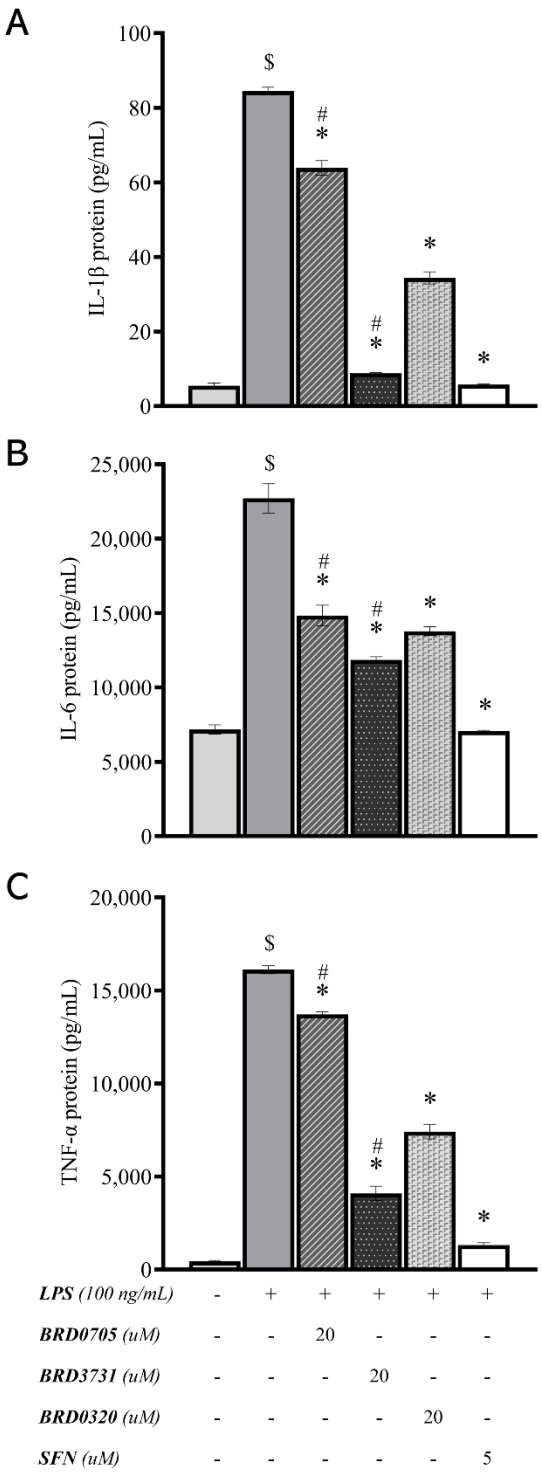

Figure 3.11. Effect of GSK3 inhibitors on the protein levels of the proinflammatory cytokines IL-1β, IL-6 and TNF-α in LPS-activated SIM-A9 cells. All compounds show a statistically significant reduction of the LPS-stimulated upregulation of the proinflammatory cytokines IL-1β (A), IL-6 (B), and TNF-α (C). Data is expressed as means ± SEM. Group comparisons were drawn using one-way ANOVA, followed by the Student-Newman-Keuls post-hoc test; * *P*-value < 0.05 (relative to the LPS-activated group); $ *P*-value < 0.05 (relative to negative [untreated] controls); # *P*-value < 0.05 (BRD0705 at any given concentration relative to BRD3731 at the corresponding concentration).

3.12. Effect of GSK3 inhibitors on the nuclear translocation of Nrf2, β-catenin, and the p65 subunit of NF-κB in LPS-activated SIM-A9 cells

To probe into the mechanistic underpinnings of the observed anti-inflammatory and anti-oxidative effects of GSK3 inhibition, nuclear protein lysates extracted from treated SIM-A9 cells were analyzed by immunoblotting for a quantitative assessment of the levels of Nrf2 and NF-κB p65 in the nucleus. The experiment was to inform whether the modulatory effects of GSK3 inhibition occur via facilitating the translocation of Nrf2 and the p65 subunit of NK-κB into the nuclear compartment, thereby promoting the transcription of their downstream targets. Figure 3.12 shows images of the immunoblots and the derived graphical representations outlining the treatment-associated modulatory trends. Nrf2 immunoblots revealed an 86.83% increase in nuclear Nrf2 in LPS-stimulated cells concurrently treated with the GSK3β inhibitor, BRD3731 (118.04% increase relative to untreated controls). LPS-stimulated cells treated with the non-selective GSK3 inhibitor, BRD0320, demonstrated a 61.4% increase in nuclear Nrf2 (88.36% increase relative to untreated controls), while BRD0705 (GSK3α inhibitor) raised the nuclear content of Nrf2 by 39.34% compared to cells treated with LPS only (62.62% more than the nuclear Nrf2 levels of untreated controls). SFN, an established electrophilic activator of Nrf2, brought about a 67.06% increase in nuclear Nrf2 compared to LPS-stimulated cells and a 94.97% increase compared to untreated controls. NF-κB immunoblots displayed a contrary trend, where GSK3 inhibition correlated with diminished nuclear levels of NF-κB p65. LPS-stimulated SIM-A9 microglia accumulated more NF-κB p65 in their nuclei (64.17% increase); SFN lowered this augmentation by 74.44%. Again, GSK3β inhibition by BRD3731 exhibited an unmatched anti-inflammatory tendency with an 82.69% drop in nuclear NF-κB p65. Pan-inhibition of GSK3 by BRD0320 in LPS-stimulated cells correlated with a 35.32% decrease in nuclear NF-κB p65. BRD0705 (GSK3α inhibitor) had almost no effect on NF-κB p65 nuclear translocation, with only a 4.01% reduction in the nuclear content of the p65 subunit. Unlike the discrepancy above outlined for Nrf2, the functional unevenness displayed by the densitometric analysis was substantiated by the statistical analysis of the data, where differences between BRD0705 (GSK3α inhibitor) and BRD3731 (GSK3β inhibitor) were statistically meaningful, as well as BRD3731 (GSK3β inhibitor) and BRD0320 (GSK3α/β inhibitor). Wherever comparisons were drawn between BRD0705 (GSK3α inhibitor) and BRD0320 (GSK3α/β inhibitor), differences therewith were determined to be statistically

inconsequential. The same statistical outcome was replicated in the analysis of data from β-catenin blots, where BRD3731 (GSK3β inhibitor) was the only GSK3 inhibitor to mediate a significant increase of β-catenin in the nucleus.

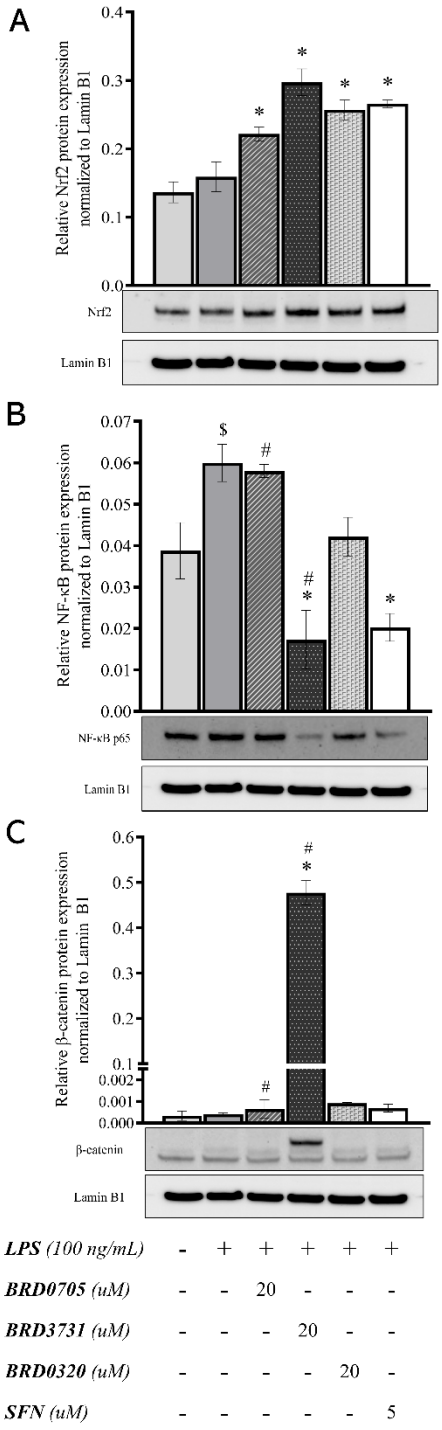

Figure 3.12. Effect of GSK3 inhibitors on the nuclear translocation of Nrf2, β-catenin, and the p65 subunit of NF-κB in LPS-stimulated SIM-A9 cells. Western immunoblots and derived graphical representation of the protein expression pattern for Nrf2 (A), NF-κB p65 (B), and β-catenin (C) are shown. Data is expressed as means ± SEM. Group comparisons were drawn using one-way ANOVA, followed by the Student-Newman-Keuls post-hoc test; * *P*-value < 0.05 (relative to the LPS-stimulated group); $ *P*-value < 0.05 (relative to negative [untreated] controls) ; # *P*-value < 0.05 (BRD0705 at any given concentration relative to BRD3731 at the corresponding concentration).

3.13. Efficiency of DsiRNA-mediated transfection of SIM-A9 cells

To determine whether the anti-inflammatory effect of the GSK-3 inhibitors was Nrf2-dependent, DsiRNA-mediated knockdown of Nrf2 was pursued as described in the "Materials and methods" section. Robustness of the transfection protocol was ascertained in two ways; first, SIM-A9 cells were reverse-transfected with a transfection control DsiRNA, tagged with TYE 563. As evident in Figure 3.13.1A and Figure 3.13.1B, only transfected cells showed fluorescence as soon as 6 h post-transfection in comparison with non-transfected control cells. Transfected cells were noted to exhibit an elongated shape rather than the predominantly rounded morphology of their non-transfected counterparts. For a quantitative assessment of transfection efficiency, an HPRT-targeting positive control DsiRNA was transduced into the cells; HPRT mRNA expression was thereafter assessed, 24 hr post-transfection. In cells transfected with the positive control DsiRNA, HPRT was silenced by 93.33% compared to cells transfected with a non-targeting negative control DsiRNA (Figure 3.13.1C). Following the same protocol, in two separate experiments, successful knockdown of Nrf2 was achieved in treatment-naïve cells, as indicated by post-transfection qPCR, with an efficiency of 87.26% (Figure 3.13.1D) and 88.47% (Figure 3.13.2) compared to cells transfected with a non-targeting negative control DsiRNA (Figure 3.13.1D). Knockdown efficiency across all treatment groups were subsequently determined and ranged between 81.39% to 88.47% (Figure 3.13.2).

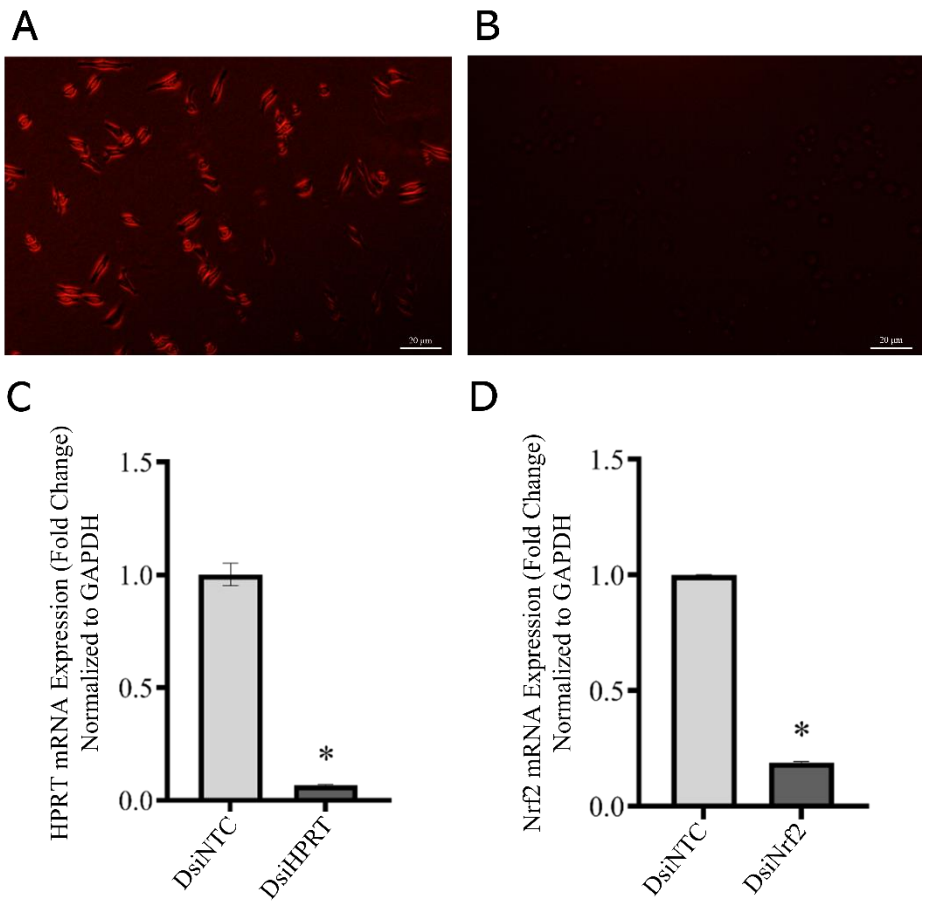

Figure 3.13.1. Efficiency of DsiRNA-mediated transfection of SIM-A9 cells. Qualitative evaluation of the transfection protocol shows fluorescence of cells transfected with TYE 563-tagged DsiRNA (A) as opposed to untransfected cells (B), which do not manifest any discernable fluorescence. Efficiency of transfection was gauged by quantitative measurement of HPRT mRNA expression, following transduction of cells with the positive control HPRT-targeting DsiRNA (C). Silencing of Nrf2 was similarly confirmed by qPCR (D), following transfection of Nrf2-targeting DsiRNAs into cells. Data is expressed as means ± SEM. Group comparisons were drawn using Welch's t-test; * *P*-value < 0.05 (relative to the NTC group).

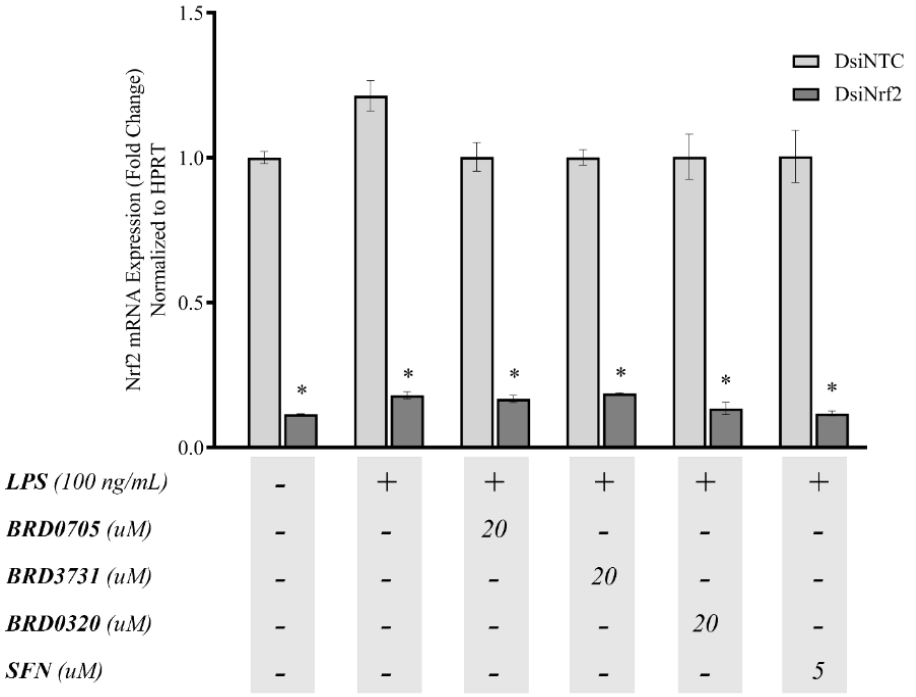

Figure 3.13.2. Knockdown efficiency of Nrf2 in DsiNrf2-transfected SIM-A9 cells. Real-time qPCR data showing the expression of Nrf2 in DsiNrf2-transfected SIM-A9 cells relative to their DsiNTC-transfected controls. Nrf2 knockdown efficiency in the DsiNrf2-transfected cells is expressed as the % decrease of Nrf2 expression in the corresponding siNTC-transfected cells. Data is expressed as means ± SEM. Comparisons between each DsiNTC and its respective DsiNrf2 were drawn using Welch's t-test; * *P*-value < 0.05 (relative to the DsiNTC group).

3.14. Effect of GSK3 inhibitors on the mRNA expression of Nrf2-driven ARE genes HO-1 and Osgin1 in DsiNrf2-transfected, LPS-activated SIM-A9 cells

As explained above, Nrf2 mRNA expression was determined to considerably drop, following DsiNrf2-mediated gene silencing. To confirm a corresponding transcriptional restriction of ARE genes, HO-1 and Osgin1 were re-assessed by qPCR, following knockdown of their transcriptional activator. The generated qPCR data suggests that there was no significant difference in HO-1 and Osgin1 mRNA expression between untreated controls, LPS-activated and LPS/GSK-3 inhibitor-treated groups (Figure 3.14). As with previous qPCR experiments, the Nrf2-activating capability of the GSK3 inhibitors was assessed in the proinflammatory (LPS-activated) context, i.e., expression in the GSK3 inhibitor-treated groups was compared to the LPS-activated group, rather than the untreated controls.

In the cells in which Nrf2 was silenced (DsiNrf2 group), BRD0705 (GSK3α inhibitor)-mediated induction of HO-1 and Osgin1 was reduced by 34.4% and 18.94%, respectively, relative to groups receiving a non-targeting negative control DsiRNA (DsiNTC). The Nrf2-inducing activity of BRD3731 (GSK3β inhibitor) noted in the DsiNTC group (122.73% increase in HO-1 and 152.42% increase in Osgin1) was likewise compromised by 119.51% for HO-1 and by 151% for Osgin1 in the DsiNrf2 group. BRD0320 (GSK3α/β inhibitor) also lost its Nrf2-activating functionality as evidenced by a 66.37% and a 69.81% drop in HO-1 and Osgin1 mRNA expression, respectively. SFN, a well-recognized Nrf2 activator, lost its ability to induce these Nrf2 targets by 195.12% for HO-1 and 348.82% for Osgin1, a substantial reversal of effect, given its remarkable efficacy in stimulating the transcription of these targets in the DsiNTC group (198.1% and 350.3% upregulation of HO-1 and Osgin1, respectively). Collectively, a loss of the anti-oxidative upregulation of HO-1 and Osgin1 by the GSK3 inhibitors was noted in Nrf2 knockdowns (DsiNrf2) compared to controls (DsiNTC).

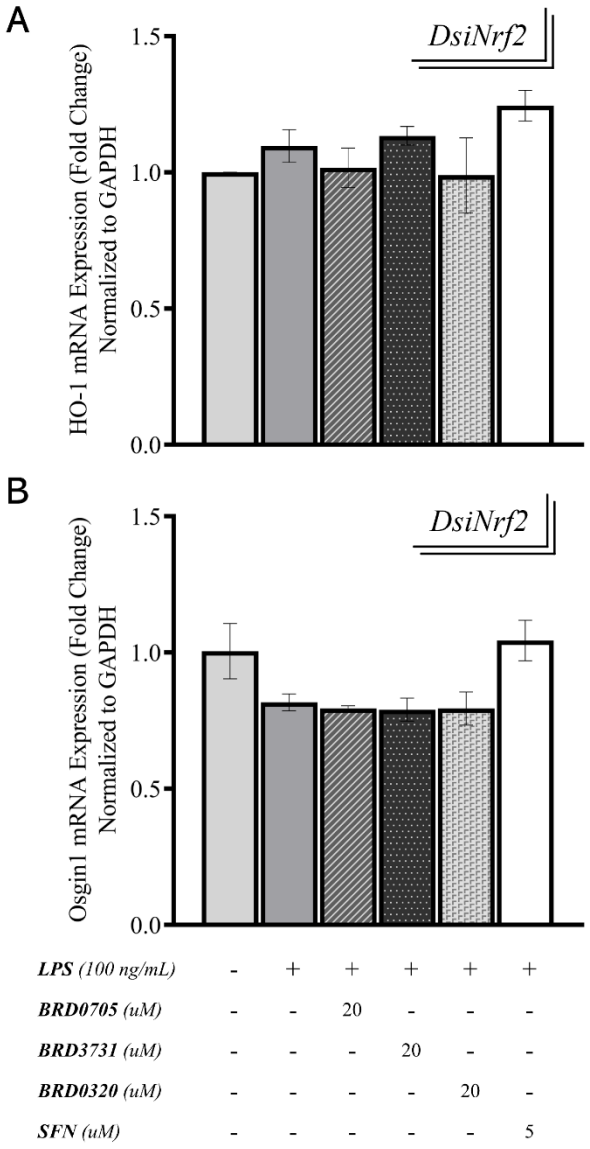

Figure 3.14. Effect of GSK3 inhibitors on the mRNA expression of Nrf2-driven ARE genes HO-1 and Osgin1 in DsiNrf2-transfected, LPS-activated SIM-A9 cells. Both HO-1 (A) and Osgin1 (B) only exhibit basal levels of expression following knockdown of Nrf2 and are not affected by any of the treatments in any manner of significance. Data is expressed as means ± SEM. Group comparisons were drawn using one-way ANOVA, followed by the Student-Newman-Keuls post-hoc test, and relay no intergroup statistical significance (*P*-value > 0.05).

3.15. Effect of GSK3 inhibitors on the mRNA expression of the proinflammatory mediators iNOS, IL-1β, IL-6 and TNF-α in DsiNrf2-transfected, LPS-stimulated SIM-A9 cells.

Having confirmed post-knockdown transcriptional suppression of Nrf2-driven genes, transcripts for proinflammatory genes were quantified by qPCR in the DsiNrf2 groups to determine whether Nrf2 silencing would compromise the above-proven anti-inflammatory function of the GSK3 inhibitors. Overall, previously relayed expression patterns remained unchanged. Reduction of iNOS mRNA expression in the DsiNrf2 group amounting to only 3.26% (BRD0705; GSK3α inhibitor), 2.34% (BRD3731; GSK3β inhibitor), 1.68% (BRD0320; GSK3α/β inhibitor) and 2.64% (SFN) of corresponding expression trends in the DsiNTC group suggested no overlap between GSK3-mediated Nrf2 activation and its repressive influence on iNOS transcription (Figure 3.15). Comparisons of treatment groups in which Nrf2 was silenced (DsiNrf2) and those in which Nrf2 expression was maintained at its basal levels (DsiNTC) determined lack of any statistical significance of the observed intergroup changes, while analysis of variations across treatments confirmed the soundness of thus far proven BRD3731 (GSK3β inhibitor) superiority to BRD0705 (GSK3α inhibitor) and BRD0320 (GSK3α/β inhibitor).

Conforming to the preceding modulatory tendency, transcription rates for IL-1β, IL-6 and TNF-α were largely analogous between the DsiNrf2 and DsiNTC groups (Figure 3.15). This was demonstrable by both the statistical and biological insignificance of the expression pattern differences between both groups. The GSK3 inhibitors comparably reversed LPS-augmented mRNA levels of the screened proinflammatory cytokines. IL-1β mRNA expression in the DsiNrf2 group only decreased by 1.68% (BRD0705; GSK3α inhibitor), 2.71% (BRD3731; GSK3β inhibitor), 2.71% (BRD0320; GSK3α/β inhibitor), and 0.04% (SFN), compared to the DsiNTC group. In relation to the DsiNTC group, levels of IL-6 mRNA in the DsiNrf2 group merely differed by 2.94% (BRD0705; GSK3α inhibitor), 2.65% (BRD3731; GSK3β inhibitor), 7.7% (BRD0320; GSK3α/β inhibitor), and 3.59% (SFN). The DsiNTC group came ahead of the DsiNrf2 group with only 1.15% (BRD0705; GSK3α inhibitor), 4.87% (BRD3731; GSK3β inhibitor), 2.03% (BRD0320), and 3.18% (SFN) higher TNF-α mRNA expression. Collectively and unlike observations made with the anti-oxidative genes HO-1 and Osgin1, the anti-inflammatory effects

of GSK3 inhibition were unaffected by Nrf2 silencing, as conveyed by the consistent expression patterns of proinflammatory markers between the DsiNrf2 and DsiNTC groups. Comparisons drawn between BRD0705 (GSK3α inhibitor), BRD3731 (GSK3β inhibitor) and BRD0320 (GSK3α/β inhibitor) once again informed of the statistical import of the differences detected therewith.

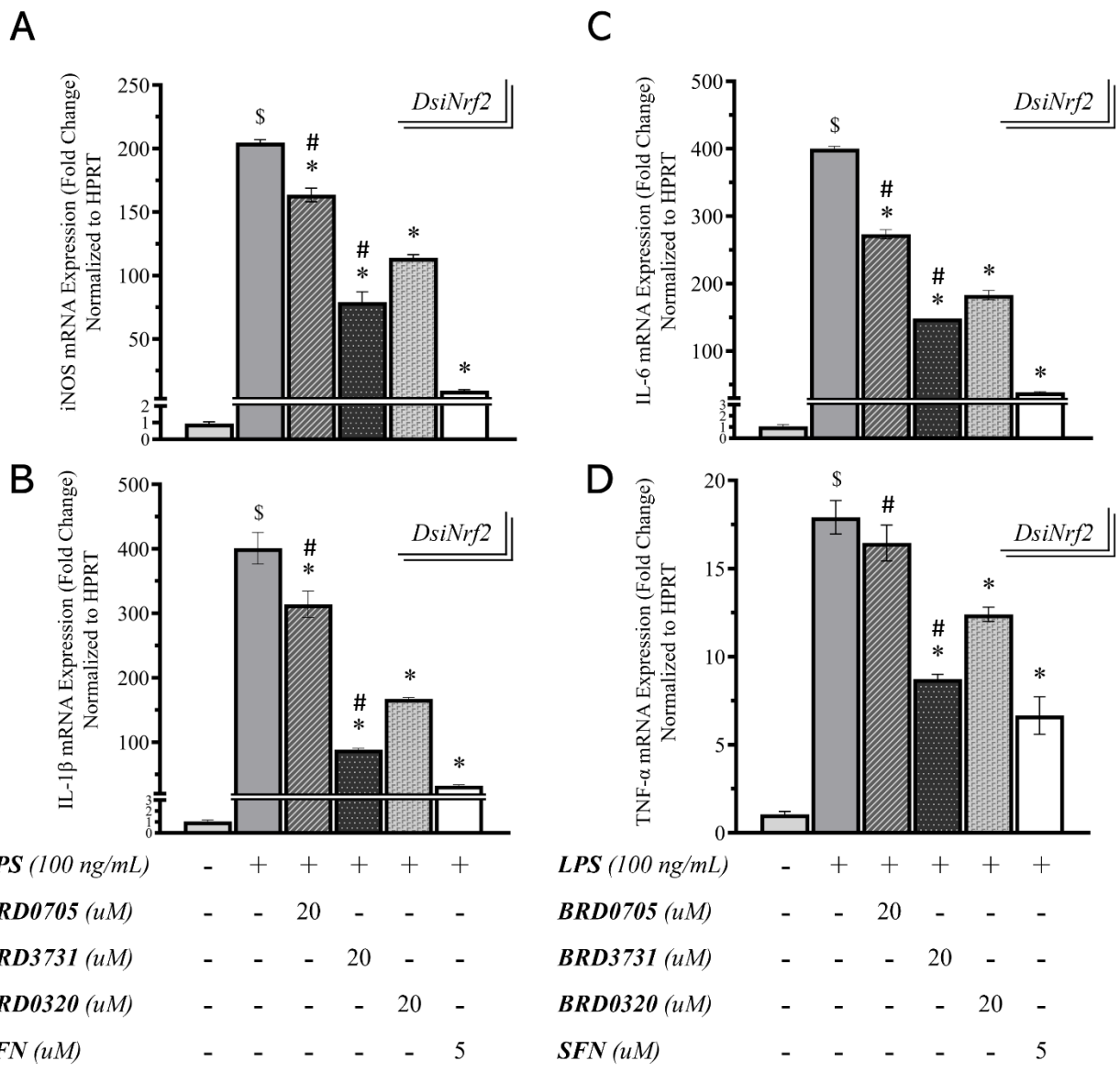

Figure 3.15. Effect of GSK3 inhibitors on the mRNA expression of the proinflammatory mediators iNOS, IL-1β, IL-6 and TNF-α in DsiNrf2-transfected, LPS-stimulated SIM-A9 cells. Target mRNA expression was quantified by real-time qPCR and normalized to HPRT. GSK3 inhibitors are shown to maintain the same pre-knockdown modulatory pattern of iNOS (A), IL-1β (B), IL-6 (C) and TNF-α (D) expression, following Nrf2 knockdown. No significance, biological or statistical, was observed between the modulatory trends effected by GSK3 inhibitors in DsiNrf2 vs DsiNTC. Data is expressed as means ± SEM. Group comparisons were drawn using one-way ANOVA, followed by the Student-Newman-Keuls post-hoc test; * *P*-value < 0.05 (relative to the LPS-stimulated group); $ *P*-value < 0.05 (relative to negative [untreated] controls); # *P*-value < 0.05 (BRD0705 at any given concentration relative to BRD3731 at the corresponding concentration).

4. DISCUSSION

Neuroinflammatory glial responses are a central component and often an inciting factor of degenerative changes in the CNS. Oxidative stress and accompanying low-grade chronic inflammation lie at the heart of the oxidative, para-inflammatory paradigm of aging and has been recently recognized as a significant yet largely overlooked pathophysiological arm of NDs. Microglia are the primary line of defense of the innate immunity in the CNS and their deprivation of hematopoietic renewal renders them particularly vulnerable to stress-induced senescence and consequent pro-degenerative deregulation of their housekeeping role. As extensively explained above, microglia have been implicated in the pathophysiological underpinnings of the most notorious NDs. Chronically activated and oxidatively stressed microglia are major aggravators of degenerative neuronal damage and their frequently exaggerated proinflammatory response often results in further disease dissemination leading to further glial dysfunction and worsening of neuronal detrition. In theory, this anomalous proinflammatory stance can either originate in microglia and go on to engender neuronal damage or may occur in consequence of neuronal pathology, which microglial incompetence can then exacerbate and end up further propagating in their fraught attempts to clear the pathological stimulus. As it happens, the heterogeneity of microglial subsets and the constant and elaborate crosstalk between neural subsets is too complex to draw clear-cut etiological models or isolate a single directional sequence of events with any degree of certainty. Modulation of activated microglial subsets, however, constitutes an increasingly sought after mitigative strategy, irrespective of the etiological precedence of pathological changes within microglia.

GSK3 has been recognized as the principal kinase to mediate tau hyperphosphorylation as well as – albeit not as fundamentally – amyloidopathy in neurons. Additionally, it has been proven to encourage the frenetic proinflammatory alias of microglia. This is particularly germane within chronically stressed microglia. Given that GSK3 is one of the key negative regulators of Nrf2, the redox master of the cell, the regulatory loop therein poses great relevance to the involvement of GSK3 in NDs, not just through its proteopathic influence, but by way of instigating oxidative stress in microglial cells. Moreover, the molecular cooperativity between GSK3 and NF-κB, a major

inflammatory player, and the inverse relationship between the latter and Nrf2 suggests a pro-oxidative, proinflammatory GSK3/NF-κB/Nrf2 regulatory loop.

As such, we theorized that inhibitory targeting of GSK3 could pose a multimodal therapeutic strategy in NDs, since not only will it check the production of toxic protein forms, but also, it should activate counter-oxidative mechanisms and repress subcellular inflammatory processes in neurons and neuroglia. It was under this conception that we sought to explore the effects of GSK3 inhibition in activated microglia in relation to NF-κB and Nrf2. Moreover, driven by the lack of research endeavors characterizing the functional differences between GSK3 isoforms, especially in relation to microglial Nrf2 activation and NF-κB-driven inflammation, we aimed to explore the differences between selective inhibition of these isoforms in terms of anti-oxidative and anti-inflammatory potential.

We chose a simple but reliable *in vitro* model for a reductionistic examination of the differences between such paralog-selective inhibition. Unlike microglial cell lines generated via viral transduction, such as BV2 and N9, SIM-A9 cells are spontaneously immortalized microglia derived from murine cerebral cortices (Nagamoto-Combs et al., 2014). SIM-A9 cells were found to retain microglial features for up to 40 passages (Dave et al., 2020), without genetic or pharmacological manipulation (Nagamoto-Combs et al., 2014). Given the above and as per various reports herein cited as well as the American Type Culture Collection (ATCC), SIM-A9 cells are expected to better emulate primary microglia than their virally or pharmacologically transformed counterparts (Nagamoto-Combs et al., 2014). LPS has been previously used to activate microglia and promote p-tau in animal models of AD (Desforges et al., 2012) and was therefore used as an alternative to recombinant cytotoxic tau oligomers to stimulate activation of SIM-A9 cells in this study, while still maintaining pertinence to the pathological context in question.

A patented GSK3 inhibitor kit developed by a team at Broad Institute Inc. (Wagner et al., 2018) was used for paralog-selective inhibition of GSK3, where BRD0705 was used as a GSK3α-selective inhibitor, BRD3731 served as our GSK3β-selective inhibitor and BRD0320 employed for non-selective inhibition of GSK3. As the traditional go-to positive control for Nrf2 activation, SFN was chosen for the purpose in this study. Based on previous work in our lab (Saleh et al.,

2021), a concentration of 5 μM was used as a positive control for an anti-inflammatory treatment as well.

First, viability of SIM-A9 cells was assessed by the MTT assay following a 24 h incubation with the investigational compounds to determine non-cytotoxic concentrations. The range of concentrations used was decided based on the original published work in which these compounds were tested. As such, viability was determined at the 10 μM, 20 μM, 40 μM and 80 μM concentrations. The 80 μM concentration was not to be tested beyond viability experiments, since it was reported to be the threshold concentration at which the compounds lose paralog-specificity (Wagner et al., 2018); it was, however, included in the MTT assays to widen the breadth of the therapeutic window of the compounds and corroborate the safety of lower concentrations, with relative certainty. As evident by the results, none of the compounds showed any meaningful cytotoxicity with maximal loss of viability recorded for 80 μM BRD3731 (GSK3β inhibitor) at 6.17% (93.83% viability compared to untreated controls).

To determine the LPS concentration that correlated with maximal microglial activation and the least cytotoxicity, incrementally increasing concentrations of LPS (10 ng/mL, 100 ng/mL, 1 μg/mL) were evaluated by the MTT assay for cytotoxicity following measurement of cellular nitrite production on exposure to LPS, which was employed as a provisional prefiguration for microglial activation. SIM-A9 cells seeded at densities of 0.5×10^5 cells/mL and 1×10^5 cells/mL were found to be largely unresponsive to LPS at all concentrations. Therefore, and again informed by previous results from our lab (Saleh et al., 2021), we opted to optimize cellular concentrations, evaluating nitrite concentration and hence microglial activation at cellular densities of 2.5×10^5 cells/mL and 5×10^5 cells/mL. Overall, variability of both the seeding density and LPS concentrations significantly affected the activation of SIM-A9 cells as revealed by our analysis, where the interaction of the two factors accounted for 20.72% of the total variance. According to our statistical analysis of the data, there was less than 0.01% chance of observing so much interaction in an experiment of this size (P-value < 0.0001) or bigger. LPS was determined to account for 27.31% of the total variance, while seeding density accounted for 51.35%. As demonstrated in Figure 3.4, a cell density of 5×10^5 cells/mL correlated with the highest response to LPS stimulation. While 10 ng/mL LPS was sufficient to occasion a significant rise in nitrite

concentration, a dose-dependent effect was noted as observed by the nitrite production levels recorded for the 100 ng/mL (560.43% increase in nitrite) and 1 μg/mL (650.8% increase in nitrite) concentrations. Given that LPS was significantly cytotoxic to SIM-A9 cells at 1 μg/mL (46.75% drop in cell viability), LPS at a concentration of 100 ng/mL was chosen to stimulate microglial activation throughout the rest of the study. To yet ensure uncompromised cellular viability following the intended experimental protocol, the cytotoxicity of treatment cocktails comprising 100 ng/mL LPS in addition to 10 μM, 20 μM, or 40 μM GSK3 inhibitors or 5 μM SFN was evaluated and, once again, no cytotoxicity was evident in any of the treatment groups.

Next, we proceeded to examine the nitrite-lowering effect of GSK3 inhibitors following microglial activation by LPS. Cells were pretreated with GSK3 inhibitors or SFN for 2 h before LPS exposure to give the compounds a head start (Eléonore Beurel & Jope, 2010; McAlpine & Werstuck, 2014; Park et al., 2014; M.-J. Wang et al., 2010), in order that repression of GSK3 can be permitted to take effect and the resultant signaling changes are not clouded by acute TLR4 stimulation. Following the 2 h pretreatment, the concentrations of the GSK3 compounds were maintained but LPS was included at a concentration of 100 ng/mL and the cells incubated for additional 24 h. BRD3731 (GSK3β inhibitor) was associated with a superlative nitrite-reducing competency, followed by BRD0705 (GSK3α inhibitor) and BRD0320 (GSK3α/β inhibitor). Beyond the lowest treatment concentration, the anti-nitrosative activity significantly varied between BRD0705 (GSK3α inhibitor) and BRD3731 (GSK3β inhibitor), which constitutes preliminary empirical evidence of BRD3731 functional precedency. Comparisons between BRD3731 (GSK3β inhibitor) and BRD0320 (GSK3α/β inhibitor) were not suggestive of a substantial difference in nitrite-reducing capacity due to paralog selectivity, and only at the highest treatment concentrations were differences between BRD0705 (GSK3α inhibitor) and BRD0320 (GSK3α/β inhibitor) determined of statistical import. These results entail that a threshold level of GSK3β inhibition is imperative for a functional drop in nitrite. Therewith, while the differences in the nitrite-extenuating efficiency of each compound was manifest and statistically significant between the 10 μM and 20 μM concentrations, no meaningful variation in potency was noted between the 20 μM and 40 μM concentrations with any of the treatments. Therefore, we chose to eliminate the 40 μM concentration from subsequent experiments and only proceed with the 10 μM and 20 μM

concentrations, which essentially emulates the pioneering study in which these compounds were first biologically characterized (Wagner et al., 2018).

To further conceive of the anti-inflammatory potential of paralog-selective GSK3 inhibition, we set out to quantitate the transcriptional rates of several proinflammatory genes using real-time polymerase chain reaction. Firstly, the mRNA expression levels of the microglial markers CD11b (Ladeby et al., 2005; Yuskaitis et al., 2009) and Iba1 (Ohsawa et al., 2004) were determined in each treatment group. We registered a significant dose-dependent decrement of the LPS-aggravated upregulation of these markers, which complied with the modulatory trend erstwhile noted, where BRD3731 (GSK3β inhibitor) was the most competent suppressor of LPS-induced proinflammatory upset. Following BRD3731, non-selective GSK3 inhibition by BRD0320 manifested a midrange modulation of these markers and BRD0705 (GSK3α inhibitor) showed the least, albeit statistically significant – and biologically non-negligible – reductive potential. The same regulatory pattern[†] was noted with all the other inflammatory markers, namely iNOS, IL-1β, IL-6, and TNF-α. Our observations agree with earlier work, herein cited, that specifically recognizes GSK3β as the isoform forward-steering inflammatory responses; while maintaining the reliability of regulatory models in which GSK3α is central, such as findings by McAlpine and colleagues, which specify that deletion of GSK3α in myeloid cells promotes an activated "M2" phenotype (Mcalpine et al., 2015).

We next proceeded with transcript quantitation by qPCR to weigh up the effect of BRD0705 (GSK3α inhibitor), BRD3731 (GSK3β inhibitor) and BRD0320 (GSK3α/β inhibitor) on activating the transcription of the ARE genes, HO-1 and Osgin1. A reversal of the modulatory tendency was observed, where BRD3731 (GSK3β inhibitor) brought on the highest mRNA expression levels for these genes, followed by BRD0320 (GSK3α/β inhibitor) and then BRD0705 (GSK3α inhibitor). Analysis of all qPCR data indicated that the functional supremacy posed by BRD3731-mediated GSK3β-selective inhibition constituted a statistically robust paradigm. Again, our findings echo

[†] On a general note, the regulatory competency of GSK3 inhibitors differed from one marker to another, where a compound could prompt substantial changes in one molecule, but only a slight alteration in another. However, and despite the unevenness within, the pattern of regulation held across all experiments, with BRD3731 (GSK3β inhibitor) always displaying the most potency. Such discrepancies, while necessitate a deeper understanding of the mechanistic basis of action for these compounds, are not atypical of GSK3 inhibition *(Yuskaitis et al., 2009)*.

earlier reports, such as work by Cuadrado et al., that recognize GSK3β, rather than GSK3α, as a non-canonical negative regulator of Nrf2, via transcriptional activation of the ARE genes HO-1 and Osgin1 (Cuadrado, Kügler, et al., 2018).

According to Wagner, Stegmaier and colleagues, BRD0705, the GSK3α-selective inhibitor, did not affect β-catenin stabilization and was associated with interrupted β-catenin signaling (Wagner et al., 2018). Given the reported coincidence of β-catenin and Nrf2 deregulation in a number of neurodegenerative contexts (Gendy et al., 2021), documented co-dependency (Bianca Marchetti, 2020), the interplay between the Wnt/β-catenin and NF-κB signaling (B. Ma & Hottiger, 2016) and another loop involving the LPS-responsive TLR4 (Zolezzi & Inestrosa, 2017) – particularly in our investigated pathological context (Jia et al., 2019; Orellana et al., 2015) and proposed mechanistic model (Gendy et al., 2021) – we opted to investigate the activity of this transcription factor in response to our treatments. We aimed to verify the variability between the GSK3 isoforms on grounds of which these compounds were designed and which pose an added advantage in a number of disease groups, in which co-morbidities can be of concern. As such, c-Myc, a target gene of the Wnt/β-catenin signaling (Herbst et al., 2014) was quantitatively assessed by qPCR. GSK3β inhibition was found to be crucial to nuclear accumulation of β-catenin as can be extrapolated from the marked c-Myc upregulation (as well as the densitometric patterning from immunoblots of β-catenin) following BRD3731 (GSK3β inhibitor) treatment. BRD0320 (GSK3α/β inhibitor) was comparatively delimited in mediating nuclear translocation of β-catenin, and BRD0705 (GSK3α inhibitor) failed to promote any tangible increase. These findings were circumsubstantiated by statistical analysis of the data, which indicated the significance of the functional distinctions observed between BRD0705 (GSK3α inhibitor) and BRD3731 (GSK3β inhibitor). Thereafter, and having formulated a picture of the proinflammatory and oxidative transcriptional landscape following our treatment protocol, we transitioned to assess the replication of the results on the protein level. For purposes of pragmatism, only the higher concentration (20 μM) of each compound was used for all experiments onwards.

Post-treatment protein levels of the proinflammatory cytokines IL-1β, IL-6, and TNF-α were assayed via ELISA. Through optimization experiments, the cell culture supernatant was determined to contain IL-1β in sparse amounts that any dilution rendered the protein content below

the detection limit of the assay. As such, undiluted samples were used for determination of IL-1β, whereas samples for IL-6 and TNF-α were diluted 20 times over. In all three assays, BRD3731 (GSK3β inhibitor) was the most efficacious counter-inflammatory compound; BRD0320 (GSK3α/β inhibitor) significantly attenuated cytokine secretion as well, whereas BRD0705 (GSK3α inhibitor) only fairly subdued their production. Comparisons drawn between selective isoform inhibition by BRD0705 (GSK3α inhibitor) and BRD3731 (GSK3β inhibitor) were yet again statistically meaningful to have occurred by chance.

We then looked into whether blunting of GSK3 activity mediates its pro-curative outcomes through tuning the nuclear content of NF-κB and Nrf2. Analysis of nuclear lysates from the relevant treatment groups by western blotting confirmed that GSK3 inhibitors hindered the nuclear translocation of the p65 subunit of NF-κB and elicited that of Nrf2, echoing the same trend theretofore identified, where BRD3731 (GSK3β inhibitor) displayed the maximum suppressive effect for NF-κB and a remarkable Nrf2 mobilizing impetus. Dual isoform inhibition by BRD0320 considerably tempered the proinflammatory NF-κB nuclear accumulation and enhanced the buildup of the anti-oxidative Nrf2, yet not as effectively as GSK3β-selective inhibition. GSK3α-selective inhibition by BRD0705 was yet again only marginally effective at altering the levels of NF-κB or Nrf2 in the nuclear compartment.

Immunoblots were also prepared for β-catenin to determine the extent to which the compounds bear upon Wnt/β-catenin signaling. Interestingly, only samples from BRD3731 (GSK3β inhibitor)-treated cells gave a chemiluminescent signal; all other groups consistently failed to signal any discernable nuclear presence of β-catenin. We attribute such an observation to the amount of protein loaded into the gel, which was capped at 15 μg/well, given the concentration of the samples and the maximum volume/well of the NuPAGE™ 10%, Bis-Tris, 1.0 mm, Mini Protein Gels (NuPAGE® Technical Guide General Information and Protocols for Using the NuPAGE® Electrophoresis System, 2010). However, since BRD3731 (GSK3β inhibitor) is prominently competent at elevating nuclear β-catenin compared to the other compounds (Wagner et al., 2018), the levels of the β-catenin protein was high enough to show up on our blots, whereas the levels from other samples were too scarce to get picked up. Such superb paralog-selective stabilization

of β-catenin entails that BRD0705 as well as other highly selective inhibitors of GSK3α could indeed solve clinical failure of GSK3 therapies, which are largely owed to inhibitor promiscuity.

We next aimed to question the mechanistic dependency of the anti-inflammatory effects of GSK3 inhibition on Nrf2/ARE signaling. To that end, we sought to silence Nrf2 mRNAs using a pool of 3 different Nrf2-targeting DsiRNAs. Given the notoriety of macrophages for being difficult-to-transfect cells and driven by the fact that reverse transfection is often more conducive to a higher transfection efficiency, SIM-A9 cells were reverse-transfected. Success of transfection was verified by microscopical examination of cells transduced with a TYE 563-labeled DsiRNA, where the transfected cells showed bright orange fluorescence, as opposed to negative controls, which remained entirely dimmed. Changes to cellular morphology and doubling time were attributed to the inherent cytotoxicity of the transfecting reagent. With initial qualitative assessment suggesting an operative transfection protocol, we utilized an HPRT-targeting positive control DsiRNA for a quantitative determination of transfection efficiency. As suggested by post-transfection qPCR data, HPRT was silenced by 93.33% in cells transfected with the HPRT-targeting DsiRNA in comparison to cells transfected with a non-targeting negative control DsiRNA. Upon confirming the efficiency of our transfection methodology, we proceeded to knockdown Nrf2 using the above outlined methodology. Quantitation of Nrf2 mRNA by qPCR revealed a silencing efficiency ranging between 81.39% to 88.47% across the various treatment groups. Moreover, HO-1 and Osgin1 transcripts were preserved at a basal level across all treatment groups; none of the GSK3 inhibitors could upregulate the ARE genes in any considerable manner, not even BRD3731 (GSK3β inhibitor) or SFN, which signifies that our knockdown carried through to the protein level and resulted in a transcriptional limitation of its target genes.

Finally, the mRNA expression[‡] of iNOS, IL-1β, IL-6, and TNF-α was once again determined by qPCR to assess the effect of Nrf2 knockdown on the anti-inflammatory activity of the GSK3 inhibitors as conveyed by the downregulation of these markers. As ascertained by the insignificance of GSK3-mediated functional differences between the DsiNrf2 and DsiNTC groups,

[‡] Here, expression was normalized to HPRT instead of GAPDH, since the latter did not maintain a stable level of expression across all treatment group following transfection. This may be attributed to post-transfection oxidative changes to GAPDH *(Butterfield et al., 2010)* on account of Nrf2 knockdown. Moreover, in some instances, small RNAs have been proven to interfere with housekeeping genes such as GAPDH and β-actin *(Sikand et al., 2012)*.

knockdown of Nrf2 was proven non-essential to the anti-inflammatory action of the GSK3 inhibitors. This suggests that true anti-inflammatory effects of Nrf2 can best be observed in conditions of chronicity, rather than acute stimulation, where NF-κB signaling takes over, and that whenever in action, is not occurring through direct negative regulation by GSK3.

Collectively, our findings consistently showed that BRD3731 (GSK3β inhibitor) maintained anti-inflammatory and anti-oxidative prepotence over BRD0320 (GSK3α/β inhibitor) and BRD0705 (GSK3α inhibitor), the latter being middling at best. From this steady modulatory pattern, we can derive that GSK3β rather than GSK3α primarily drives inflammatory and pro-oxidative processes, and its inhibition is thus more therapeutically consequential. As such, treatments selectively targeting GSK3β (BRD3731) are likely to be of superior medicinal outcome than same-dose paralog-non-discriminating treatments (BRD0320), where GSK3β is inhibited at a rate that is only fractional of that achieved by targeted inhibition, at any given concentration. Where the dosing regimen is unchanged, treatments selectively targeting GSK3α, with no antagonism of GSK3β whatsoever, produce much milder effects, as proven by our results for BRD0705 (GSK3α inhibitor).

Notwithstanding the above, and in light of promising reports that recognize a potential remedial benefit for GSK3α in neurodegenerative/neuroinflammatory pathologies (Draffin et al., 2021; Dunning et al., 2015; Kaidanovich-Beilin et al., 2009; McAlpine et al., 2015; Phiel et al., 2003; J. Zhou et al., 2013), targeted inhibition of GSK3α should not be altogether disregarded as a therapeutic strategy, especially in disease groups of known vulnerability to β-catenin-driven pathologies, such as cancer. As evidenced by our experiments, GSK3α inhibition – despite the mediocrity of its effects when compared to GSK3β inhibition – was capable of moderating pro-pathological molecular changes. On the other hand, the superb selectivity of the BRD0705 for GSK3α combined with its inability to activate β-catenin-mediated transcription unveiled a crucial cog in the mechanistic machinery under study. Consistent with the literature (Koistinaho et al., 2011; Ougolkov & Billadeau, 2006) and as outlined in Figure 4.1., β-catenin seems to be more consequential a player in this loop than was anticipated, whereby its maximal activation by BRD03731 and absence thereof with BRD0705 coincided with attenuated NF-κB signaling and

modulation of the inflammatory response in consequence. Such an observation can be corroborated in BRD3731-treated β-catenin knockouts and constitutes a significant future corollary of this work.

Furthermore, and in keeping with previously acknowledged mechanistic models, it would also seem that GSK3 exerts its proinflammatory function directly through stimulating NF-κB signaling (Hoeflich et al., 2000) and promoting the production of proinflammatory molecules (NO, IL-1β, IL-6, and TNF-α), rather than via Nrf2/ARE signaling. The upregulated inflammatory mediators then go on to stimulate the upregulation of the microglial surface markers of activation (Avik Roy et al., 2006; X. Zhou et al., 2005). It would therefore make for a cogent argument to state that while GSK3 is a mutual modulatory factor linking NF-κB activation and Nrf2 inhibition, its regulatory effect on the two pathways is not codependent.

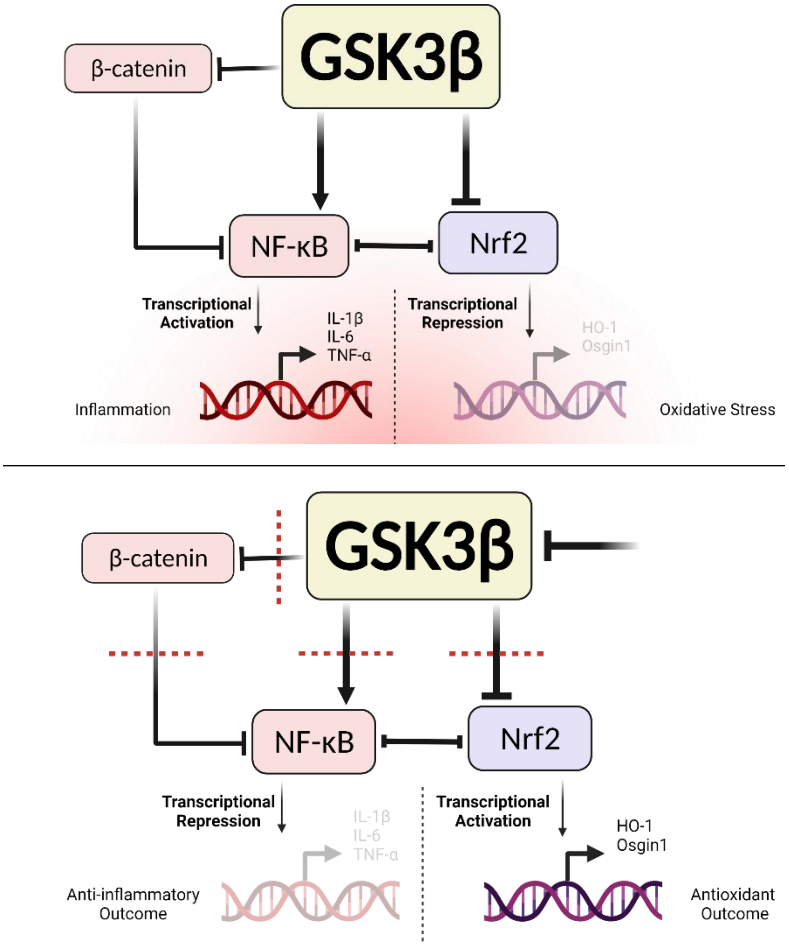

Figure 4.1. A schematic outlining the GSK3/Nrf2/NF-κB regulatory model underlying GSK3 inhibition in SIM-A9 microglia, as evinced by findings in this study.

5. CONCLUSION AND FUTURE PERSPECTIVES

Our data accentuates the significance of the dysregulated GSK3/Nrf2/NF-kB regulatory network in activated microglial cells and emphasizes the multimodal therapeutic potential of GSK3 inhibition in neurodegenerative diseases. The evidence herein provided suggests that suppression of GSK3 in activated SIM-A9 cells impart anti-inflammatory and anti-oxidative effects. Moreover, we present proof that paralog-selectivity of GSK3 inhibition is of utmost consequence to its anti-inflammatory and anti-oxidative effects, which were maximal with GSK3β-selective inhibition. This as stated earlier signifies the functional superiority of GSK3β to GSK3α, at least as far as anti-inflammatory and anti-oxidative functions are concerned.

Further examination of paralog-distinctive features within the presented regulatory network in more complex experimental constructs – such as those involving neural organoids and transgenic animal models – would be particularly beneficial since it affords the phenotypic heterogeneity of microglia and can better recapitulate the relevant molecular pathophysiological backdrop. Moreover, results of this study warrants further investigation of the utility of GSK3α-selective inhibition, especially in experimental set ups that best reiterate the pathophysiological contexts and disease groups which can benefit from a non GSK3β-targeting treatments.

Working beyond the limitations of simplistic *in vitro* systems would provide invaluable insights to the intricate crosstalk between neural subpopulations and offer a more categorical assessment of the molecular mechanisms that are most clinically relevant, which should render the findings of a more translational value.

REFERENCES

Abbott, A. (2018). Is “friendly fire” in the brain provoking Alzheimer’s disease? news-feature. *Nature*, *556*(7702), 426–428. https://doi.org/10.1038/D41586-018-04930-7

Ahmed, S. M. U., Luo, L., Namani, A., Wang, X. J., & Tang, X. (2017). Nrf2 signaling pathway: Pivotal roles in inflammation. *Biochimica et Biophysica Acta (BBA) - Molecular Basis of Disease*, *1863*(2), 585–597. https://doi.org/10.1016/J.BBADIS.2016.11.005

Ajami, B., Bennett, J. L., Krieger, C., Tetzlaff, W., & Rossi, F. M. V. (2007). Local self-renewal can sustain CNS microglia maintenance and function throughout adult life. *Nature Neuroscience 2007 10:12*, *10*(12), 1538–1543. https://doi.org/10.1038/nn2014

Ajmone-Cat, M. A., D’Urso, M. C., di Blasio, G., Brignone, M. S., De Simone, R., & Minghetti, L. (2016). Glycogen synthase kinase 3 is part of the molecular machinery regulating the adaptive response to LPS stimulation in microglial cells. *Brain, Behavior, and Immunity*, *55*, 225–235. https://doi.org/10.1016/J.BBI.2015.11.012

Akiyama, H., Barger, S., Barnum, S., Bradt, B., Bauer, J., Cole, G. M., Cooper, N. R., Eikelenboom, P., Emmerling, M., Fiebich, B. L., Finch, C. E., Frautschy, S., Griffin, W. S. T., Hampel, H., Hull, M., Landreth, G., Lue, L., Mrak, R., Mackenzie, I. R., … Wyss–Coray, T. (2000). Inflammation and Alzheimer’s disease. *Neurobiology of Aging*, *21*(3), 383. /pmc/articles/PMC3887148/

Alarcón-Aguilar, A., Luna-López, A., Ventura-Gallegos, J. L., Lazzarini, R., Galván-Arzate, S., González-Puertos, V. Y., Morán, J., Santamaría, A., & Königsberg, M. (2014). Primary cultured astrocytes from old rats are capable to activate the Nrf2 response against MPP+ toxicity after tBHQ pretreatment. *Neurobiology of Aging*, *35*(8), 1901–1912. https://doi.org/10.1016/J.NEUROBIOLAGING.2014.01.143

Avila, J., León-Espinosa, G., García, E., García-Escudero, V., Hernández, F., & Defelipe, J. (2012). Tau phosphorylation by GSK3 in different conditions. *International Journal of Alzheimer’s Disease*. https://doi.org/10.1155/2012/578373

Bachiller, S., Jiménez-Ferrer, I., Paulus, A., Yang, Y., Swanberg, M., Deierborg, T., & Boza-Serrano, A. (2018). Microglia in neurological diseases: A road map to brain-disease dependent-inflammatory response. In *Frontiers in Cellular Neuroscience* (Vol. 12, p. 488). Frontiers Media S.A. https://doi.org/10.3389/fncel.2018.00488

Bahn, G., Park, J. S. J.-S., Yun, U. J., Lee, Y. J., Choi, Y., Park, J. S. J.-S., Baek, S. H., Choi, B. Y., Cho, Y. S., Kim, H. K., Han, J. J.-W., Sul, J. H., Baik, S.-H., Lim, J., Wakabayashi, N., Bae, S. H., Han, J. J.-W., Arumugam, T. V., Mattson, M. P., & Jo, D.-G. (2019). NRF2/ARE pathway negatively regulates BACE1 expression and ameliorates cognitive deficits in mouse Alzheimer’s models. *Proceedings of the National Academy of Sciences*, *116*(25), 12516–12523. https://doi.org/10.1073/PNAS.1819541116

Baird, L., Swift, S., Llères, D., & Dinkova-Kostova, A. T. (2014). Monitoring Keap1–Nrf2 interactions in single live cells. *Biotechnology Advances*, *32*(6), 1133–1144. https://doi.org/10.1016/J.BIOTECHADV.2014.03.004

Barone, M. C., Sykiotis, G. P., & Bohmann, D. (2011). Genetic activation of Nrf2 signaling is sufficient to ameliorate neurodegenerative phenotypes in a Drosophila model of Parkinson’s disease. *Disease Models & Mechanisms*, *4*(5), 701. https://doi.org/10.1242/DMM.007575

Beggs, S., & Salter, M. W. (2016). SnapShot: Microglia in Disease. In *Cell* (Vol. 165, Issue 5,

pp. 1294-1294.e1). Cell Press. https://doi.org/10.1016/j.cell.2016.05.036
Beurel, Eleonore, Grieco, S. F., & Jope, R. S. (2015). Glycogen synthase kinase-3 (GSK3): regulation, actions, and diseases. *Pharmacology & Therapeutics*, *0*, 114. https://doi.org/10.1016/J.PHARMTHERA.2014.11.016
Beurel, Eléonore, & Jope, R. S. (2009). Lipopolysaccharide-induced interleukin-6 production is controlled by glycogen synthase kinase-3 and STAT3 in the brain. *Journal of Neuroinflammation 2009 6:1*, *6*(1), 1–11. https://doi.org/10.1186/1742-2094-6-9
Beurel, Eléonore, & Jope, R. S. (2010). Glycogen synthase kinase-3 regulates inflammatory tolerance in astrocytes. *Neuroscience*, *169*(3), 1063. https://doi.org/10.1016/J.NEUROSCIENCE.2010.05.044
Beurel, Eléonore, Jope, R. S., E, B., RS, J., Beurel, E., Jope, R. S., E, B., & RS, J. (2009). Lipopolysaccharide-induced interleukin-6 production is controlled by glycogen synthase kinase-3 and STAT3 in the brain. *Journal of Neuroinflammation 2009 6:1*, *6*(1), 1–11. https://doi.org/10.1186/1742-2094-6-9
Biase, L. M. De, Schuebel, K. E., Fusfeld, Z. H., Jair, K., Hawes, I. A., Cimbro, R., Zhang, H.-Y., Liu, Q.-R., Shen, H., Xi, Z.-X., Goldman, D., & Bonci, A. (2017). Local Cues Establish and Maintain Region-Specific Phenotypes of Basal Ganglia Microglia. *Neuron*, *95*(2), 341-356.e6. https://doi.org/10.1016/J.NEURON.2017.06.020
Boche, D., Perry, V. H., & Nicoll, J. A. R. (2013). Review: Activation patterns of microglia and their identification in the human brain. *Neuropathology and Applied Neurobiology*, *39*(1), 3–18. https://doi.org/10.1111/NAN.12011
Brandes, M. S., & Gray, N. E. (2020). NRF2 as a Therapeutic Target in Neurodegenerative Diseases: *Https://Doi.Org/10.1177/1759091419899782*, *12*. https://doi.org/10.1177/1759091419899782
Brown, G. C. (2007). Mechanisms of inflammatory neurodegeneration: iNOS and NADPH oxidase. *Biochemical Society Transactions*, *35*(5), 1119–1121. https://doi.org/10.1042/BST0351119
Butterfield, D. A., Hardas, S. S., & Lange, M. L. B. (2010). Oxidatively Modified Glyceraldehyde-3-Phosphate Dehydrogenase (GAPDH) and Alzheimer Disease: Many Pathways to Neurodegeneration. *Journal of Alzheimer's Disease : JAD*, *20*(2), 369. https://doi.org/10.3233/JAD-2010-1375
Calder, P. C., Bosco, N., Bourdet-Sicard, R., Capuron, L., Delzenne, N., Doré, J., Franceschi, C., Lehtinen, M. J., Recker, T., Salvioli, S., & Visioli, F. (2017). Health relevance of the modification of low grade inflammation in ageing (inflammageing) and the role of nutrition. *Ageing Research Reviews*, *40*, 95–119. https://doi.org/10.1016/J.ARR.2017.09.001
Carvalho, C., Santos, M. S., Oliveira, C. R., & Moreira, P. I. (2015). Alzheimer's disease and type 2 diabetes-related alterations in brain mitochondria, autophagy and synaptic markers. *Biochimica et Biophysica Acta (BBA) - Molecular Basis of Disease*, *1852*(8), 1665–1675. https://doi.org/10.1016/J.BBADIS.2015.05.001
Chen, M., & Xu, H. (2015). Parainflammation, chronic inflammation and age-related macular degeneration. *Journal of Leukocyte Biology*, *98*(5), 713. https://doi.org/10.1189/JLB.3RI0615-239R
Chen, P.-C., Vargas, M. R., Pani, A. K., Smeyne, R. J., Johnson, D. A., Kan, Y. W., & Johnson, J. A. (2009). Nrf2-mediated neuroprotection in the MPTP mouse model of Parkinson's disease: Critical role for the astrocyte. *Proceedings of the National Academy of Sciences of the United States of America*, *106*(8), 2933. https://doi.org/10.1073/PNAS.0813361106

Chen, X., Hu, Y., Cao, Z., Liu, Q., & Cheng, Y. (2018). Cerebrospinal Fluid Inflammatory Cytokine Aberrations in Alzheimer's Disease, Parkinson's Disease and Amyotrophic Lateral Sclerosis: A Systematic Review and Meta-Analysis. *Frontiers in Immunology*, *9*(SEP). https://doi.org/10.3389/FIMMU.2018.02122

Chen, Z., & Trapp, B. D. (2016). Microglia and neuroprotection. *Journal of Neurochemistry*, *136*, 10–17. https://doi.org/10.1111/jnc.13062

Cheng, Y., Wang, C., Huang, W., Tsai, C., Chen, C., Shen, C., Chi, C., & Lin, C. (2009). Staphylococcus aureus induces microglial inflammation via a glycogen synthase kinase 3beta-regulated pathway. *Infection and Immunity*, *77*(9), 4002–4008. https://doi.org/10.1128/IAI.00176-09

Chitnis, T., & Weiner, H. L. (2017). CNS inflammation and neurodegeneration. *The Journal of Clinical Investigation*, *127*(10), 3577–3587. https://doi.org/10.1172/JCI90609

Chou, R. C., Kane, M., Ghimire, S., Gautam, S., & Gui, J. (2016). Treatment for Rheumatoid Arthritis and Risk of Alzheimer's Disease: A Nested Case-Control Analysis. *CNS Drugs*, *30*(11), 1111. https://doi.org/10.1007/S40263-016-0374-Z

Chowdhry, S., Zhang, Y., McMahon, M., Sutherland, C., Cuadrado, A., & Hayes, J. D. (2012). Nrf2 is controlled by two distinct β-TrCP recognition motifs in its Neh6 domain, one of which can be modulated by GSK-3 activity. *Oncogene 2013 32:32*, *32*(32), 3765–3781. https://doi.org/10.1038/onc.2012.388

Cole, A. R., Knebel, A., Morrice, N. A., Robertson, L. A., Irving, A. J., Connolly, C. N., & Sutherland, C. (2004). GSK-3 Phosphorylation of the Alzheimer Epitope within Collapsin Response Mediator Proteins Regulates Axon Elongation in Primary Neurons. *The Journal of Biological Chemistry*, *279*(48), 50176. https://doi.org/10.1074/JBC.C400412200

Colton, C. A. (2009). Heterogeneity of Microglial Activation in the Innate Immune Response in the Brain. *Journal of Neuroimmune Pharmacology 2009 4:4*, *4*(4), 399–418. https://doi.org/10.1007/S11481-009-9164-4

Cross, D. A. E., Alessi, D. R., Cohen, P., Andjelkovich, M., & Hemmings, B. A. (1995). Inhibition of glycogen synthase kinase-3 by insulin mediated by protein kinase B. *Nature 1995 378:6559*, *378*(6559), 785–789. https://doi.org/10.1038/378785a0

Cuadrado, A., Kügler, S., & Lastres-Becker, I. (2018). Pharmacological targeting of GSK-3 and NRF2 provides neuroprotection in a preclinical model of tauopathy. *Redox Biology*, *14*, 522–534. https://doi.org/10.1016/j.redox.2017.10.010

Cuadrado, A., Manda, G., Hassan, A., Alcaraz, M. J., Barbas, C., Daiber, A., Ghezzi, P., León, R., López, M. G., Oliva, B., Pajares, M., Rojo, A. I., Robledinos-Antón, N., Valverde, A. M., Guney, E., & Schmidt, H. H. H. W. (2018). Transcription Factor NRF2 as a Therapeutic Target for Chronic Diseases: A Systems Medicine Approach. *Pharmacological Reviews*, *70*(2), 348–383. https://doi.org/10.1124/PR.117.014753

Cuadrado, A., Martín-Moldes, Z., Ye, J., & Lastres-Becker, I. (2014). Transcription Factors NRF2 and NF-κB Are Coordinated Effectors of the Rho Family, GTP-binding Protein RAC1 during Inflammation. *The Journal of Biological Chemistry*, *289*(22), 15244. https://doi.org/10.1074/JBC.M113.540633

Cullinan, S. B., Gordan, J. D., Jin, J., Harper, J. W., & Diehl, J. A. (2004). The Keap1-BTB Protein Is an Adaptor That Bridges Nrf2 to a Cul3-Based E3 Ligase: Oxidative Stress Sensing by a Cul3-Keap1 Ligase. *Molecular and Cellular Biology*, *24*(19), 8477–8486. https://doi.org/10.1128/MCB.24.19.8477-8486.2004

Cunningham, C. L., Martínez-Cerdeño, V., & Noctor, S. C. (2013). Microglia Regulate the

Number of Neural Precursor Cells in the Developing Cerebral Cortex. *Journal of Neuroscience*, *33*(10), 4216–4233. https://doi.org/10.1523/JNEUROSCI.3441-12.2013

Dave, K. M., Ali, L., & Manickam, D. S. (2020). Characterization of the SIM-A9 cell line as a model of activated microglia in the context of neuropathic pain. *PLoS ONE*, *15*(4), e0231597. https://doi.org/10.1371/journal.pone.0231597

Desforges, N. M., Hebron, M. L., Algarzae, N. K., Lonskaya, I., & Moussa, C. E. H. (2012). Fractalkine mediates communication between pathogenic proteins and microglia: Implications of anti-inflammatory treatments in different stages of neurodegenerative diseases. *International Journal of Alzheimer's Disease*. https://doi.org/10.1155/2012/345472

Dinkova-Kostova, A. T., Holtzclaw, W. D., Cole, R. N., Itoh, K., Wakabayashi, N., Katoh, Y., Yamamoto, M., & Talalay, P. (2002). Direct evidence that sulfhydryl groups of Keap1 are the sensors regulating induction of phase 2 enzymes that protect against carcinogens and oxidants. *Proceedings of the National Academy of Sciences*, *99*(18), 11908–11913. https://doi.org/10.1073/PNAS.172398899

Dinkova-Kostova, A. T., Kostov, R. V., & Kazantsev, A. G. (2018). The role of Nrf2 signaling in counteracting neurodegenerative diseases. *The FEBS Journal*, *285*(19), 3576–3590. https://doi.org/10.1111/FEBS.14379

DiSabato, D., Quan, N., & Godbout, J. P. (2016). Neuroinflammation: The Devil is in the Details. *Journal of Neurochemistry*, *139*(Suppl 2), 136. https://doi.org/10.1111/JNC.13607

Dong, Y., Stewart, T., Bai, L., Li, X., Xu, T., Iliff, J., Shi, M., Zheng, D., Yuan, L., Wei, T., Yang, X., & Zhang, J. (2020). Coniferaldehyde attenuates Alzheimer's pathology via activation of Nrf2 and its targets. *Theranostics*, *10*(1), 179–200. https://doi.org/10.7150/THNO.36722

Doorn, K. J., Goudriaan, A., Blits-Huizinga, C., Bol, J. G. J. M., Rozemuller, A. J., Hoogland, P. V. J. M., Lucassen, P. J., Drukarch, B., Berg, W. D. J. van de, & Dam, A.-M. van. (2014). Increased Amoeboid Microglial Density in the Olfactory Bulb of Parkinson's and Alzheimer's Patients. *Brain Pathology*, *24*(2), 152–165. https://doi.org/10.1111/BPA.12088

Draffin, J. E., Sánchez-Castillo, C., Fernández-Rodrigo, A., Sánchez-Sáez, X., Ávila, J., Wagner, F. F., & Esteban, J. A. (2021). GSK3α, not GSK3β, drives hippocampal NMDAR-dependent LTD via tau-mediated spine anchoring. *The EMBO Journal*, *40*(2), e105513. https://doi.org/10.15252/EMBJ.2020105513

Duda, P., Wiśniewski, J., Wójtowicz, T., Wójcicka, O., Jaśkiewicz, M., Drulis-Fajdasz, D., Rakus, D., McCubrey, J. A., & Gizak, A. (2018). Targeting GSK3 signaling as a potential therapy of neurodegenerative diseases and aging. *Https://Doi.Org/10.1080/14728222.2018.1526925*, *22*(10), 833–848. https://doi.org/10.1080/14728222.2018.1526925

Dunning, C. J., McGauran, G., Willén, K., Gouras, G. K., O'Connell, D. J., & Linse, S. (2015). Direct High Affinity Interaction between Aβ42 and GSK3α Stimulates Hyperphosphorylation of Tau. A New Molecular Link in Alzheimer's Disease? *ACS Chemical Neuroscience*, *7*(2), 161–170. https://doi.org/10.1021/ACSCHEMNEURO.5B00262

Erblich, B., Zhu, L., Etgen, A. M., Dobrenis, K., & Pollard, J. W. (2011). Absence of Colony Stimulation Factor-1 Receptor Results in Loss of Microglia, Disrupted Brain Development and Olfactory Deficits. *PLOS ONE*, *6*(10), e26317. https://doi.org/10.1371/JOURNAL.PONE.0026317

Fang, X., Yu, S. X., Lu, Y., Bast, R. C., Jr., Woodgett, J. R., & Mills, G. B. (2000). Phosphorylation and inactivation of glycogen synthase kinase 3 by protein kinase A. *Proceedings of the National Academy of Sciences of the United States of America*, *97*(22), 11960. https://doi.org/10.1073/PNAS.220413597

Foresti, R., Bains, S. K., Pitchumony, T. S., De Castro Brás, L. E., Drago, F., Dubois-Randé, J. L., Bucolo, C., & Motterlini, R. (2013). Small molecule activators of the Nrf2-HO-1 antioxidant axis modulate heme metabolism and inflammation in BV2 microglia cells. *Pharmacological Research*, *76*, 132–148. https://doi.org/10.1016/J.PHRS.2013.07.010

Frame, S., & Cohen, P. (2001). GSK3 takes centre stage more than 20 years after its discovery. *Biochemical Journal*, *359*(Pt 1), 1. https://doi.org/10.1042/0264-6021:3590001

Friling, R. S., Bergelson, S., & Daniel, V. (1992). Two adjacent AP-1-like binding sites form the electrophile-responsive element of the murine glutathione S-transferase Ya subunit gene. *Proceedings of the National Academy of Sciences*, *89*(2), 668–672. https://doi.org/10.1073/PNAS.89.2.668

Furukawa, M., & Xiong, Y. (2005). BTB Protein Keap1 Targets Antioxidant Transcription Factor Nrf2 for Ubiquitination by the Cullin 3-Roc1 Ligase. *Molecular and Cellular Biology*, *25*(1), 162–171. https://doi.org/10.1128/MCB.25.1.162-171.2005

Fuse, Y., & Kobayashi, M. (2017). Conservation of the Keap1-Nrf2 System: An Evolutionary Journey through Stressful Space and Time. *Molecules 2017, Vol. 22, Page 436*, *22*(3), 436. https://doi.org/10.3390/MOLECULES22030436

Gendy, A., Soubh, A., Al-Mokaddem, A., & Kotb El-Sayed, M. (2021). Dimethyl fumarate protects against intestinal ischemia/reperfusion lesion: Participation of Nrf2/HO-1, GSK-3β and Wnt/β-catenin pathway. *Biomedicine & Pharmacotherapy*, *134*, 111130. https://doi.org/10.1016/J.BIOPHA.2020.111130

Ginhoux, F., Greter, M., Leboeuf, M., Nandi, S., See, P., Gokhan, S., Mehler, M. F., Conway, S. J., Ng, L. G., Stanley, E. R., Samokhvalov, I. M., & Merad, M. (2010). Fate mapping analysis reveals that adult microglia derive from primitive macrophages. *Science*, *330*(6005), 841–845. https://doi.org/10.1126/SCIENCE.1194637

Gopal, S., Mikulskis, A., Gold, R., Fox, R. J., Dawson, K. T., & Amaravadi, L. (2017). Evidence of activation of the Nrf2 pathway in multiple sclerosis patients treated with delayed-release dimethyl fumarate in the Phase 3 DEFINE and CONFIRM studies: *Https://Doi.Org/10.1177/1352458517690617*, *23*(14), 1875–1883. https://doi.org/10.1177/1352458517690617

Graeber, M.B., Kösel, S., Egensperger, R., Banati, R. B., Müller, U., Bise, K., Hoff, P., Möller, H. J., Fujisawa, K., & Mehraein, P. (1997). Rediscovery of the case described by Alois Alzheimer in 1911: historical, histological and molecular genetic analysis. *Neurogenetics 1997 1:1*, *1*(1), 73–80. https://doi.org/10.1007/S100480050011

Graeber, Manuel B., Li, W., & Rodriguez, M. L. (2011). Role of microglia in CNS inflammation. In *FEBS Letters* (Vol. 585, Issue 23, pp. 3798–3805). No longer published by Elsevier. https://doi.org/10.1016/j.febslet.2011.08.033

Guzman-Martinez, L., Maccioni, R. B., Andrade, V., Navarrete, L. P., Pastor, M. G., & Ramos-Escobar, N. (2019). Neuroinflammation as a common feature of neurodegenerative disorders. *Frontiers in Pharmacology*, *10*(SEP). https://doi.org/10.3389/FPHAR.2019.01008/FULL

Hagemeyer, N., Hanft, K.-M., Akriditou, M.-A., Unger, N., Park, E. S., Stanley, E. R., Staszewski, O., Dimou, L., & Prinz, M. (2017). Microglia contribute to normal

myelinogenesis and to oligodendrocyte progenitor maintenance during adulthood. *Acta Neuropathologica 2017 134:3*, *134*(3), 441–458. https://doi.org/10.1007/S00401-017-1747-1

Hanger, D. P., Anderton, B. H., & Noble, W. (2009). Tau phosphorylation: the therapeutic challenge for neurodegenerative disease. *Trends in Molecular Medicine*, *15*(3), 112–119. https://doi.org/10.1016/J.MOLMED.2009.01.003

Hanisch, U.-K., & Kettenmann, H. (2007). Microglia: active sensor and versatile effector cells in the normal and pathologic brain. *Nature Neuroscience 2007 10:11*, *10*(11), 1387–1394. https://doi.org/10.1038/nn1997

Harvey, K., & Marchetti, B. (2014). Regulating Wnt signaling: a strategy to prevent neurodegeneration and induce regeneration. *Journal of Molecular Cell Biology*, *6*(1), 1–2. https://doi.org/10.1093/JMCB/MJU002

Hayes, J., & Dinkova-Kostova, A. T. (2014). The Nrf2 regulatory network provides an interface between redox and intermediary metabolism. *Trends in Biochemical Sciences*, *39*(4), 199–218. https://doi.org/10.1016/J.TIBS.2014.02.002

Hemonnot, A.-L., Hua, J., Ulmann, L., & Hirbec, H. (2019). Microglia in Alzheimer Disease: Well-Known Targets and New Opportunities. *Frontiers in Aging Neuroscience*, *0*(JUL), 233. https://doi.org/10.3389/FNAGI.2019.00233

Heneka, M. T., Kummer, M. P., Stutz, A., Delekate, A., Schwartz, S., Vieira-Saecker, A., Griep, A., Axt, D., Remus, A., Tzeng, T.-C., Gelpi, E., Halle, A., Korte, M., Latz, E., & Golenbock, D. T. (2012). NLRP3 is activated in Alzheimer's disease and contributes to pathology in APP/PS1 mice. *Nature 2012 493:7434*, *493*(7434), 674–678. https://doi.org/10.1038/nature11729

Herbst, A., Jurinovic, V., Krebs, S., Thieme, S. E., Blum, H., Göke, B., & Kolligs, F. T. (2014). Comprehensive analysis of β-catenin target genes in colorectal carcinoma cell lines with deregulated Wnt/β-catenin signaling. *BMC Genomics 2014 15:1*, *15*(1), 1–15. https://doi.org/10.1186/1471-2164-15-74

Herzog, C., Pons Garcia, L., Keatinge, M., Greenald, D., Moritz, C., Peri, F., & Herrgen, L. (2019). Rapid clearance of cellular debris by microglia limits secondary neuronal cell death after brain injury in vivo. *Development*, *146*(9). https://doi.org/10.1242/DEV.174698

Hickman, S., Izzy, S., Sen, P., Morsett, L., & Khoury, J. El. (2018). Microglia in neurodegeneration. *Nature Neuroscience*, *21*(10), 1359. https://doi.org/10.1038/S41593-018-0242-X

Hoeflich, K. P., Luo, J., Rubie, E. A., Tsao, M.-S., Jin, O., & Woodgett, J. R. (2000). Requirement for glycogen synthase kinase-3β in cell survival and NF-κB activation. *Nature 2000 406:6791*, *406*(6791), 86–90. https://doi.org/10.1038/35017574

Hoffmeister, L., Diekmann, M., Brand, K., & Huber, R. (2020). GSK3: A Kinase Balancing Promotion and Resolution of Inflammation. *Cells*, *9*(4). https://doi.org/10.3390/CELLS9040820

Holmström, K. M., Baird, L., Zhang, Y., Hargreaves, I., Chalasani, A., Land, J. M., Stanyer, L., Yamamoto, M., Dinkova-Kostova, A. T., & Abramov, A. Y. (2013). Nrf2 impacts cellular bioenergetics by controlling substrate availability for mitochondrial respiration. *Biology Open*, *2*(8), 761–770. https://doi.org/10.1242/BIO.20134853

Hong, S., Dissing-Olesen, L., & Stevens, B. (2016). New insights on the role of microglia in synaptic pruning in health and disease. *Current Opinion in Neurobiology*, *36*, 128–134. https://doi.org/10.1016/J.CONB.2015.12.004

Hoshiko, M., Arnoux, I., Avignone, E., Yamamoto, N., & Audinat, E. (2012). Deficiency of the Microglial Receptor CX3CR1 Impairs Postnatal Functional Development of Thalamocortical Synapses in the Barrel Cortex. *Journal of Neuroscience*, *32*(43), 15106–15111. https://doi.org/10.1523/JNEUROSCI.1167-12.2012

Ichimura, Y., Waguri, S., Sou, Y., Kageyama, S., Hasegawa, J., Ishimura, R., Saito, T., Yang, Y., Kouno, T., Fukutomi, T., Hoshii, T., Hirao, A., Takagi, K., Mizushima, T., Motohashi, H., Lee, M.-S., Yoshimori, T., Tanaka, K., Yamamoto, M., & Komatsu, M. (2013). Phosphorylation of p62 Activates the Keap1-Nrf2 Pathway during Selective Autophagy. *Molecular Cell*, *51*(5), 618–631. https://doi.org/10.1016/J.MOLCEL.2013.08.003

Itoh, K., Wakabayashi, N., Katoh, Y., Ishii, T., Igarashi, K., Engel, J. D., & Yamamoto, M. (1999). Keap1 represses nuclear activation of antioxidant responsive elements by Nrf2 through binding to the amino-terminal Neh2 domain. *Genes & Development*, *13*(1), 76–86. https://doi.org/10.1101/GAD.13.1.76

Itoh, K., Wakabayashi, N., Katoh, Y., Ishii, T., O'Connor, T., & Yamamoto, M. (2003). Keap1 regulates both cytoplasmic-nuclear shuttling and degradation of Nrf2 in response to electrophiles. *Genes to Cells*, *8*(4), 379–391. https://doi.org/10.1046/J.1365-2443.2003.00640.X

Jazwa, A., Rojo, A. I., Innamorato, N. G., Hesse, M., Fernández-Ruiz, J., & Cuadrado, A. (2011). Pharmacological targeting of the transcription factor NRf2 at the basal ganglia provides disease modifying therapy for experimental parkinsonism. *Antioxidants and Redox Signaling*, *14*(12), 2347–2360. https://doi.org/10.1089/ARS.2010.3731

Jia, L., Piña-Crespo, J., & Li, Y. (2019). Restoring Wnt/β-catenin signaling is a promising therapeutic strategy for Alzheimer's disease. *Molecular Brain 2019 12:1*, *12*(1), 1–11. https://doi.org/10.1186/S13041-019-0525-5

Jiang-Shieh, Y. F., Wu, C. H., Chang, M. L., Shieh, J. Y., & Wen, C. Y. (2003). Regional heterogeneity in immunoreactive macrophages/microglia in the rat pineal gland. *Journal of Pineal Research*, *35*(1), 45–53. https://doi.org/10.1034/J.1600-079X.2003.00054.X

Jiang, Z.-Y., Chu, H.-X., Xi, M.-Y., Yang, T.-T., Jia, J.-M., Huang, J.-J., Guo, X.-K., Zhang, X.-J., You, Q.-D., & Sun, H.-P. (2013). Insight into the Intermolecular Recognition Mechanism between Keap1 and IKKβ Combining Homology Modelling, Protein-Protein Docking, Molecular Dynamics Simulations and Virtual Alanine Mutation. *PLoS ONE*, *8*(9), 75076. https://doi.org/10.1371/JOURNAL.PONE.0075076

Jimenez-Sanchez, M., Licitra, F., Underwood, B. R., & Rubinsztein, D. C. (2017). Huntington's Disease: Mechanisms of Pathogenesis and Therapeutic Strategies. *Cold Spring Harbor Perspectives in Medicine*, *7*(7), 1–22. https://doi.org/10.1101/CSHPERSPECT.A024240

Johnson, D. A., & Johnson, J. A. (2015). Nrf2—a therapeutic target for the treatment of neurodegenerative diseases. *Free Radical Biology & Medicine*, *88*(Pt B), 253. https://doi.org/10.1016/J.FREERADBIOMED.2015.07.147

Judge, A., Garriga, C., Arden, N. K., Lovestone, S., Prieto-Alhambra, D., Cooper, C., & Edwards, C. J. (2017). Protective effect of antirheumatic drugs on dementia in rheumatoid arthritis patients. *Alzheimer's & Dementia: Translational Research & Clinical Interventions*, *3*(4), 612–621. https://doi.org/10.1016/J.TRCI.2017.10.002

Jurga, A. M., Paleczna, M., & Kuter, K. Z. (2020). Overview of General and Discriminating Markers of Differential Microglia Phenotypes. *Frontiers in Cellular Neuroscience*, *0*, 198. https://doi.org/10.3389/FNCEL.2020.00198

Kaidanovich-Beilin, O., Lipina, T. V, Takao, K., van Eede, M., Hattori, S., Laliberté, C., Khan,

M., Okamoto, K., Chambers, J. W., Fletcher, P. J., MacAulay, K., Doble, B. W., Henkelman, M., Miyakawa, T., Roder, J., & Woodgett, J. R. (2009). Abnormalities in brain structure and behavior in GSK-3alpha mutant mice. *Molecular Brain 2009 2:1*, *2*(1), 1–23. https://doi.org/10.1186/1756-6606-2-35

Kamphuis, W., Kooijman, L., Schetters, S., Orre, M., & Hol, E. M. (2016). Transcriptional profiling of CD11c-positive microglia accumulating around amyloid plaques in a mouse model for Alzheimer's disease. *Biochimica et Biophysica Acta (BBA) - Molecular Basis of Disease*, *1862*(10), 1847–1860. https://doi.org/10.1016/J.BBADIS.2016.07.007

Kandar, Chandi C., Sen, D., & Maity, A. (2021). Anti-inflammatory Potential of GSK-3 Inhibitors. *Current Drug Targets*, *22*(13), 1464–1476. https://doi.org/10.2174/1389450122666210118150313

Kandar, Chandi Charan, Sen, D., Maity, A., Sen, D., Kandar, C. C., Sen, D., Maity, A., Sen, D., & Kandar, C. C. (2021). Anti-inflammatory Potential of GSK-3 Inhibitors. *Current Drug Targets*, *22*(13), 1464–1476. https://doi.org/10.2174/1389450122666210118150313

Kanninen, K., Malm, T. M., Jyrkkänen, H. K., Goldsteins, G., Keksa-Goldsteine, V., Tanila, H., Yamamoto, M., Ylä-Herttuala, S., Levonen, A. L., & Koistinaho, J. (2008). Nuclear factor erythroid 2-related factor 2 protects against beta amyloid. *Molecular and Cellular Neuroscience*, *39*(3), 302–313. https://doi.org/10.1016/J.MCN.2008.07.010

Kanno, T., Tanaka, K., Yanagisawa, Y., Yasutake, K., Hadano, S., Yoshii, F., Hirayama, N., & Ikeda, J. E. (2012). A novel small molecule, N-(4-(2-pyridyl)(1,3-thiazol-2-yl))-2-(2,4,6-trimethylphenoxy) acetamide, selectively protects against oxidative stress-induced cell death by activating the Nrf2–ARE pathway: Therapeutic implications for ALS. *Free Radical Biology and Medicine*, *53*(11), 2028–2042. https://doi.org/10.1016/J.FREERADBIOMED.2012.09.010

Katoh, Y., Itoh, K., Yoshida, E., Miyagishi, M., Fukamizu, A., & Yamamoto, M. (2001). Two domains of Nrf2 cooperatively bind CBP, a CREB binding protein, and synergistically activate transcription. *Genes to Cells*, *6*(10), 857–868. https://doi.org/10.1046/J.1365-2443.2001.00469.X

Keren-Shaul, H., Spinrad, A., Weiner, A., Matcovitch-Natan, O., Dvir-Szternfeld, R., Ulland, T. K., David, E., Baruch, K., Lara-Astaiso, D., Toth, B., Itzkovitz, S., Colonna, M., Schwartz, M., & Amit, I. (2017). A Unique Microglia Type Associated with Restricting Development of Alzheimer's Disease. *Cell*, *169*(7), 1276-1290.e17. https://doi.org/10.1016/J.CELL.2017.05.018

Kerr, F., Sofola-Adesakin, O., Ivanov, D. K., Gatliff, J., Perez-Nievas, B. G., Bertrand, H. C., Martinez, P., Callard, R., Snoeren, I., Cochemé, H. M., Adcott, J., Khericha, M., Castillo-Quan, J. I., Wells, G., Noble, W., Thornton, J., & Partridge, L. (2017). Direct Keap1-Nrf2 disruption as a potential therapeutic target for Alzheimer's disease. *PLOS Genetics*, *13*(3), e1006593. https://doi.org/10.1371/JOURNAL.PGEN.1006593

Kobayashi, A., Kang, M.-I., Okawa, H., Ohtsuji, M., Zenke, Y., Chiba, T., Igarashi, K., & Yamamoto, M. (2004). Oxidative Stress Sensor Keap1 Functions as an Adaptor for Cul3-Based E3 Ligase To Regulate Proteasomal Degradation of Nrf2. *Molecular and Cellular Biology*, *24*(16). https://doi.org/10.1128/MCB.24.16.7130-7139.2004

Kobayashi, E. H., Suzuki, T., Funayama, R., Nagashima, T., Hayashi, M., Sekine, H., Tanaka, N., Moriguchi, T., Motohashi, H., Nakayama, K., & Yamamoto, M. (2016). Nrf2 suppresses macrophage inflammatory response by blocking proinflammatory cytokine transcription. *Nature Communications 2016 7:1*, *7*(1), 1–14. https://doi.org/10.1038/ncomms11624

Koistinaho, J., Malm, T., & Goldsteins, G. (2011). Glycogen synthase kinase-3β: A mediator of inflammation in Alzheimer's disease? *International Journal of Alzheimer's Disease*. https://doi.org/10.4061/2011/129753

Kubben, N., Zhang, W., Wang, L., Voss, T. C., Yang, J., Qu, J., Liu, G.-H., & Misteli, T. (2016). Repression of the antioxidant NRF2 pathway in premature aging. *Cell*, *165*(6), 1361. https://doi.org/10.1016/J.CELL.2016.05.017

Kumar, H., HW, L., SV, M., BW, K., S, K., IS, K., & DK, C. (2012). The role of free radicals in the aging brain and Parkinson's Disease: convergence and parallelism. *International Journal of Molecular Sciences*, *13*(8), 10478–10504. https://doi.org/10.3390/IJMS130810478

Kwon, H. S., & Koh, S.-H. (2020). Neuroinflammation in neurodegenerative disorders: the roles of microglia and astrocytes. *Translational Neurodegeneration 2020 9:1*, *9*(1), 1–12. https://doi.org/10.1186/S40035-020-00221-2

Kwon, S., Ma, S., Hwang, J., Lee, S., & Jang, C. (2015). Involvement of the Nrf2/HO-1 signaling pathway in sulfuretin-induced protection against amyloid beta25-35 neurotoxicity. *Neuroscience*, *304*, 14–28. https://doi.org/10.1016/J.NEUROSCIENCE.2015.07.030

L'episcopo, F., Serapide, M., Tirolo, C., Testa, N., Caniglia, S., Morale, M., Pluchino, S., & Marchetti, B. (2011). A Wnt1 regulated Frizzled-1/β-Catenin signaling pathway as a candidate regulatory circuit controlling mesencephalic dopaminergic neuron-astrocyte crosstalk: Therapeutical relevance for neuron survival and neuroprotection. *Molecular Neurodegeneration*, *6*(1), 49–49. https://doi.org/10.1186/1750-1326-6-49

L'Episcopo, F., Tirolo, C., Testa, N., Caniglia, S., Morale, M., Cossetti, C., D'Adamo, P., Zardini, E., Andreoni, L., Ihekwaba, A., Serra, P., Franciotta, D., Martino, G., Pluchino, S., & Marchetti, B. (2010). Reactive astrocytes and Wnt/β-catenin signaling link nigrostriatal injury to repair in 1-methyl-4-phenyl-1,2,3,6-tetrahydropyridine model of Parkinson's disease. *Neurobiology of Disease*, *41*(2), 508–527. https://doi.org/10.1016/J.NBD.2010.10.023

L'Episcopo, F., Tirolo, C., Testa, N., Caniglia, S., Morale, M., Deleidi, M., Serapide, M., Pluchino, S., & Marchetti, B. (2012). Plasticity of subventricular zone neuroprogenitors in MPTP (1-methyl-4-phenyl-1,2,3,6-tetrahydropyridine) mouse model of Parkinson's disease involves cross talk between inflammatory and Wnt/β-catenin signaling pathways: functional consequences for neuropr. *The Journal of Neuroscience : The Official Journal of the Society for Neuroscience*, *32*(6), 2062–2085. https://doi.org/10.1523/JNEUROSCI.5259-11.2012

L'Episcopo, F., Tirolo, C., Testa, N., Caniglia, S., Morale, M., Impagnatiello, F., Pluchino, S., & Marchetti, B. (2013). Aging-induced Nrf2-ARE pathway disruption in the subventricular zone drives neurogenic impairment in parkinsonian mice via PI3K-Wnt/β-catenin dysregulation. *The Journal of Neuroscience : The Official Journal of the Society for Neuroscience*, *33*(4), 1462–1485. https://doi.org/10.1523/JNEUROSCI.3206-12.2013

L'Episcopo, F., Tirolo, C., Testa, N., Caniglia, S., Morale, M., Serapide, M., Pluchino, S., & Marchetti, B. (2014). Wnt/β-catenin signaling is required to rescue midbrain dopaminergic progenitors and promote neurorepair in ageing mouse model of Parkinson's disease. *Stem Cells (Dayton, Ohio)*, *32*(8), 2147–2163. https://doi.org/10.1002/STEM.1708

Ladeby, R., Wirenfeldt, M., Garcia-Ovejero, D., Fenger, C., Dissing-Olesen, L., Dalmau, I., & Finsen, B. (2005). Microglial cell population dynamics in the injured adult central nervous system. *Brain Research Reviews*, *48*(2), 196–206. https://doi.org/10.1016/J.BRAINRESREV.2004.12.009

Lastres-Becker, I., Innamorato, N. G., Jaworski, T., Rábano, A., Kügler, S., Van Leuven, F., & Cuadrado, A. (2014). Fractalkine activates NRF2/NFE2L2 and heme oxygenase 1 to restrain tauopathy-induced microgliosis. *Brain*, *137*(1), 78–91. https://doi.org/10.1093/BRAIN/AWT323

Lastres-BeckerIsabel, J., G.-Y., H., S., J., C., KüglerSebastian, RábanoAlberto, & CuadradoAntonio. (2016). Repurposing the NRF2 Activator Dimethyl Fumarate as Therapy Against Synucleinopathy in Parkinson's Disease. *Https://Home.Liebertpub.Com/Ars*, *25*(2), 61–77. https://doi.org/10.1089/ARS.2015.6549

Lauretti, E., Dincer, O., & Praticò, D. (2020). Glycogen synthase kinase-3 signaling in Alzheimer's disease. *Biochimica et Biophysica Acta (BBA) - Molecular Cell Research*, *1867*(5), 118664. https://doi.org/10.1016/J.BBAMCR.2020.118664

Lee, D. C., Rizer, J., Selenica, M.-L. B., Reid, P., Kraft, C., Johnson, A., Blair, L., Gordon, M. N., Dickey, C. A., & Morgan, D. (2010). LPS- induced inflammation exacerbates phospho-tau pathology in rTg4510 mice. *Journal of Neuroinflammation*, *7*, 56. https://doi.org/10.1186/1742-2094-7-56

Lee, G., & Leugers, C. J. (2012). Tau and Tauopathies. *Progress in Molecular Biology and Translational Science*, *107*, 263. https://doi.org/10.1016/B978-0-12-385883-2.00004-7

Lenz, K. M., & Nelson, L. H. (2018). Microglia and Beyond: Innate Immune Cells As Regulators of Brain Development and Behavioral Function. *Frontiers in Immunology*, *0*(APR), 698. https://doi.org/10.3389/FIMMU.2018.00698

Levonen, A.-L., Landar, A., Ramachandran, A., Ceasar, E. K., Dickinson, D. A., Zanoni, G., Morrow, J. D., & Darley-Usmar, V. M. (2004). Cellular mechanisms of redox cell signalling: role of cysteine modification in controlling antioxidant defences in response to electrophilic lipid oxidation products. *Biochemical Journal*, *378*(2), 373–382. https://doi.org/10.1042/BJ20031049

Leyh, J., Paeschke, S., Mages, B., Michalski, D., Nowicki, M., Bechmann, I., & Winter, K. (2021). Classification of Microglial Morphological Phenotypes Using Machine Learning. *Frontiers in Cellular Neuroscience*, *0*, 241. https://doi.org/10.3389/FNCEL.2021.701673

Li, D., Liu, Z., Chen, W., Yao, M., & Li, G. (2014). Association of glycogen synthase kinase-3β with Parkinson's disease (Review). *Molecular Medicine Reports*, *9*(6), 2043–2050. https://doi.org/10.3892/MMR.2014.2080

Li, Q., & Barres, B. A. (2017). Microglia and macrophages in brain homeostasis and disease. *Nature Reviews Immunology 2017 18:4*, *18*(4), 225–242. https://doi.org/10.1038/nri.2017.125

Li, W., Yu, S., Liu, T., Kim, J. H., Blank, V., Li, H., & Kong, A. N. T. (2008). Heterodimerization with small Maf proteins enhances nuclear retention of Nrf2 via masking the NESzip motif. *Biochimica et Biophysica Acta - Molecular Cell Research*, *1783*(10), 1847–1856. https://doi.org/10.1016/J.BBAMCR.2008.05.024

Liu, G. H., Qu, J., & Shen, X. (2008). NF-κB/p65 antagonizes Nrf2-ARE pathway by depriving CBP from Nrf2 and facilitating recruitment of HDAC3 to MafK. *Biochimica et Biophysica Acta (BBA) - Molecular Cell Research*, *1783*(5), 713–727. https://doi.org/10.1016/J.BBAMCR.2008.01.002

Liu, Y., Deng, Y., Liu, H., Yin, C., Li, X., & Gong, Q. (2016). Hydrogen sulfide ameliorates learning memory impairment in APP/PS1 transgenic mice: A novel mechanism mediated by the activation of Nrf2. *Pharmacology Biochemistry and Behavior*, *150–151*, 207–216. https://doi.org/10.1016/J.PBB.2016.11.002

Lively, S., & Schlichter, L. C. (2018). Microglia Responses to Pro-inflammatory Stimuli (LPS, IFNγ+TNFα) and Reprogramming by Resolving Cytokines (IL-4, IL-10). *Frontiers in Cellular Neuroscience*, *0*, 215. https://doi.org/10.3389/FNCEL.2018.00215

Llano, D., Li, J., Waring, J., Ellis, T., Devanarayan, V., Witte, D., & Lenz, R. (2012). Cerebrospinal fluid cytokine dynamics differ between Alzheimer disease patients and elderly controls. *Alzheimer Disease and Associated Disorders*, *26*(4), 322–328. https://doi.org/10.1097/WAD.0B013E31823B2728

Lochhead, P. A., Kinstrie, R., Sibbet, G., Rawjee, T., Morrice, N., & Cleghon, V. (2006). A Chaperone-Dependent GSK3β Transitional Intermediate Mediates Activation-Loop Autophosphorylation. *Molecular Cell*, *24*(4), 627–633. https://doi.org/10.1016/J.MOLCEL.2006.10.009

Lou, H., Jing, X., Wei, X., Shi, H., Ren, D., & Zhang, X. (2014). Naringenin protects against 6-OHDA-induced neurotoxicity via activation of the Nrf2/ARE signaling pathway. *Neuropharmacology*, *79*, 380–388. https://doi.org/10.1016/J.NEUROPHARM.2013.11.026

Lyons, A., Griffin, R. J., Costelloe, C. E., Clarke, R. M., & Lynch, M. A. (2007). IL-4 attenuates the neuroinflammation induced by amyloid-β in vivo and in vitro. *Journal of Neurochemistry*, *101*(3), 771–781. https://doi.org/10.1111/J.1471-4159.2006.04370.X

Ma, B., & Hottiger, M. O. (2016). Crosstalk between Wnt/β-Catenin and NF-κB Signaling Pathway during Inflammation. *Frontiers in Immunology*, *0*(SEP), 378. https://doi.org/10.3389/FIMMU.2016.00378

Ma, K., Guo, J., Li, L., & Liu, X. (2019). The phenotypical induction and damage effect of peptidoglycan on microglia. *International Journal of Clinical and Experimental Medicine*, *12*(9), 11497–11503.

Ma, Q. (2013). Role of Nrf2 in Oxidative Stress and Toxicity. *Annual Review of Pharmacology and Toxicology*, *53*, 401. https://doi.org/10.1146/ANNUREV-PHARMTOX-011112-140320

Manczak, M., Kandimalla, R., Yin, X., & Reddy, P. H. (2018). Hippocampal mutant APP and amyloid beta-induced cognitive decline, dendritic spine loss, defective autophagy, mitophagy and mitochondrial abnormalities in a mouse model of Alzheimer's disease. *Human Molecular Genetics*, *27*(8), 1332–1342. https://doi.org/10.1093/HMG/DDY042

Marchetti, B, & Pluchino, S. (2013). Wnt your brain be inflamed? Yes, it Wnt! *Trends in Molecular Medicine*, *19*(3), 144–156. https://doi.org/10.1016/J.MOLMED.2012.12.001

Marchetti, Bianca. (2020). Nrf2/Wnt resilience orchestrates rejuvenation of glia-neuron dialogue in Parkinson's disease. *Redox Biology*, *36*, 101664–101664. https://doi.org/10.1016/J.REDOX.2020.101664

Martin, M., Rehani, K., Jope, R. S., & Michalek, S. M. (2005). Toll-like receptor—mediated cytokine production is differentially regulated by glycogen synthase kinase 3. *Nature Immunology*, *6*(8), 777. https://doi.org/10.1038/NI1221

Mcalpine, C. S., Huang, A., Emdin, A., Banko, N. S., Beriault, D. R., Shi, Y., & Werstuck, G. H. (2015). Deletion of myeloid GSK3α attenuates atherosclerosis and promotes an M2 macrophage phenotype. *Arteriosclerosis, Thrombosis, and Vascular Biology*, *35*(5), 1113–1122. https://doi.org/10.1161/ATVBAHA.115.305438

McAlpine, C. S., Huang, A., Emdin, A., Banko, N. S., Beriault, D. R., Shi, Y., & Werstuck, G. H. (2015). Deletion of Myeloid GSK3α Attenuates Atherosclerosis and Promotes an M2 Macrophage Phenotype. *Arteriosclerosis, Thrombosis, and Vascular Biology*, *35*(5), 1113–1122. https://doi.org/10.1161/ATVBAHA.115.305438

McAlpine, C. S., & Werstuck, G. H. (2014). Protein kinase R-like endoplasmic reticulum kinase and glycogen synthase kinase-3α/β regulate foam cell formation. *Journal of Lipid Research*, *55*(11), 2320. https://doi.org/10.1194/JLR.M051094

McMahon, M., Itoh, K., Yamamoto, M., & Hayes, J. D. (2003). Keap1-dependent Proteasomal Degradation of Transcription Factor Nrf2 Contributes to the Negative Regulation of Antioxidant Response Element-driven Gene Expression *. *Journal of Biological Chemistry*, *278*(24), 21592–21600. https://doi.org/10.1074/JBC.M300931200

Meakin, P., S, C., RS, S., FB, A., SV, W., RJ, M., AT, D.-K., JF, D., JD, H., & ML, A. (2014). Susceptibility of Nrf2-null mice to steatohepatitis and cirrhosis upon consumption of a high-fat diet is associated with oxidative stress, perturbation of the unfolded protein response, and disturbance in the expression of metabolic enzymes but not with i. *Molecular and Cellular Biology*, *34*(17), 3305–3320. https://doi.org/10.1128/MCB.00677-14

Medunjanin, S., Schleithoff, L., Fiegehenn, C., Weinert, S., Zuschratter, W., & Braun-Dullaeus, R. C. (2016). GSK-3β controls NF-kappaB activity via IKKγ/NEMO. *Scientific Reports 2016 6:1*, *6*(1), 1–11. https://doi.org/10.1038/srep38553

Michell-Robinson, M. A., Touil, H., Healy, L. M., Owen, D. R., Durafourt, B. A., Bar-Or, A., Antel, J. P., & Moore, C. S. (2015). Roles of microglia in brain development, tissue maintenance and repair. *Brain*, *138*(5), 1138–1159. https://doi.org/10.1093/BRAIN/AWV066

Mills, C. D., Kincaid, K., Alt, J. M., Heilman, M. J., & Hill, A. M. (2000). M-1/M-2 Macrophages and the Th1/Th2 Paradigm. *The Journal of Immunology*, *164*(12), 6166–6173. https://doi.org/10.4049/JIMMUNOL.164.12.6166

Moi, P., Chan, K., Asunis, I., Cao, A., & Kan, Y. W. (1994). Isolation of NF-E2-related factor 2 (Nrf2), a NF-E2-like basic leucine zipper transcriptional activator that binds to the tandem NF-E2/AP1 repeat of the beta-globin locus control region. *Proceedings of the National Academy of Sciences of the United States of America*, *91*(21), 9926. https://doi.org/10.1073/PNAS.91.21.9926

Morales, I., Farías, G. A., Cortes, N., & B.Maccioni, R. (2016). Neuroinflammation and Neurodegeneration. *Update on Dementia*. https://doi.org/10.5772/64545

Morgan, D., Gordon, M. N., Tan, J., Wilcock, D., & Rojiani, A. M. (2005). Dynamic Complexity of the Microglial Activation Response in Transgenic Models of Amyloid Deposition: Implications for Alzheimer Therapeutics. *Journal of Neuropathology & Experimental Neurology*, *64*(9), 743–753. https://doi.org/10.1097/01.JNEN.0000178444.33972.E0

Morgan, M. J., & Liu, Z. (2010). Crosstalk of reactive oxygen species and NF-κB signaling. *Cell Research 2011 21:1*, *21*(1), 103–115. https://doi.org/10.1038/cr.2010.178

Motohashi, H., O'Connor, T., Katsuoka, F., Engel, J. D., & Yamamoto, M. (2002). Integration and diversity of the regulatory network composed of Maf and CNC families of transcription factors. *Gene*, *294*(1–2), 1–12. https://doi.org/10.1016/S0378-1119(02)00788-6

Nagamoto-Combs, K., Kulas, J., & Combs, C. K. (2014). A novel cell line from spontaneously immortalized murine microglia. *Journal of Neuroscience Methods*, *233*, 187–198. https://doi.org/10.1016/j.jneumeth.2014.05.021

Nahman, S., Belmaker, R., & Azab, A. N. (2011). Effects of lithium on lipopolysaccharide-induced inflammation in rat primary glia cells: *Http://Dx.Doi.Org/10.1177/1753425911421512*, *18*(3), 447–458. https://doi.org/10.1177/1753425911421512

Napetschnig, J., & Wu, H. (2013). Molecular Basis of NF-κB Signaling. *Annual Review of*

Biophysics, *42*(1), 443. https://doi.org/10.1146/ANNUREV-BIOPHYS-083012-130338
Nassar, A., & Azab, A. N. (2014). Effects of Lithium on Inflammation. *ACS Chemical Neuroscience*, *5*(6), 451–458. https://doi.org/10.1021/CN500038F
Neumann, H., Kotter, M. R., & Franklin, R. J. M. (2009). Debris clearance by microglia: an essential link between degeneration and regeneration. *Brain*, *132*(2), 288. https://doi.org/10.1093/BRAIN/AWN109
Newby, D., Prieto-Alhambra, D., Duarte-Salles, T., Ansell, D., Pedersen, L., van der Lei, J., Mosseveld, M., Rijnbeek, P., James, G., Alexander, M., Egger, P., Podhorna, J., Stewart, R., Perera, G., Avillach, P., Grosdidier, S., Lovestone, S., & Nevado-Holgado, A. J. (2020). Methotrexate and relative risk of dementia amongst patients with rheumatoid arthritis: a multi-national multi-database case-control study. *Alzheimer's Research & Therapy 2020 12:1*, *12*(1), 1–10. https://doi.org/10.1186/S13195-020-00606-5
Nimmerjahn, A., Kirchhoff, F., & Helmchen, F. (2005). Neuroscience: Resting microglial cells are highly dynamic surveillants of brain parenchyma in vivo. *Science*, *308*(5726), 1314–1318. https://doi.org/10.1126/SCIENCE.1110647
Nioi, P., Nguyen, T., Sherratt, P. J., & Pickett, C. B. (2005). The Carboxy-Terminal Neh3 Domain of Nrf2 Is Required for Transcriptional Activation. *Molecular and Cellular Biology*, *25*(24), 10895–10906. https://doi.org/10.1128/MCB.25.24.10895-10906.2005
Nolan, Y., Maher, F. O., Martin, D. S., Clarke, R. M., Brady, M. T., Bolton, A. E., Mills, K. H. G., & Lynch, M. A. (2005). Role of Interleukin-4 in Regulation of Age-related Inflammatory Changes in the Hippocampus *. *Journal of Biological Chemistry*, *280*(10), 9354–9362. https://doi.org/10.1074/JBC.M412170200
Norden, D. M., & Godbout, J. P. (2013). Review: Microglia of the aged brain: primed to be activated and resistant to regulation. *Neuropathology and Applied Neurobiology*, *39*(1), 19–34. https://doi.org/10.1111/j.1365-2990.2012.01306.x
NuPAGE ® Technical Guide General information and protocols for using the NuPAGE ® electrophoresis system. (2010, October 29). https://tools.thermofisher.com/content/sfs/manuals/nupage_tech_man.pdf
Ohsawa, K., Imai, Y., Sasaki, Y., & Kohsaka, S. (2004). Microglia/macrophage-specific protein Iba1 binds to fimbrin and enhances its actin-bundling activity. *Journal of Neurochemistry*, *88*(4), 844–856. https://doi.org/10.1046/J.1471-4159.2003.02213.X
Okun, E., Mattson, M. P., & Arumugam, T. V. (2010). Involvement of Fc Receptors in Disorders of the Central Nervous System. *Neuromolecular Medicine*, *12*(2), 164. https://doi.org/10.1007/S12017-009-8099-5
Onuska, K. M. (2020). The Dual Role of Microglia in the Progression of Alzheimer's Disease. *Journal of Neuroscience*, *40*(8), 1608–1610. https://doi.org/10.1523/JNEUROSCI.2594-19.2020
Orellana, A. M. M., Vasconcelos, A. R., Leite, J. A., Lima, L. de S., Andreotti, D. Z., Munhoz, C. D., Kawamoto, E. M., & Scavone, C. (2015). Age-related neuroinflammation and changes in AKT-GSK-3β and WNT/ β-CATENIN signaling in rat hippocampus. *Aging (Albany NY)*, *7*(12), 1094. https://doi.org/10.18632/AGING.100853
Ougolkov, A. V., & Billadeau, D. D. (2006). Targeting GSK-3: A promising approach for cancer therapy? *Future Oncology*, *2*(1), 91–100. https://doi.org/10.2217/14796694.2.1.91/ASSET/IMAGES/LARGE/GRAPHIC11.JPEG
Owyang, A., Masuda, E. S., Payan, D. G., Park, G., Lau, D., Torneros, A., Pablo, F. S., Bhamidipati, S., Singh, R., & Duncton, M. A. J. (2016). R970, A Selective Activator of

Nrf2, is Efficacious in a Murine Model of Multiple Sclerosis. *The Journal of Immunology*, *196*(1 Supplement).

Paolicelli, R. C., Bolasco, G., Pagani, F., Maggi, L., Scianni, M., Panzanelli, P., Giustetto, M., Ferreira, T. A., Guiducci, E., Dumas, L., Ragozzino, D., & Gross, C. T. (2011). Synaptic pruning by microglia is necessary for normal brain development. *Science*, *333*(6048), 1456–1458. https://doi.org/10.1126/SCIENCE.1202529

Park, D. W., Jiang, S., Liu, Y., Siegal, G. P., Inoki, K., Abraham, E., & Zmijewski, J. W. (2014). GSK3β-dependent inhibition of AMPK potentiates activation of neutrophils and macrophages and enhances severity of acute lung injury. *Https://Doi.Org/10.1152/Ajplung.00165.2014*, *307*(10), L735–L745. https://doi.org/10.1152/AJPLUNG.00165.2014

Perdiguero, E. G., Klapproth, K., Schulz, C., Busch, K., Azzoni, E., Crozet, L., Garner, H., Trouillet, C., Bruijn, M. F. de, Geissmann, F., & Rodewald, H.-R. (2015). Tissue-resident macrophages originate from yolk sac-derived erythro-myeloid progenitors. *Nature*, *518*(7540), 547. https://doi.org/10.1038/NATURE13989

Peress, N. S., Fleit, H. B., Perillo, E., Kuljis, R., & Pezzullo, C. (1993). Identification of FcγRI, II and III on normal human brain ramified microglia and on microglia in senile plaques in Alzheimer's disease. *Journal of Neuroimmunology*, *48*(1), 71–79. https://doi.org/10.1016/0165-5728(93)90060-C

Peri, F., & Nüsslein-Volhard, C. (2008). Live Imaging of Neuronal Degradation by Microglia Reveals a Role for v0-ATPase a1 in Phagosomal Fusion In Vivo. *Cell*, *133*(5), 916–927. https://doi.org/10.1016/J.CELL.2008.04.037

Perry, V. H., & Teeling, J. (2013). Microglia and macrophages of the central nervous system: the contribution of microglia priming and systemic inflammation to chronic neurodegeneration. *Seminars in Immunopathology 2013 35:5*, *35*(5), 601–612. https://doi.org/10.1007/S00281-013-0382-8

Petersen, M. A., & Dailey, M. E. (2004). Diverse microglial motility behaviors during clearance of dead cells in hippocampal slices. *Glia*, *46*(2), 195–206. https://doi.org/10.1002/GLIA.10362

Petrillo, S., Schirinzi, T., Lazzaro, G. Di, D'Amico, J., Colona, V. L., Bertini, E., Pierantozzi, M., Mari, L., Mercuri, N. B., Piemonte, F., & Pisani, A. (2020). Systemic Activation of Nrf2 Pathway in Parkinson's Disease. *Movement Disorders*, *35*(1), 180–184. https://doi.org/10.1002/MDS.27878

Phiel, C. J., Wilson, C. A., Lee, V. M.-Y., & Klein, P. S. (2003). GSK-3α regulates production of Alzheimer's disease amyloid-β peptides. *Nature 2003 423:6938*, *423*(6938), 435–439. https://doi.org/10.1038/nature01640

Prasad, K. N., & Bondy, S. C. (2016). Inhibition of Early Biochemical Defects in Prodromal Huntington's disease by Simultaneous Activation of Nrf2 and Elevation of Multiple Micronutrients. *Current Aging Science*, *9*(1), 61–70. https://doi.org/10.2174/1874609809666151124231127

Quinti, L., Naidu, S. D., Träger, U., Chen, X., Kegel-Gleason, K., Llères, D., Connolly, C., Chopra, V., Low, C., Moniot, S., Sapp, E., Tousley, A. R., Vodicka, P., Kanegan, M. J. Van, Kaltenbach, L. S., Crawford, L. A., Fuszard, M., Higgins, M., Miller, J. R. C., … Kazantsev, A. G. (2017). KEAP1-modifying small molecule reveals muted NRF2 signaling responses in neural stem cells from Huntington's disease patients. *Proceedings of the National Academy of Sciences*, *114*(23), E4676–E4685.

https://doi.org/10.1073/PNAS.1614943114
Rada, P., Rojo, A. I., Chowdhry, S., McMahon, M., Hayes, J. D., & Cuadrado, A. (2011). SCF/ -TrCP Promotes Glycogen Synthase Kinase 3-Dependent Degradation of the Nrf2 Transcription Factor in a Keap1-Independent Manner. *Molecular and Cellular Biology*, *31*(6), 1121–1133. https://doi.org/10.1128/MCB.01204-10
Raes, G., Baetselier, P. De, Noël, W., Beschin, A., Brombacher, F., & Gh., G. H. (2002). Differential expression of FIZZ1 and Ym1 in alternatively versus classically activated macrophages. *Journal of Leukocyte Biology*, *71*(4), 597–602. https://doi.org/10.1189/JLB.71.4.597
Raes, G., Noël, W., Beschin, A., Brys, L., De Baetselier, P., & Hassanzadeh, G. G. (2002). FIZZ1 and Ym as tools to discriminate between differentially activated macrophages. *Developmental Immunology*, *9*(3), 151–159. https://doi.org/10.1080/1044667031000137629
Rahal, A., Kumar, A., Singh, V., Yadav, B., Tiwari, R., Chakraborty, S., & Dhama, K. (2014). Oxidative Stress, Prooxidants, and Antioxidants: The Interplay. *BioMed Research International*, *2014*. https://doi.org/10.1155/2014/761264
Ramkumar, A., Jong, B. Y., & Ori-McKenney, K. M. (2018). ReMAPping the microtubule landscape: How phosphorylation dictates the activities of microtubule-associated proteins. *Developmental Dynamics*, *247*(1), 138–155. https://doi.org/10.1002/DVDY.24599
Ransohoff, R. M. (2016). How neuroinflammation contributes to neurodegeneration. *Science*, *353*(6301), 777–783. https://doi.org/10.1126/SCIENCE.AAG2590
Ren, P., Chen, J., Li, B., Zhang, M., Yang, B., Guo, X., Chen, Z., Cheng, H., Wang, P., Wang, S., Wang, N., Zhang, G., Wu, X., Ma, D., Guan, D., & Zhao, R. (2020). Nrf2 Ablation Promotes Alzheimer's Disease-Like Pathology in APP/PS1 Transgenic Mice: The Role of Neuroinflammation and Oxidative Stress. *Oxidative Medicine and Cellular Longevity*, *2020*. https://doi.org/10.1155/2020/3050971
Rojo, A. I., Innamorato, N. G., Martín-Moreno, A. M., Ceballos, M. L. De, Yamamoto, M., & Cuadrado, A. (2010). Nrf2 regulates microglial dynamics and neuroinflammation in experimental Parkinson's disease. *Glia*, *58*(5), 588–598. https://doi.org/10.1002/GLIA.20947
Rojo, A. I., Pajares, M., Rada, P., Nuñez, A., Nevado-Holgado, A. J., Killik, R., Leuven, F. Van, Ribe, E., Lovestone, S., Yamamoto, M., & Cuadrado, A. (2017). NRF2 deficiency replicates transcriptomic changes in Alzheimer's patients and worsens APP and TAU pathology. *Redox Biology*, *13*, 444. https://doi.org/10.1016/J.REDOX.2017.07.006
Roy, A, Jana, A., Yatish, K., Freidt, M., Fung, Y., Martinson, J., & Pahan, K. (2008). Reactive oxygen species up-regulate CD11b in microglia via nitric oxide: Implications for neurodegenerative diseases. *Free Radical Biology & Medicine*, *45*(5), 686–699. https://doi.org/10.1016/J.FREERADBIOMED.2008.05.026
Roy, Avik, Fung, Y. K., Liu, X., & Pahan, K. (2006). Up-regulation of Microglial CD11b Expression by Nitric Oxide. *The Journal of Biological Chemistry*, *281*(21), 14971. https://doi.org/10.1074/JBC.M600236200
Rushmore, T. H., Morton, M. R., & Pickett, C. B. (1991). The antioxidant responsive element. Activation by oxidative stress and identification of the DNA consensus sequence required for functional activity. *J Biol Chem*, *266*(18), 11632–11639. https://doi.org/10.1016/S0021-9258(18)99004-6
Rushworth, S. A., Zaitseva, L., Murray, M. Y., Shah, N. M., Bowles, K. M., & MacEwan, D. J. (2012). The high Nrf2 expression in human acute myeloid leukemia is driven by NF-κB and

underlies its chemo-resistance. *Blood*, *120*(26), 5188–5198. https://doi.org/10.1182/BLOOD-2012-04-422121

Saleh, H. A., Ramdan, E., Elmazar, M. M., Azzazy, H. M. E., & Abdelnaser, A. (2021). Comparing the protective effects of resveratrol, curcumin and sulforaphane against LPS/IFN-γ-mediated inflammation in doxorubicin-treated macrophages. *Scientific Reports 2021 11:1*, *11*(1), 1–16. https://doi.org/10.1038/s41598-020-80804-1

Sanada, F., Taniyama, Y., Muratsu, J., Otsu, R., Shimizu, H., Rakugi, H., & Morishita, R. (2018). Source of Chronic Inflammation in Aging. *Frontiers in Cardiovascular Medicine*, *5*, 12. https://doi.org/10.3389/FCVM.2018.00012

Schafer, D. P., Lehrman, E. K., Kautzman, A. G., Koyama, R., Mardinly, A. R., Yamasaki, R., Ransohoff, R. M., Greenberg, M. E., Barres, B. A., & Stevens, B. (2012). Microglia Sculpt Postnatal Neural Circuits in an Activity and Complement-Dependent Manner. *Neuron*, *74*(4), 691–705. https://doi.org/10.1016/J.NEURON.2012.03.026

Scolnick, E., Cottrell, J. R., Wagner, F. F., Holson, E., Lewis, M. C., Bear, M. F., Stoppel, L., & Heynen, A. (2016). *Uses of paralog-selective inhibitors of GSK3 kinases* (Patent No. US20160375006A1). https://patents.google.com/patent/US20160375006A1/en?oq=US20160375006+A1

Shinozaki, Y., Nomura, M., Iwatsuki, K., Moriyama, Y., Gachet, C., & Koizumi, S. (2014). Microglia trigger astrocyte-mediated neuroprotection via purinergic gliotransmission. *Scientific Reports 2014 4:1*, *4*(1), 1–11. https://doi.org/10.1038/srep04329

Siebert, A., Desai, V., Chandrasekaran, K., Fiskum, G., & Jafri, M. S. (2009). Nrf2 activators provide neuroprotection against 6-hydroxydopamine toxicity in rat organotypic nigrostriatal cocultures. *Journal of Neuroscience Research*, *87*(7), 1659–1669. https://doi.org/10.1002/JNR.21975

Sigfridsson, E., Marangoni, M., Hardingham, G. E., Horsburgh, K., & Fowler, J. H. (2020). Deficiency of Nrf2 exacerbates white matter damage and microglia/macrophage levels in a mouse model of vascular cognitive impairment. *Journal of Neuroinflammation 2020 17:1*, *17*(1), 1–15. https://doi.org/10.1186/S12974-020-02038-2

Sikand, K., Singh, J., Ebron, J. S., & Shukla, G. C. (2012). Housekeeping Gene Selection Advisory: Glyceraldehyde-3-Phosphate Dehydrogenase (GAPDH) and β-Actin Are Targets of miR-644a. *PLoS ONE*, *7*(10). https://doi.org/10.1371/JOURNAL.PONE.0047510

Silva-Islas, C. A., & Maldonado, P. D. (2018). Canonical and non-canonical mechanisms of Nrf2 activation. *Pharmacological Research*, *134*, 92–99. https://doi.org/10.1016/J.PHRS.2018.06.013

Simoni, E., Serafini, M. M., Caporaso, R., Marchetti, C., Racchi, M., Minarini, A., Bartolini, M., Lanni, C., & Rosini, M. (2017). Targeting the Nrf2/Amyloid-Beta Liaison in Alzheimer's Disease: A Rational Approach. *ACS Chemical Neuroscience*, *8*(7), 1618–1627. https://doi.org/10.1021/ACSCHEMNEURO.7B00100

Solovjov, D. A., Pluskota, E., & Plow, E. F. (2005). Distinct Roles for the α and β Subunits in the Functions of Integrin αMβ2*. *Journal of Biological Chemistry*, *280*(2), 1336–1345. https://doi.org/10.1074/JBC.M406968200

Song, X., Shapiro, S., Goldman, D. L., Casadevall, A., Scharff, M., & Lee, S. C. (2002). Fcγ Receptor I- and III-Mediated Macrophage Inflammatory Protein 1α Induction in Primary Human and Murine Microglia. *Infection and Immunity*, *70*(9), 5177. https://doi.org/10.1128/IAI.70.9.5177-5184.2002

Song, X., Tanaka, S., Cox, D., & Lee, S. C. (2004). Fcγ receptor signaling in primary human

microglia: differential roles of PI-3K and Ras/ERK MAPK pathways in phagocytosis and chemokine induction. *Journal of Leukocyte Biology*, *75*(6), 1147–1155. https://doi.org/10.1189/JLB.0403128

Sotolongo, K., Ghiso, J., & Rostagno, A. (2020). Nrf2 activation through the PI3K/GSK-3 axis protects neuronal cells from Aβ-mediated oxidative and metabolic damage. *Alzheimer's Research & Therapy 2020 12:1*, *12*(1), 1–22. https://doi.org/10.1186/S13195-019-0578-9

Soutar, M. P. M., Kim, W.-Y., Williamson, R., Peggie, M., Hastie, C. J., McLauchlan, H., Snider, W. D., Gordon-Weeks, P. R., & Sutherland, C. (2010). Evidence that glycogen synthase kinase-3 isoforms have distinct substrate preference in the brain. *Journal of Neurochemistry*, *115*(4), 974–983. https://doi.org/10.1111/J.1471-4159.2010.06988.X

Squarzoni, P., Oller, G., Hoeffel, G., Pont-Lezica, L., Rostaing, P., Low, D., Bessis, A., Ginhoux, F., & Garel, S. (2014). Microglia Modulate Wiring of the Embryonic Forebrain. *Cell Reports*, *8*(5), 1271–1279. https://doi.org/10.1016/J.CELREP.2014.07.042

Stambolic, V., & Woodgett, J. R. (1994). Mitogen inactivation of glycogen synthase kinase-3 beta in intact cells via serine 9 phosphorylation. *Biochemical Journal*, *303*(Pt 3), 701. https://doi.org/10.1042/BJ3030701

Stelzmann, R. A., Schnitzlein, H. N., & Murtagh, F. R. (1995). An english translation of alzheimer's 1907 paper, "über eine eigenartige erkankung der hirnrinde." *Clinical Anatomy*, *8*(6), 429–431. https://doi.org/10.1002/CA.980080612

Streit, W. J. (2002). Microglia as neuroprotective, immunocompetent cells of the CNS. *Glia*, *40*(2), 133–139. https://doi.org/10.1002/GLIA.10154

Streit, W. J., Mrak, R. E., & Griffin, W. S. T. (2004). Microglia and neuroinflammation: A pathological perspective. *Journal of Neuroinflammation*, *1*(1), 14. https://doi.org/10.1186/1742-2094-1-14

Sun, Z., Zhang, S., Chan, J. Y., & Zhang, D. D. (2007). Keap1 Controls Postinduction Repression of the Nrf2-Mediated Antioxidant Response by Escorting Nuclear Export of Nrf2. *Molecular and Cellular Biology*, *27*(18), 6334–6349. https://doi.org/10.1128/MCB.00630-07

Suschek, C., Schnorr, O., & Kolb-Bachofen, V. (2004). The role of iNOS in chronic inflammatory processes in vivo: is it damage-promoting, protective, or active at all? *Current Molecular Medicine*, *4*(7), 763–775. https://doi.org/10.2174/1566524043359908

Sutherland, C, Leighton, I. A., & Cohen, P. (1993). Inactivation of glycogen synthase kinase-3 beta by phosphorylation: new kinase connections in insulin and growth-factor signalling. *Biochemical Journal*, *296*(Pt 1), 15. https://doi.org/10.1042/BJ2960015

Sutherland, Calum. (2011). What Are the bona fide GSK3 Substrates? *International Journal of Alzheimer's Disease*, *2011*, 24. https://doi.org/10.4061/2011/505607

Svahn, A. J., Graeber, M. B., Ellett, F., Lieschke, G. J., Rinkwitz, S., Bennett, M. R., & Becker, T. S. (2013). Development of ramified microglia from early macrophages in the zebrafish optic tectum. *Developmental Neurobiology*, *73*(1), 60–71. https://doi.org/10.1002/DNEU.22039

Telakowski-Hopkins, C. A., King, R. G., & Pickett, C. B. (1988). Glutathione S-transferase Ya subunit gene: identification of regulatory elements required for basal level and inducible expression. *Proceedings of the National Academy of Sciences*, *85*(4), 1000–1004. https://doi.org/10.1073/PNAS.85.4.1000

Terwel, D., Muyllaert, D., Dewachter, I., Borghgraef, P., Croes, S., Devijver, H., & Leuven, F. Van. (2008). Amyloid Activates GSK-3β to Aggravate Neuronal Tauopathy in Bigenic

Mice. *The American Journal of Pathology*, *172*(3), 786. https://doi.org/10.2353/AJPATH.2008.070904
Thompson, K. K., & Tsirka, S. E. (2017). The Diverse Roles of Microglia in the Neurodegenerative Aspects of Central Nervous System (CNS) Autoimmunity. *International Journal of Molecular Sciences*, *18*(3). https://doi.org/10.3390/IJMS18030504
Tonelli, C., Chio, I. I. C., & Tuveson, D. A. (2018). Transcriptional Regulation by Nrf2. *Https://Home.Liebertpub.Com/Ars*, *29*(17), 1727–1745. https://doi.org/10.1089/ARS.2017.7342
Tong, K. I., Katoh, Y., Kusunoki, H., Itoh, K., Tanaka, T., & Yamamoto, M. (2006). Keap1 Recruits Neh2 through Binding to ETGE and DLG Motifs: Characterization of the Two-Site Molecular Recognition Model. *Molecular and Cellular Biology*, *26*(8), 2887–2900. https://doi.org/10.1128/MCB.26.8.2887-2900.2006
Toral-Rios, D., Pichardo-Rojas, P. S., Alonso-Vanegas, M., & Campos-Peña, V. (2020). GSK3β and Tau Protein in Alzheimer's Disease and Epilepsy. *Frontiers in Cellular Neuroscience*, *0*, 19. https://doi.org/10.3389/FNCEL.2020.00019
Townsend, B. E., & Johnson, R. W. (2016). Sulforaphane induces Nrf2 target genes and attenuates inflammatory gene expression in microglia from brain of young adult and aged mice. *Experimental Gerontology*, *73*, 42. https://doi.org/10.1016/J.EXGER.2015.11.004
Tummala, K. S., Kottakis, F., & Bardeesy, N. (2016). NRF2: Translating the Redox Code. *Trends in Molecular Medicine*, *22*(10), 829. https://doi.org/10.1016/J.MOLMED.2016.08.002
Ueno, M., Fujita, Y., Tanaka, T., Nakamura, Y., Kikuta, J., Ishii, M., & Yamashita, T. (2013). Layer V cortical neurons require microglial support for survival during postnatal development. *Nature Neuroscience 2013 16:5*, *16*(5), 543–551. https://doi.org/10.1038/nn.3358
Uruno, A., Matsumaru, D., Ryoke, R., Saito, R., Kadoguchi, S., Saigusa, D., Saito, T., Saido, T. C., Kawashima, R., & Yamamoto, M. (2020). Nrf2 Suppresses Oxidative Stress and Inflammation in App Knock-In Alzheimer's Disease Model Mice . *Molecular and Cellular Biology*, *40*(6). https://doi.org/10.1128/MCB.00467-19
User Bulletin #2 ABI PRISM 7700 Sequence Detection System. (n.d.). Retrieved October 17, 2021, from http://tools.thermofisher.com/content/sfs/manuals/cms_040980.pdf
van Roon-Mom, W. M., Pepers, B. A., 't Hoen, P. A., Verwijmeren, C. A., den Dunnen, J. T., Dorsman, J. C., & van Ommen, G. B. (2008). Mutant huntingtin activates Nrf2-responsive genes and impairs dopamine synthesis in a PC12 model of Huntington's disease. *BMC Molecular Biology 2008 9:1*, *9*(1), 1–13. https://doi.org/10.1186/1471-2199-9-84
Vargas, M. R., Johnson, D. A., Sirkis, D. W., Messing, A., & Johnson, J. A. (2008). Nrf2 Activation in Astrocytes Protects against Neurodegeneration in Mouse Models of Familial Amyotrophic Lateral Sclerosis. *The Journal of Neuroscience*, *28*(50), 13574. https://doi.org/10.1523/JNEUROSCI.4099-08.2008
Varnum, M. M., & Ikezu, T. (2012). The classification of microglial activation phenotypes on neurodegeneration and regeneration in Alzheimer's disease brain. *Archivum Immunologiae et Therapiae Experimentalis*, *60*(4), 251. https://doi.org/10.1007/S00005-012-0181-2
Velagapudi, R., El-Bakoush, A., & Olajide, O. A. (2018). Activation of Nrf2 Pathway Contributes to Neuroprotection by the Dietary Flavonoid Tiliroside. *Molecular Neurobiology 2018 55:10*, *55*(10), 8103–8123. https://doi.org/10.1007/S12035-018-0975-2
Velagapudi, R., Kumar, A., Bhatia, H. S., El-Bakoush, A., Lepiarz, I., Fiebich, B. L., & Olajide,

O. A. (2017). Inhibition of neuroinflammation by thymoquinone requires activation of Nrf2/ARE signalling. *International Immunopharmacology*, *48*, 17–29. https://doi.org/10.1016/J.INTIMP.2017.04.018

Venegas, C., Kumar, S., Franklin, B. S., Dierkes, T., Brinkschulte, R., Tejera, D., Vieira-Saecker, A., Schwartz, S., Santarelli, F., Kummer, M. P., Griep, A., Gelpi, E., Beilharz, M., Riedel, D., Golenbock, D. T., Geyer, M., Walter, J., Latz, E., & Heneka, M. T. (2017). Microglia-derived ASC specks cross-seed amyloid-β in Alzheimer's disease. *Nature 2017 552:7685*, *552*(7685), 355–361. https://doi.org/10.1038/nature25158

Wagner, F. F., Benajiba, L., Campbell, A. J., Weïwer, M., Sacher, J. R., Gale, J. P., Ross, L., Puissant, A., Alexe, G., Conway, A., Back, M., Pikman, Y., Galinsky, I., Deangelo, D. J., Stone, R. M., Kaya, T., Shi, X., Robers, M. B., Machleidt, T., … Holson, E. B. (2018). Exploiting an asp-glu "switch" in glycogen synthase kinase 3 to design paralog-selective inhibitors for use in acute myeloid leukemia. *Science Translational Medicine*, *10*(431). https://doi.org/10.1126/SCITRANSLMED.AAM8460

Walker, K. A. (2019). Inflammation and neurodegeneration: chronicity matters. *Aging (Albany NY)*, *11*(1), 3. https://doi.org/10.18632/AGING.101704

Wang, F., Lu, Y., Qi, F., Su, Q., Wang, L., You, C., Che, F., & Yu, J. (2014). Effect of the human SOD1-G93A gene on the Nrf2/ARE signaling pathway in NSC-34 cells. *Molecular Medicine Reports*, *9*(6), 2453–2458. https://doi.org/10.3892/MMR.2014.2087

Wang, H., Liu, K., Geng, M., Gao, P., Wu, X., Hai, Y., Li, Y., Li, Y., Luo, L., Hayes, J. D., Wang, X. J., & Tang, X. (2013). RXRα Inhibits the NRF2-ARE Signaling Pathway through a Direct Interaction with the Neh7 Domain of NRF2. *Cancer Research*, *73*(10), 3097–3108. https://doi.org/10.1158/0008-5472.CAN-12-3386

Wang, M.-J., Huang, H.-Y., Chen, W.-F., Chang, H.-F., & Kuo, J.-S. (2010). Glycogen synthase kinase-3β inactivation inhibits tumor necrosis factor-α production in microglia by modulating nuclear factor κB and MLK3/JNK signaling cascades. *Journal of Neuroinflammation 2010 7:1*, *7*(1), 1–18. https://doi.org/10.1186/1742-2094-7-99

Wang, M., & Kaufman, R. J. (2014). The impact of the endoplasmic reticulum protein-folding environment on cancer development. *Nature Reviews Cancer 2014 14:9*, *14*(9), 581–597. https://doi.org/10.1038/nrc3800

Wang, Q., Li, W.-X., Dai, S.-X., Guo, Y.-C., Han, F.-F., Zheng, J.-J., Li, G.-H., & Huang, J.-F. (2017). Meta-Analysis of Parkinson's Disease and Alzheimer's Disease Revealed Commonly Impaired Pathways and Dysregulation of NRF2-Dependent Genes. *Journal of Alzheimer's Disease*, *56*(4), 1525–1539. https://doi.org/10.3233/JAD-161032

Wang, W.-Y., Tan, M.-S., Yu, J.-T., & Tan, L. (2015). Role of pro-inflammatory cytokines released from microglia in Alzheimer's disease. *Annals of Translational Medicine*, *3*(10), 7–7. https://doi.org/10.3978/J.ISSN.2305-5839.2015.03.49

Wardyn, J. D., Ponsford, A. H., & Sanderson, C. M. (2015). Dissecting molecular cross-talk between Nrf2 and NF-κB response pathways. *Biochemical Society Transactions*, *43*(4), 621. https://doi.org/10.1042/BST20150014

Williamson, T. P., Johnson, D. A., & Johnson, J. A. (2012). Activation of the Nrf2-ARE pathway by siRNA knockdown of Keap1 reduces oxidative stress and provides partial protection from MPTP-mediated neurotoxicity. *Neurotoxicology*, *33*(3), 272. https://doi.org/10.1016/J.NEURO.2012.01.015

Winston, J. T., Strack, P., Beer-Romero, P., Chu, C. Y., Elledge, S. J., & Harper, J. W. (1999). The SCFβ-TRCP–ubiquitin ligase complex associates specifically with phosphorylated

destruction motifs in IκBα and β-catenin and stimulates IκBα ubiquitination in vitro. *Genes & Development*, *13*(3), 270. https://doi.org/10.1101/GAD.13.3.270

Wood-Kaczmar, A., Kraus, M., Ishiguro, K., Philpott, K. L., & Gordon-Weeks, P. R. (2009). An alternatively spliced form of glycogen synthase kinase-3β is targeted to growing neurites and growth cones. *Molecular and Cellular Neuroscience*, *42*(3), 184–194. https://doi.org/10.1016/J.MCN.2009.07.002

Woodgett, J. R. (1991). cDNA cloning and properties of glycogen synthase kinase-3. *Methods in Enzymology*, *200*(C), 564–577. https://doi.org/10.1016/0076-6879(91)00172-S

Wooten, M. W., Geetha, T., Seibenhener, M. L., Babu, J. R., Diaz-Meco, M. T., & Moscat, J. (2005). The p62 Scaffold Regulates Nerve Growth Factor-induced NF-κB Activation by Influencing TRAF6 Polyubiquitination *. *Journal of Biological Chemistry*, *280*(42), 35625–35629. https://doi.org/10.1074/JBC.C500237200

Wu, C. H., Chien, H. F., Chang, C. Y., & Ling, E. A. (1997). Heterogeneity of antigen expression and lectin labeling on microglial cells in the olfactory bulb of adult rats. *Neuroscience Research*, *28*(1), 67–75. https://doi.org/10.1016/S0168-0102(97)01178-4

Wu, Y., Dissing-Olesen, L., MacVicar, B. A., & Stevens, B. (2015). Microglia: Dynamic Mediators of Synapse Development and Plasticity. *Trends in Immunology*, *36*(10), 605. https://doi.org/10.1016/J.IT.2015.08.008

Xue, Q., Yan, Y., Zhang, R., & Xiong, H. (2018). Regulation of iNOS on Immune Cells and Its Role in Diseases. *International Journal of Molecular Sciences*, *19*(12). https://doi.org/10.3390/IJMS19123805

Yamazaki, H., Tanji, K., Wakabayashi, K., Matsuura, S., & Itoh, K. (2015). Role of the Keap1/Nrf2 pathway in neurodegenerative diseases. *Pathology International*, *65*(5), 210–219. https://doi.org/10.1111/PIN.12261

Yang, Y., Jiang, S., Yan, J., Li, Y., Xin, Z., Lin, Y., & Qu, Y. (2015). An overview of the molecular mechanisms and novel roles of Nrf2 in neurodegenerative disorders. *Cytokine & Growth Factor Reviews*, *26*(1), 47–57. https://doi.org/10.1016/J.CYTOGFR.2014.09.002

Yin, J., Valin, K. L., Dixon, M. L., & Leavenworth, J. W. (2017). The Role of Microglia and Macrophages in CNS Homeostasis, Autoimmunity, and Cancer. *Journal of Immunology Research*, *2017*. https://doi.org/10.1155/2017/5150678

Yoshiyama, Y., Higuchi, M., Zhang, B., Huang, S.-M., Iwata, N., Saido, T. C., Maeda, J., Suhara, T., Trojanowski, J. Q., & Lee, V. M.-Y. (2007). Synapse Loss and Microglial Activation Precede Tangles in a P301S Tauopathy Mouse Model. *Neuron*, *53*(3), 337–351. https://doi.org/10.1016/J.NEURON.2007.01.010

Yu, H., Yuan, B., Chu, Q., Wang, C., & Bi, H. (2019). Protective roles of isoastilbin against Alzheimer's disease via Nrf2-mediated antioxidation and anti-apoptosis. *International Journal of Molecular Medicine*, *43*(3), 1406–1416. https://doi.org/10.3892/IJMM.2019.4058

Yu, I.-C. I., Paraiso, H. C., Kuo, P.-C., Scofield, B. A., Sweazey, R. D., Chang, F.-L., & Yen, J.-H. (2019). Functional Nrf2 restrains inflammatory and transcriptional phenotypes in microglia and its deficiency recapitulates the aging phenotype. *The Journal of Immunology*, *202*(1 Supplement).

Yu, M., Li, H., Liu, Q., Liu, F., Tang, L., Li, C., Yuan, Y., Zhan, Y., Xu, W., Li, W., Chen, H., Ge, C., Wang, J., & Yang, X. (2011). Nuclear factor p65 interacts with Keap1 to repress the Nrf2-ARE pathway. *Cellular Signalling*, *23*(5), 883–892. https://doi.org/10.1016/J.CELLSIG.2011.01.014

Yunna, C., Mengru, H., Lei, W., & Weidong, C. (2020). Macrophage M1/M2 polarization. *European Journal of Pharmacology*, *877*, 173090. https://doi.org/10.1016/J.EJPHAR.2020.173090

Yuskaitis, C. J., Jope, R. S., CJ, Y., RS, J., Yuskaitis, C. J., & Jope, R. S. (2009). Glycogen synthase kinase-3 regulates microglial migration, inflammation, and inflammation-induced neurotoxicity. *Cellular Signalling*, *21*(2). https://doi.org/10.1016/J.CELLSIG.2008.10.014

Zhang, D. D., & Hannink, M. (2003). Distinct Cysteine Residues in Keap1 Are Required for Keap1-Dependent Ubiquitination of Nrf2 and for Stabilization of Nrf2 by Chemopreventive Agents and Oxidative Stress. *Molecular and Cellular Biology*, *23*(22), 8137. https://doi.org/10.1128/MCB.23.22.8137-8151.2003

Zhang, D. D., Lo, S.-C., Cross, J. V., Templeton, D. J., & Hannink, M. (2004). Keap1 Is a Redox-Regulated Substrate Adaptor Protein for a Cul3-Dependent Ubiquitin Ligase Complex. *Molecular and Cellular Biology*, *24*(24), 10941–10953. https://doi.org/10.1128/MCB.24.24.10941-10953.2004

Zhang, J.-S., Herreros-Villanueva, M., Koenig, A., Deng, Z., de Narvajas, A. A.-M., Gomez, T. S., Meng, X., Bujanda, L., Ellenrieder, V., Li, X. K., Kaufmann, S. H., & Billadeau, D. D. (2014). Differential activity of GSK-3 isoforms regulates NF-κB and TRAIL- or TNFα induced apoptosis in pancreatic cancer cells. *Cell Death & Disease 2014 5:3*, *5*(3), e1142–e1142. https://doi.org/10.1038/cddis.2014.102

Zheng, Y., Zhu, G., He, J., Wang, G., Li, D., & Zhang, F. (2019). Icariin targets Nrf2 signaling to inhibit microglia-mediated neuroinflammation. *International Immunopharmacology*, *73*, 304–311. https://doi.org/10.1016/J.INTIMP.2019.05.033

Zhou, J., Freeman, T. A., Ahmad, F., Shang, X., Mangano, E., Gao, E., Farber, J., Wang, Y., Ma, X.-L., Woodgett, J., Vagnozzi, R. J., Lal, H., & Force, T. (2013). GSK-3α is a central regulator of age-related pathologies in mice. *The Journal of Clinical Investigation*, *123*(4), 1821. https://doi.org/10.1172/JCI64398

Zhou, X., Gao, X.-P., Fan, J., Liu, Q., Anwar, K. N., Frey, R. S., & Malik, A. B. (2005). LPS activation of Toll-like receptor 4 signals CD11b/CD18 expression in neutrophils. *Https://Doi.Org/10.1152/Ajplung.00327.2004*, *288*(4 32-4), 655–662. https://doi.org/10.1152/AJPLUNG.00327.2004

Zhou, Y., Wang, X., Ying, W., Wu, D., & Zhong, P. (2019). Cryptotanshinone Attenuates Inflammatory Response of Microglial Cells via the Nrf2/HO-1 Pathway. *Frontiers in Neuroscience*, *0*, 852. https://doi.org/10.3389/FNINS.2019.00852

Zolezzi, J. M., & Inestrosa, N. C. (2017). Wnt/TLR Dialog in Neuroinflammation, Relevance in Alzheimer's Disease. *Frontiers in Immunology*, *0*(FEB), 187. https://doi.org/10.3389/FIMMU.2017.00187

Zou, Y., Hong, B., Fan, L., Zhou, L., Liu, Y., Wu, Q., Zhang, X., & Dong, M. (2012). Protective effect of puerarin against beta-amyloid-induced oxidative stress in neuronal cultures from rat hippocampus: involvement of the GSK-3β/Nrf2 signaling pathway. *Http://Dx.Doi.Org/10.3109/10715762.2012.742518*, *47*(1), 55–63. https://doi.org/10.3109/10715762.2012.742518

Zuo, L., Prather, E. R., Stetskiv, M., Garrison, D. E., Meade, J. R., Peace, T. I., & Zhou, T. (2019). Inflammaging and Oxidative Stress in Human Diseases: From Molecular Mechanisms to Novel Treatments. *International Journal of Molecular Sciences 2019, Vol. 20, Page 4472*, *20*(18), 4472. https://doi.org/10.3390/IJMS20184472